Elsevier Editorial System(tm) for Applied Surface Science

Manuscript Draft

Manuscript Number: APSUSC-D-18-10130R1

Title: Au nanoparticles decorated on activated coke via a facile preparation for efficient catalytic reduction of nitrophenols and azo dyes

Article Type: Full Length Article

Keywords: Au nanoparticles; Activated coke; Catalytic reduction; Nitrophenols; Azo dyes.

Corresponding Author: Professor Guangming Zeng, Ph.D.

Corresponding Author's Institution: Hunan University

First Author: Yukui Fu

Order of Authors: Yukui Fu; Piao Xu; Danlian Huang; Guangming Zeng, Ph.D.; Cui Lai; Lei Qin; Bisheng Li; Jiangfan He; Huan Yi; Min Cheng; Chen Zhang

Ms. Ref. No.: APSUSC-D-18-10130

Title: Au nanoparticles decorated on activated coke via a facile preparation for efficient catalytic reduction of nitrophenols and azo dyes

Journal: Applied Surface Science

Dear Editor, Prof. Franklin Tao, and Reviewer

Thanks for your valuable suggestions and comments on our manuscript entitled "Au nanoparticles decorated on activated coke via a facile preparation for efficient catalytic reduction of nitrophenols and azo dyes" (**Ms. Ref. No.: APSUSC-D-18-10130**). It is very helpful for us to make improvement.

We have read and considered all the comments and suggestions carefully, and tried our best to revise the manuscript according to the comments of reviewers. On behalf of my co-authors, I would like to provide a detailed list (point by point) of responses to each item of the reviewers' comments. We also highlighted our revisions in the manuscript in red so that reviewers/Editors could easily identify them. We hope that the editor and the reviewers will be satisfied with our responses to the 'comments' and the revisions for our original manuscript.

Thanks and best regards.

Yours sincerely,

Guangming Zeng

***Highlights (for review)**

1. Activated coke (AC) with a graphite-like layer crystallite structure as a promising support for metal nanoparticles.

2. Au nanoparticles supported on AC for efficient catalytic reduction of nitrophenols and azo dyes.

3. Mechanism of the synergistic effect between Au NPs and AC towards the reduction of nitrophenols.

Ms. Ref. No.: APSUSC-D-18-10130

Title: Au nanoparticles decorated on activated coke via a facile preparation for efficient catalytic reduction of nitrophenols and azo dyes

Journal: Applied Surface Science

Dear Editor and Reviewer

Thanks for your valuable suggestions and comments on our article (**Ms. Ref. No.: APSUSC-D-18-10130**). It is very helpful for us to make improvement. We have read and considered all the comments and suggestions carefully, and tried our best to revise the manuscript according to the comments of reviewers. On behalf of my co-authors, I would like to provide a detailed list (point by point) of responses to each item of the reviewers' comments. We also highlighted our revisions in the manuscript in red so that reviewers could easily identify them. We hope that the editor and the reviewers will be satisfied with our responses to the 'comments' and the revisions for our original manuscript.

Thanks and best regards.

Yours sincerely,

Guangming Zeng

Revisions based on Reviewer

General Comments:

This manuscript brings a study on the catalytic performance of activated coke (AC) supported gold nanoparticles for the reduction of nitrophenols and azo dyes. The activities of the catalytic reduction excelled most of the reported catalysts with similar structures. Texture and surface properties of the catalysts were illustrated by a comprehensive investigation of combined characterizations including XRD, TEM, FTIR, XPS. A mechanism was proposed at the same time. There are, nonetheless, some problems should be concerned before the publication of this article.

Response:

We are very appreciated for the reviewer's valuable comments and thoughtful suggestions on our manuscript. The suggestion is quite helpful and important to improve our manuscript. We have revised the manuscript carefully to make it clearer than the previous version. The specific revisions are presented as follows.

Specific comments:

Comment 1:

What is this "tight interaction" (line 162) exactly? How did this "tight interaction" decrease the XRD intensities of AC specifically with such a low Au amount? Please rule out the influence of the synthesis process on the crystallinity of AC instead of the Au NPs per se.

Response:

Thank you very much for your valuable comments and we highly agree with your suggestions. To better figure out the implications of the change of diffraction peak, we have supplemented the XRD spectrum of activated coke reacted with ascorbic acid only ("AC+AA" in Fig.1 in revised manuscript) and found the peak at nearly 29.4° disappeared in this spectrum. This indicates the synthesis process has an influence on the crystallinity of activated coke. The oxidation of ascorbic acid used in our research (10 mL, 0.1 M) would affect the hydrogen bonding of hydrogen and oxygen atom, thus affecting the interplanar spacing and crystallinity of activated coke.

But it's worth noting that the peak at 26.66° was present in all XRD spectra and the peak intensity decreased with the increase of Au loading amount. It indicates the loading of Au NPs over activated coke would affect the activated coke crystallinity. The increase of Au loading amount may occupy more grain boundaries and affected the interplanar spacing of activated coke, thus leading to a decrease of crystalline quality of activated coke, which indicates that Au NPs interacted with activated coke. Since the ascorbic acid was indispensable in the synthesis of Au NPs supported on activated coke, it's hard to rule out the influence of the synthesis process on the crystallinity of activated coke instead of the Au NPs per se. To clarify the results more clearly, we have revised this part (Line 160-172, Page 9~10 in revised manuscript). Thanks very much for the advice again.

- (Line 160-165, Page 9) The peak intensity at 26.66° decreased with increase of AC loading amount. The increase of Au loading amount may occupy more grain

boundaries and affected the interplanar spacing of AC [31, 40], thus leading to a decrease of crystalline quality of AC. The above results could also be inferred that the interaction may exist between Au and AC, as demonstrated as follows in TEM, FTIR and XPS.

- (Line 165-172, Page 10) What's more, the peak at nearly 29.4° corresponding to AC was also detected over virgin AC. Interestingly, compared with the virgin AC, the peak at 29.4° disappeared in XRD pattern of AC that reacted with AA only. This indicates the synthesis process has an influence on the crystallinity of activated coke. As reported by Costanzo et al., the oxidation or reduction of ascorbic acid would affect the hydrogen bonding of hydrogen and oxygen atom [41, 42], thus resulting in a decrease of crystalline quality of AC.

- **References**

[31] Y. Xie, C. Li, L. Zhao, J. Zhang, G. Zeng, X. Zhang, W. Zhang, S. Tao, Experimental study on Hg^0 removal from flue gas over columnar MnO_x-CeO_2/activated coke, Applied Surface Science, 333 (2015) 59-67.

[40] L. Ouarez, A. Chelouche, T. Touam, R. Mahiou, D. Djouadi, A. Potdevin, Au-doped ZnO sol-gel thin films: An experimental investigation on physical and photoluminescence properties, Journal of Luminescence, 203 (2018) 222-229.

[41] F. Costanzo, M. Sulpizi, J. Vandevondele, R.G.D. Valle, M. Sprik, Ab initiomolecular dynamics study of ascorbic acid in aqueous solution, Molecular Physics, 105 (2007) 17-23.

[42] H. Li, Y. Liu, Y. Yang, D. Yang, J. Sun, Influences of hydrogen bonding dynamics on adsorption of ethyl mercaptan onto functionalized activated carbons: A DFT/TDDFT study, Journal of Photochemistry and Photobiology A: Chemistry, 291 (2014) 9-15.

- (Line 183, Page 11)

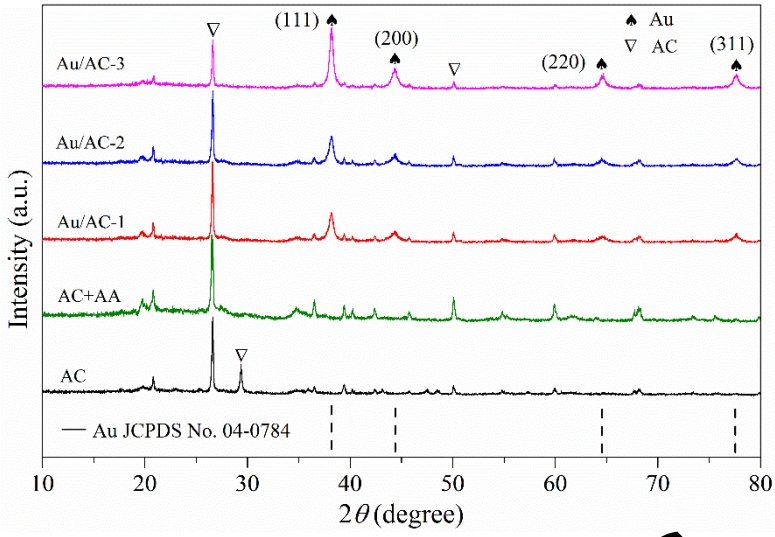

Fig. 1. X-ray diffraction patterns of virgin AC and Au/AC catalysts with different Au content.

Comment 2:

There seems to be a large amount of small Au particles from the TEM image (Fig. 2C) as well as the STEM-HAADF image (Fig. S1A). Considering the widely known fact that Au NPs with a size larger than 5 nm generally present little catalytic activity (Hutchings, G. (2009). A golden future. Nature chemistry, 1(7), 584. Corma, A., & Serna, P. (2006). Chemoselective hydrogenation of nitro compounds with supported gold catalysts. Science, 313(5785), 332-334.), do please provide (S)TEM images with higher resolution and recount the size distributions. Maybe these small particles are the actual active species?

Response:

Thank you for your valuable comments. According to your suggestions, we have supplemented TEM images with higher resolution and SEM images in **Fig.2D and**

Fig. S2. According to the TEM images with higher resolution (**Fig. 2C and 2D, Fig. S2B and S2C**), we have recounted the size distributions based on more than 200 Au NPs and the size distributions was 14.9 ± 10.8 nm. The Au NPs with a size smaller than 5 nm accounted for 14%. This was because the pore structure of activated coke restricted the growing of Au NPs adsorbed into the activated coke.

Besides, we have read more literatures to better understand the relationship between Au NPs size and active species. As reported by Hutchings, Corma and Serna et al., Au NPs with the size of 2–5 nm can exhibit higher activity in catalytic oxidation of carbon monoxide, hydrochlorination of acetylene and hydrogenation of nitro compounds. In addition, we also found some interesting results that the actual active species were affected by many factors, such as the particle size, shape as well as the reaction system and conditions (temperatures and pressures). For example, Nautiyal et al. have synthesized Au NPs with various shapes and sizes and found that the catalytic activity was influenced by their shape and size. They have demostrated that penta and hexagonal nanoparticles exhibit good catalytic activity despite their larger size (80–85 nm) as compared to spherical particles. It also can be found that under diferent catalytic reaction system and condition, the Au NPs with various size can exhibit a relatively higher catalytic activity to some extent. In the catalytic system of nitrophenols reduction, Tang et al. have synthesized Au@CMK-3-O with Au NPs size of 10 nm. Zeng et al. have developed PDA-g-C_3N_4/$Au_{(3)}$ catalyst and the Au NPs size was in average diameter of 26.1 ± 4.7 nm. This indicates that Au NPs with about relatively larger size could also exhibit high catalytic activity in the catalytic system

of nitrophenols reduction. Thus, we briefly summarized the Au NPs size on different Au-based catalysts in resent research.

Catalysts	Particle size (nm)	k_{app} (s^{-1})	Catalytic system	Reaction condition	Ref
Au@ZIF-8	3.1 ± 0.9	-	Oxidation of CO	>300°C	[1]
Au/TiO_2	25	-	Aerobic oxidation of aniline	100°C	[2]
Au/Fe_2O_3	11.8	-	Oxidation of Volatile organic compounds	354°C	[3]
Au/C	10.5	-	Oxidation of glycerol	60 °C	[4]
Au/γ-Fe_2O_3	6.7 ± 2.3	-	Oxidation of 1,4-butanediol	140°C	[5]
Au/AC (Activated carbon)	1-15	0.035	Selective hydrogenation of m-DNB	250 °C	[6]
Au/SC_M	9.99 ± 1.63	0.16	Degradation of quinclorac	Room temperature	[7]
Au NPs	6.2	0.0475	Reduction of nitrophenol reduction	Room temperature	[8]
PVCL-CD-Au hybrid	6.0 ± 0.3	0.025	Reduction of aromatic nitro-compounds	Room temperature	[9]
Au NPs	with various shape and sizes	-	Reduction of nitrophenol	Room temperature	[10]
PDA-g-$C_3N_4/Au_{(3)}$	26.1	0.054	Reduction of nitrophenol	Room temperature	[11]
Au@CMK-3-O	10	0.0048	Reduction of p-nitrophenol	Room temperature	[12]

Reference

[1] H.-L. Jiang, B. Liu, T. Akita, M. Haruta, H. Sakurai, Q. Xu, Au@ZIF-8: CO oxidation over gold nanoparticles deposited to metal− organic framework, Journal of the American Chemical Society, 131 (2009) 11302-11303.

[2] P. Haider, B. Kimmerle, F. Krumeich, W. Kleist, J.-D. Grunwaldt, A. Baiker, Gold-Catalyzed Aerobic Oxidation of Benzyl Alcohol: Effect of Gold Particle Size on Activity and Selectivity in Different Solvents, Catalysis Letters, 125 (2008) 169-176.

[3] S.A.C. Carabineiro, X. Chen, O. Martynyuk, N. Bogdanchikova, M. Avalos-Borja, A. Pestryakov, P.B. Tavares, J.J.M. Órfão, M.F.R. Pereira, J.L. Figueiredo, Gold supported on metal oxides for volatile organic compounds total oxidation, Catalysis Today, 244 (2015) 103-114.

[4] B.N. Zope, D.D. Hibbitts, M. Neurock, R.J. Davis, Reactivity of the gold/water interface during selective oxidation catalysis, Science, 330 (2010) 74-78.

[5] J. Huang, W.-L. Dai, K. Fan, Remarkable support crystal phase effect in Au/FeO_x catalyzed oxidation of 1,4-butanediol to γ-butyrolactone, Journal of Catalysis, 266 (2009) 228-235.

[6] F. Cárdenas-Lizana, Z.M.D. Pedro, S. Gómez-Quero, L. Kiwi-Minsker, M.A. Keane, Carbon supported gold and silver: Application in the gas phase hydrogenation of m-dinitrobenzene, Journal of Molecular Catalysis A: Chemical, 408 (2015) 138-146.
[7] G. Shi, Y. Li, G. Xi, Q. Xu, Z. He, Y. Liu, J. Zhang, J. Cai, Rapid green synthesis of gold nanocatalyst for high-efficiency degradation of quinclorac, J Hazard Mater, 335 (2017) 170-177.
[8] P. Suchomel, L. Kvitek, R. Prucek, A. Panacek, A. Halder, S. Vajda, R. Zboril, Simple size-controlled synthesis of Au nanoparticles and their size-dependent catalytic activity, Sci Rep, 8 (2018) 4589.
[9] H. Jia, D. Schmitz, A. Ott, A. Pich, Y. Lu, Cyclodextrin modified microgels as "nanoreactor" for the generation of Au nanoparticles with enhanced catalytic activity, J. Mater. Chem. A, 3 (2015) 6187-6195.
[10] M. Kumari, A. Mishra, S. Pandey, S.P. Singh, V. Chaudhry, M.K. Mudiam, S. Shukla, P. Kakkar, C.S. Nautiyal, Physico-Chemical Condition Optimization during Biosynthesis lead to development of Improved and Catalytically Efficient Gold Nano Particles, Sci Rep, 6 (2016) 27575.
[11] L. Qin, D. Huang, P. Xu, G. Zeng, C. Lai, Y. Fu, H. Yi, B. Li, C. Zhang, M. Cheng, C. Zhou, X. Wen, In-situ deposition of gold nanoparticles onto polydopamine-decorated g-C_3N_4 for highly efficient reduction of nitroaromatics in environmental water purification, Journal of colloid and interface science, 534 (2018) 357-369.
[12] P. Guo, L. Tang, J. Tang, G. Zeng, B. Huang, H. Dong, Y. Zhang, Y. Zhou, Y. Deng, L. Ma, S. Tan, Catalytic reduction-adsorption for removal of p-nitrophenol and its conversion p-aminophenol from water by gold nanoparticles supported on oxidized mesoporous carbon, Journal of colloid and interface science, 469 (2016) 78-85.

Thanks very much for the advice again. The detailed revisions are presented as follows.

- (Line 191-194, Page 11) From Fig. 2C and 2D, it could be observed that Au NPs with a size smaller than 5 nm existed in AC, with interplanar spacing of 0.235 nm corresponding to the (111) crystal planes. This was because the pore structure of AC restricted the growing of Au NPs adsorbed into the AC.
- (Line 201-205, Page 12) Base on the Fig. 2C, Fig. 2D, Fig. S2B and Fig. S2C, the particle size of Au NPs supported on AC was counted for at least 200 nanoparticles, which would make the size distributions more representative and accurate. Fig. 2F shows the presence of dispersed Au NPs with a diameter of 14.9 ± 10.8 nm.

- (Line 212, Page 12)

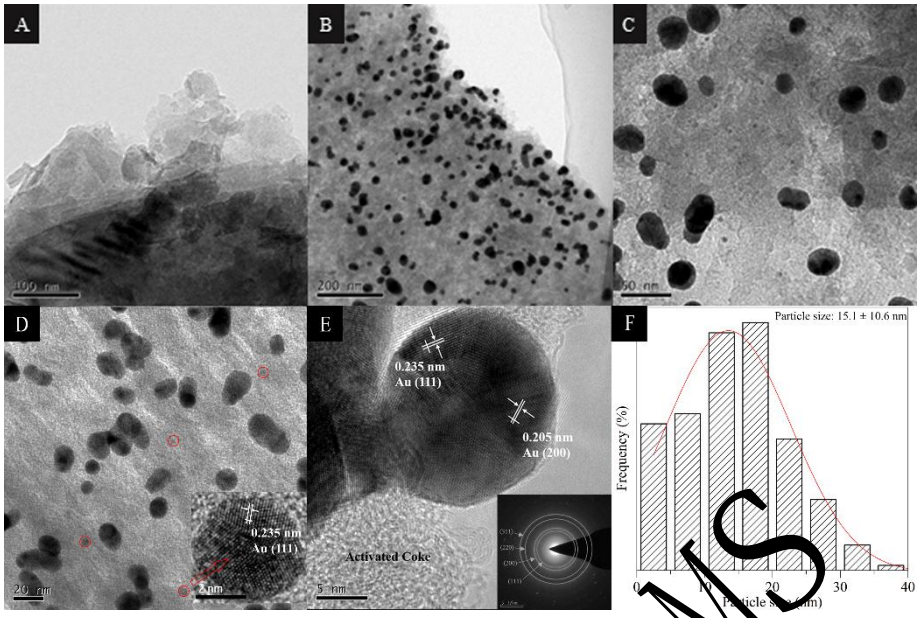

Fig. 2. TEM images of virgin AC (A) and the Au/AC-3 catalyst (B, C and D) (the inset is HRTEM image of the tiny NPs); HRTEM image (E) of Au/AC-3 catalyst (the inset is SAED pattern); Size distribution of Au NPs (F).

- (Supporting information, Line 15, Page 2)

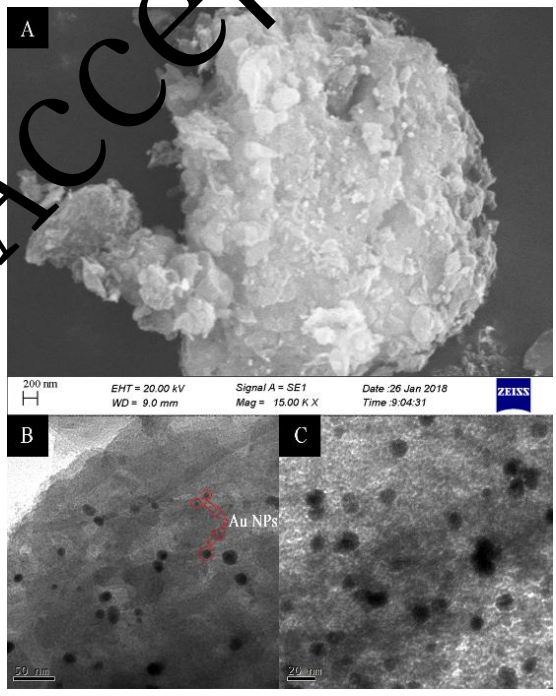

Fig. S2. SEM image (A) and TEM images (B and C) of Au/AC-3.

Comment 3:

The statement from line 201~202, as I quote, "As shown in Fig. 3, the spectrum of AC is similar to the activated carbon", is confusing.

Response:

Thanks so much for reviewer's valuable comment. At present, there are many studies about activated carbon as a support for metal noble nanoparticles anchoring, while a relatively few studies about activated coke. Activated coke possesses mesopore and macropore structure, which is different from the active carbon with micropore structure. This can reduce the influence of internal diffusion on the general rate of adsorption and catalytic process greatly. Hence, we utilized activated coke as a support for Au NPs anchoring for organic transformation in wastewater treatment. In the previous discussion, the comparison in activated coke and activated carbon aimed to compare the similar research and get more information about spatial structure of activated coke. To avoid confusing the readership, we have removed the sentence "As shown in Fig. 3, the spectrum of AC is similar to the activated carbon" and revised the discussion in the revised manuscript (Line 217-223, Page 13). Thanks very much for the advice again.

- (Line 217-223, Page 13) In the region of 3600-3200 cm^{-1}, the most pronounced broad and intense band around 3421 cm^{-1} was due to the overlapping of –OH as exhibited in the FTIR spectrum of activated carbon or a displaced amino group [38, 44]. And the band located at 2362 cm^{-1} was assigned to the vibration of C=O [45]. The peaks at 1635 and 1445 cm^{-1} corresponded to the skeletal vibrations

stretching of aromatic C=C [19]. The peak at 1037 cm^{-1} represented a stretching vibration of C-O or primary alcohols[46].

Comment 4:

The 4f5/2 and 4f7/2 are mislabeled in Fig. 4D.

Response:

Thanks so much for pointing out the incorrect picture. We are sorry that we mislabeled the 4f5/2 and 4f7/2 in Fig.4. We have checked our manuscript carefully to avoid the similar mistakes in the revised manuscript (Line 265, Page 15). Thanks very much for the advice again.

- (Line 265, Page 15)

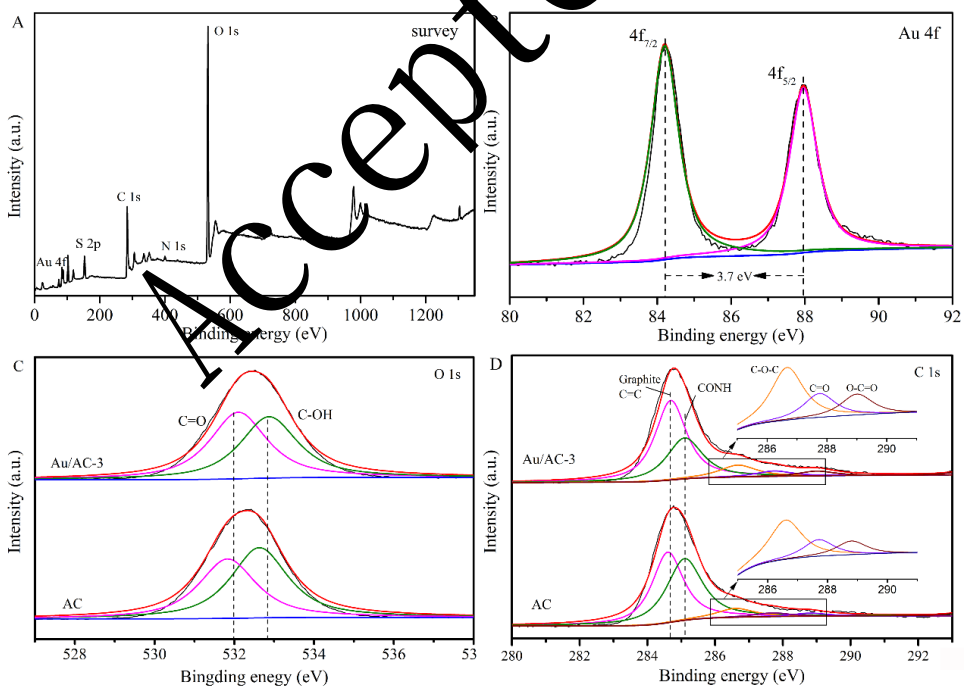

Fig. 4. XPS survey spectra (A) of Au/AC-3 catalyst; High-resolution XPS spectra of O 1s (B), C1s (C) and Au 4f (D) of Au/AC-3 and AC.

Comment 5:

The units of calculated TOF in line 312~313 are mol·g^{-1}·s^{-1}, while this variable was defined there as "moles of 4-NP reduced by per mole of Au per hour". Also, the definition of TOF is more recommended to be a normalization of catalytic conversion of reactants by the number of surface sites (more accurately, active sites).

Response:

Thanks so much for reviewer's valuable comments and we highly agree with your suggestions. In this case, we have read many literatures to better understand the definition of TOF and found it is necessary to figure out the number of active sites in a catalyst for calculation of TOF. It is difficult to calculate accurately the active sites for many heterogeneous catalytic reactions. The most critical in calculation TOF is that active sites in heterogeneous catalyst may undergo agglomeration or re-dispersion during the catalytic process, resulting in difference between each active sites. In addition, the determination of Au NPs dispersion obtained by chemisorption is often needed for the basic TOF calculation.

Nonetheless, it can be found that another feasible way for TOF calculation has been utilized in some studies. For instance, Hu et al. has calculated TOF of all samples from low to high Au NPs loading amounts are 0.076, 0.21, 0.24 and 0.055 mmol g^{-1} s^{-1}, respectively (J. Mater. Chem. A, 2014, 2, 13471-13478). Zhao has calculated that TOF of the g-C_3N_4/Au/P25 Z-scheme system is 259 mmol h^{-1} g^{-1}, which is 30 times higher than that of pristine g-C_3N_4 (Int. J. Hydrogen Energy, 2016, 41(15), 6277-6287). Dandia et al. has calculated TOF of 18.03×10^{-5} mol g^{-1} min^{-1} (defined as

number of moles of produced per gram of catalyst used per min) of Ag NPs/GO composite catalyst (Tetrahedron Lett., 2017, 58(12), 1170-1175). Based on the essential aim of the catalytic activity evaluation, this feasible expression is easy to calculate and can represent the catalytic activity of catalysts. Thus, we utilize this feasible way to calculate TOF. And we are sorry that we made a mistake in the expression of TOF. The sentence "moles of 4-NP reduced by per mole of Au per hour" was corrected by "moles of 4-NP reduced by per gram of Au per second" (Line 327-329, Page 18). Thanks very much for the advice again.

- (Line 327-329, Page 18) According to the previous research, the turn-over frequency (TOF: moles of 4-NP reduced by per gram of Au NPs per second) has been calculated to estimate the catalytic efficiency of catalysts in our research [61, 62].

- **References**

[61] Y. Qiu, Z. Ma, P. Hu, Environmentally benign magnetic chitosan/Fe_3O_4 composites as reductant and stabilizer for anchoring Au NPs and their catalytic reduction of 4-nitrophenol, Journal of Materials Chemistry A, 2 (2014) 13471-13478.

[62] W. Zhao, L. Xie, M. Zhang, Z. Ai, H. Xi, Y. Li, Q. Shi, J. Chen, Enhanced photocatalytic activity of all-solid-state g-C_3N_4/Au/P25 Z-scheme system for visible-light-driven H_2 evolution, International Journal of Hydrogen Energy, 41 (2016) 6277-6287.

Comment 6:

Why did the rate constant become constant (Fig. 7A) with the catalyst dosage more than 9 mg?

Response:

Thank you for your valuable comments and professional guidance. In our research, the rate constant k_{app} increased intensively as the catalyst dosage increased to 9 mg,

while it increased slowly as the catalyst dosage increased from 9 to 12 mg. This could be ascribed to that the reactants were saturated that even more availability sites of active catalytic surfaces could not further enhance the reaction rate at the same initial concentration of 4-NP. We have revised this part in the revised manuscript (Line 355-362, Page 20~21). Thanks very much for the advice again.

- (Line 355-362, Page 20~21) However, the rate constant k_{app} increased slowly as the catalyst dosage increased from 9 to 12 mg. When the dosage was over 9 mg and reached 12 mg, the increasing amount of rate constant k_{app} was very small, from 0.1916 to 0.2210 s^{-1}. This could be ascribed to that the reactants were saturated that even more availability sites of active catalytic surfaces could not further enhance the reaction rate at the same initial concentration of 4-NP [71]. For the balance of the highest rate and minimum catalyst dosage in the concept of economic friendly, the catalyst dosage of 9 mg was used with the current experimental condition.
- **References**

[71] L. Qin, D. Huang, P. Xu, G. Zeng, C. Lai, Y. Fu, H. Yi, B. Li, C. Zhang, M. Cheng, C. Zhou, X. Wen, In-situ deposition of gold nanoparticles onto polydopamine-decorated g-C_3N_4 for highly efficient reduction of nitroaromatics in environmental water purification, Journal of colloid and interface science, 534 (2018) 357-369.

Comment 7:

In section 3.4, were the azo dyes degraded or adsorbed? What were these dyes degraded into? Please provide evidence and references for the statement "It has been known the disappearance of the color indicates that the azo bonds of the molecules

were reductive degradation from -N=N- bonds to -HN-NH- bonds, forming colorless products" in line 444~446.

Response:

Thanks so much for reviewer's suggestions. According to reviewer's comment, we have utilized the as-prepared Au nanoparticles/activated coke-3 (Au/AC-3) catalyst to adsorb congo red, methyl orange and erichrome black T, and measured BET surface area. In addition, UV-Vis spectrophotometer was applied to determine the formation of intermediate products. The results show that Au/AC-3 possesses relatively low adsorption ability. Besides, after adding $NaBH_4$ to trigger the catalytic reaction, the reaction completed within several seconds, accompanied with the occurrence of the new characteristic adsorption peaks at about 250 nm on each UV-vis absorption spectra. According to previous studies, the peak at about 250 nm was originated from the absorption from aromatic intermediates, which may ascribed to the two sides of the cleavage azo bond or their derivatives. Thus, it can be concluded that most of azo dyes were removed by the catalytic degradation of Au/AC-3. We have revised this part and supplemented relative references in the revised manuscript (Line 460-493, Page 27~28). The detailed revisions are given below.

- (Line 460-493, Page 27~28) As shown in Fig. S6, the initial maximum absorbance of CR, EBT and MO was at 495, 526 and 465 nm [81]. After the as-prepared Au/AC-3 was tried on CR, EBT and MO adsorption, the characteristic peaks in the corresponding UV-Vis spectra of CR, EBT and MO decreased within initial 15 min (Fig. S6A, Fig. S6C and Fig. S6E). With

continuously stirring for another 15 min, these solutions achieved the adsorption equilibrium, with the adsorption efficiency of 30%, 35% and 12% for CR, EBT and MO, respectively. Especially, the adsorption efficiency of MO by Au/AC-3 was 32% at first 15 min and then decreased to 12% until equilibrium was achieved. Besides, the BET surface area (S_{BET}), pore volume, and average pore size of Au/AC-3 were determined to be 21.383 m^2 g^{-1}, 0.0938 cm^3 g^{-1} and 17.55 nm (Table S2). It validates that Au/AC-3 possesses low adsorption ability [82].

Then, the reductant $NaBH_4$ was added to the above solution for triggering the catalytic degradation. As we can see from Fig. S6B, the characteristic peaks at 344 and 495 nm ascribed to the CR decreased rapidly over reaction time. However, a new peak at 250 nm occurred with the decolorization of solutions within several seconds (Fig. S7). After reaction, there was almost no absorbance at 344 and 495 nm, and the absorbance at 250 nm was maximized, confirming that the removal of CR and the formation of intermediates were caused by catalytic degradation [83]. Similarly, the characteristic peaks of EBT and MO disappeared accompanied with the decolorization within several seconds after adding the Au/AC-3 catalysts (Fig. S7), while the new peaks at 240 and 258 nm were emerged corresponding to the produced intermediates of EBT and MO (Fig. S6D and Fig. S6E) [84, 85].

To sum up, the characteristic peaks of azo dyes decreased and the color of these solutions was decolorization during the reaction. Besides, new peaks were formed in the UV- range, suggesting azo dyes was indeed degraded, instead of

just being absorbed by Au/AC-3 and the –N=N– bonds of azo dyes was broken down by Au/AC-3 [84]. The emerging absorption at about 250 nm appeared simultaneously with –N=N– cleavage, indicating that there were newly produced colorless compounds [71]. These peaks were originated from the absorption from aromatic intermediates, which may ascribed to the two sides of the cleavage azo bond or their derivatives, corresponding to the results in previous reports [83, 84]. Thus, the most of azo dyes were removed by the catalytic degradation by Au/AC-3. As is well-known, adsorption process can play a critical role on the removal of pollutants, including catalysis [19].

- **References**

[81] C. Umamaheswari, A. Lakshmanan, N.S. Nagarajan, Green synthesis, characterization and catalytic degradation studies of gold nanoparticles against congo red and methyl orange, J Photochem Photobiol B, 178 (2018) 33-39.

[82] U. Tyagi, N. Anand, D. Kumar, Synergistic effect of modified activated carbon and ionic liquid in the conversion of microcrystalline cellulose to 5-Hydroxymethyl Furfural, Bioresour Technol, 267 (2018) 326-332.

[83] Y. Zhu, X. Cao, Y. Cheng, T. Zhu, Performances and structures of functional microbial communities in the mono azo dye decolorization and mineralization stages, Chemosphere, 210 (2018) 1051-1060.

[84] W. Zhong, T. Jiang, Y. Dang, J. He, S.-Y. Chen, C.-H. Kuo, D. Kriz, Y. Meng, A.G. Meguerdichian, S.L. Suib, Mechanism studies on methyl orange dye degradation by perovskite-type $LaNiO_{3-\delta}$ under dark ambient conditions, Applied Catalysis A: General, 549 (2018) 302-309.

[85] N. Srivastava, M. Mukhopadhyay, Biosynthesis of SnO_2 Nanoparticles Using Bacterium Erwinia herbicola and Their Photocatalytic Activity for Degradation of Dyes, Industrial & Engineering Chemistry Research, 53 (2014) 13971-13979.

- (Supporting information, Line 21, Page 4)

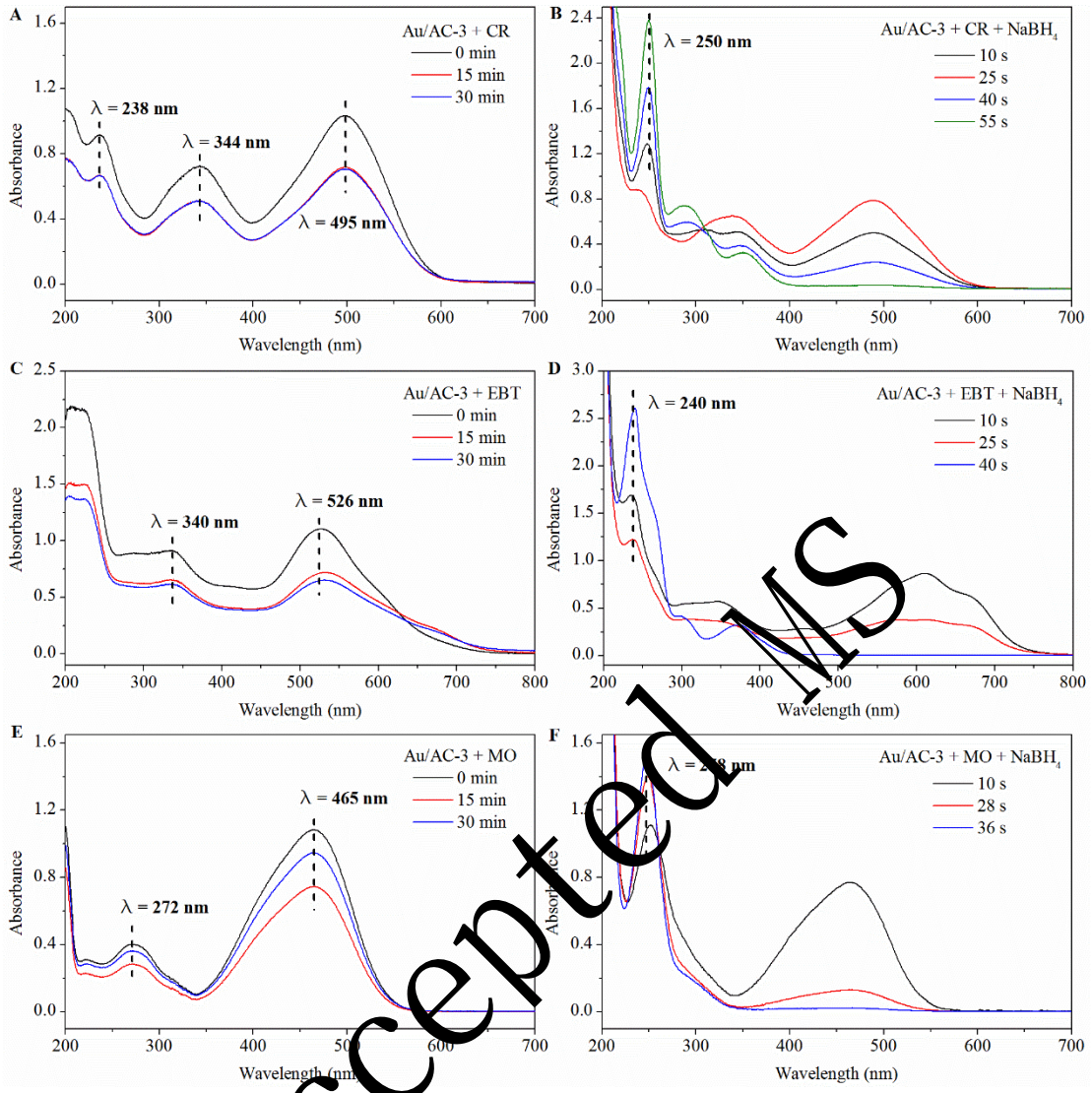

Fig. S6. Time-dependent UV-Vis absorption spectra of the absoption of CR (A), EBT (C) and MO(E) by Au/AC-3; Time-dependent UV-vis absorption spectra of the reductive degradation of CR (B), EBT (D), MO (F) catalyzed by Au/AC-3.

- (Supporting information, Line 32, Page 6) **Table S2.** Physical parameters of Au/AC-3 obtanied by N_2 adsorption-desorption analysis.

Sample	BET surface area (m^2 g^{-1})	Pore volume (cm^3 g^{-1})	Average pore size (nm)
Au/AC-3	21.383	0.0938	17.55

Comment 8:

The phrasing and grammar of this article could benefit from some polishing to eliminate mistakes like "prolong time" (line 41), "NPs was dispersed" (line 306), "was easily separated by easily centrifugation" (line 367). Words should be chosen more carefully. More examples are not listed.

Response:

Many thanks for your suggestions, which are of great importance to improve our manuscript. According to your suggestions, we have polished the whole manuscript carefully to eliminate any grammar error and typos. Some of the detailed revisions are list as follows.

1) (Line 10~13, Page 2) "Activated coke (AC), exhibiting excellent properties with a graphite-like layer crystallite structure, possesses mesopore and macropore structures which can reduce the influence of internal diffusion on the general rate of adsorption and catalytic process greatly." was revised to "Activated coke (AC) exhibits excellent properties with a graphite-like layer crystallite structure and possesses mesopore and macropore structures, which can reduce the influence of internal diffusion on the general rate of adsorption and catalytic process greatly."
2) (Line 13~15, Page 2) "In this work, we used AC as a support for gold nanoparticles anchoring to prepare Au nanoparticles/AC catalysts via a facile synthesis using ascorbic acid as a mild reducing agent." was revised to "In this work, AC was served as a support for gold nanoparticles (Au NPs) anchoring to prepare Au /AC catalysts via a facile synthesis using ascorbic acid as a mild

reducing agent."

3) (Line 17, Page 2) "experimental" was revised to "experiment".

4) (Line 20, Page 2) "were" was revised to "was".

5) (Line 27, Page 2) "shed" was revised to "sheds".

6) (Line 34, Page 4) "owing to" was revised to "because".

7) (Line 41, Page 4) "shows" was revised to "exhibits".

8) (Line 41, Page 4) "a prolong time" was revised to "a long time".

9) (Line 86, Page 6) "enhancing" was revised to "enhanced".

10) (Line 96, Page 6) "were" was revised to "was".

11) (Line 107, Page 7) "perchased" was revised to "purchased".

12) (Line 125, Page 8) "activities" was revised to "activity".

13) (Line 126, Page 8) "were" was revised to "was".

14) (Line 126, Page 8) All the "UV-is" in previous manuscript was revised to "UV-Vis".

15) (Line 179, Page 10) "match" was revised to "matched".

16) (Line 181, Page 10) "heightens" was revised to "heightened".

17) (Line 181, Page 10) "can" was revised to "could".

18) (Line 181~182, Page 10) "turn into larger nanoparticles" was revised to "formation of larger Au NPs".

19) (Line 190~191, Page 11) "As revealed from Fig. 2B, the Au NPs are uniformly distributed on the stacking AC layers." was revised to "As revealed from Fig. 2B, the Au NPs were dispersed uniformly on the stacking AC layers."

20) (Line 197~198, Page 11) "Moreover, the SAED pattern as indicated in Fig. 2F, displays the characteristic rings for the (111), (200), (220) and (311) planes of fcc Au." was revised to "Moreover, the SAED pattern was inserted in Fig. 2E, displaying the characteristic rings for the (111), (200), (220) and (311) planes of fcc Au."

21) (Line 227, Page 13) "indicates" was revised to "indicated".

22) (Line 231, Page 13) "is" was revised to "was".

23) (Line 242, Page 14) "index" was revised to "indexed".

24) (Line 244, Page 14) "are" was revised to "were"

25) (Line 246, Page 14) "are" was revised to "were".

26) (Line 249, Page 14) "are" was revised to "were".

27) (Line 255, Page 15) "can" was revised to "could".

28) (Line 257, Page 15) "can be" was revised to "were".

29) (Line 260, Page 15) "decrease" was revised to "decreased".

30) (Line 260, Page 15) "is" was revised to "was".

31) (Line 262, Page 15) "which might be attributed" was revised to "owing to".

32) (Line 270, Page 16) "materials" was revised to "material".

33) (Line 273~275, Page 16) "After the additional of $NaBH_4$ in the 4-nitreophenol, the color of the mixture aqueous turned to bright yellow rapidly which means the 4-nitreophenol was converted into nitrophenolate anion ($C_6H_4NO_3^-$)." was revised to " After the additional of $NaBH_4$ in the 4-NP, the color of the mixture aqueous turned to bright yellow rapidly, indicating the 4-NP was converted into

nitrophenolate anion ($C_6H_4NO_3^-$)."

34) (Line 276, Page 16) "indexes" was revised to "indexed".

35) (Line 282, Page 16) "decreases" was revised to "decreased".

36) (Line 282, Page 16) "appears" was revised to "appeared".

37) (Line 294, Page 17) "is" was revised to "was".

38) (Line 297, Page 17) "provide" was revised to "provided".

39) (Line 298, Page 17) "was used excess" was revised to "was excess".

40) (Line 306, Page 17) "is" was revised to "was".

41) (Line 316, Page 18) "is" was revised to "was".

42) (Line 317, Page 18) "is" was revised to "was".

43) (Line 319, Page 18) "increases" was revised to "increased".

44) (Line 321, Page 18) "was" was revised to "were".

45) (Line 369, Page 21) "is" was revised to "was".

46) (Line 376, Page 21) "band" was revised to "bands".

47) (Line 376, Page 21) "is" was revised to "were".

48) (Line 378, Page 22) "decreases" was revised to "decreased".

49) (Line 378, Page 22) "along with the color of the mixture solution fading" was revised to "accompanied with decolorization".

50) (Line 382, Page 22) "is" was revised to "was".

51) (Line 392~393, Page 23) "the Au/AC was easily separated by easily centrifugation" was revised to "the Au/AC could be easily separated by centrifugation from reaction solution".

52) (Line 396, Page 24) "exhibits" was revised to "exhibited".

53) (Line 398, Page 24) "have" was revised to "has".

54) (Line 415, Page 25) "decreases" was revised to "decreased".

55) (Line 422, Page 25) "desorb" was revised to "were desorbed".

56) (Line 434~437, Page 26) "AC can promote the adsorption of reactants which provides a higher concentration of nitrophenols near to Au NPs on AC, leading to more opportunity for nitrophenols molecules to exposed onto active sites of the catalysts, accelerating the reaction kinetics " was revised to " AC can promote the adsorption of reactants, which provides a higher concentration of nitrophenols near to Au NPs on AC. This could provide more opportunity for nitrophenols molecules to expose onto active sites of the catalysts and thus accelerate the reaction kinetics."

57) (Line 437~440, Page 26) "AC possesses a graphite-like layer crystallite structure, which is beneficial for the adsorption of 4-NP via π-π stacking interactions, leading to shorter distance between 4-NP and Au NPs supported on AC." was revised to " AC possesses a graphite-like layer crystallite structure, which is beneficial for the adsorption of 4-NP via π-π stacking interactions. This can shorten the distance between 4-NP and Au NPs supported on AC."

58) (Line 493~495, Page 28~29) "Compared with other reported catalytic degradation study of azo dyes, the reductive degradation catalyzed by Au/AC catalyst is obviously superior to that by other catalysts" was revised to "Compared with other study of catalytic degradation of azo dyes, the reductive

degradation efficiency of Au/AC catalyst is obviously superior to that of other catalysts ".

59) (Line 506, Page 29) "exposed" was revised to "expose".

60) (Line 510, Page 29) "was" was revised to "were".

61) (Line 512, Page 29) "manifests" was revised to "manifested".

Au nanoparticles decorated on activated coke via a facile preparation for efficient catalytic reduction of nitrophenols and azo dyes

Yukui Fu [a,b,1], Piao Xu [a,b,1], Danlian Huang [a,b,1], Guangming Zeng [a,b,*], Cui Lai [a,b,*], Lei Qin [a,b], Bisheng Li [a,b], Jiangfan He [a, b], Huan Yi [a,b], Min Cheng [a,b], Chen Zhang [a,b]

[a] *College of Environmental Science and Engineering, Hunan University, Changsha, 410082, PR China,*

[b] *Key Laboratory of Environmental Biology and Pollution Control, Hunan University, Ministry of Education*

* Corresponding author.

E-mail address: zgming@hnu.edu.cn (G.M. Zeng) and laicui@hnu.edu.cn (C.Lai).

1 These authors contributed equally to this article.

Abstract

Activated coke (AC) exhibits excellent properties with a graphite-like layer crystallite structure and possesses mesopore and macropore structures, which can reduce the influence of internal diffusion on the general rate of adsorption and catalytic process greatly. In this work, AC was served as a support for gold nanoparticles (Au NPs) anchoring to prepare Au /AC catalysts via a facile synthesis using ascorbic acid as a mild reducing agent. The morphology and structure of catalysts were characterized by XRD, TEM, FTIR, and XPS analysis. Our experiment results showed that the abundant functional groups on the surface of AC play a vital role in the immobilization of Au NPs. Au/AC was employed as a highly efficient catalyst with a rate constant of 0.1916 s^{-1} for the reduction of 4-nitrophenols by $NaBH_4$. Au/AC was also tested for the catalytic reduction of other nitrophenols (2-nitrophenol and 2, 4-dinitrophenol) and azo dyes (congo red, methyl orange and erichrome black T), demonstrating that Au/AC exhibited superior catalytic efficiency compared with other Au NPs catalysts. The catalysts showed good reusability, with conversion of 84% in the reduction of 4-NP in 20 s after six cycles. The Au/AC with high TOF has potential to be a workable and efficient catalyst in industrial applications. Present study not only provides a facile preparation route of catalysts using AC as a promising support, but also sheds light on the understanding of mechanism of the synergistic effect between Au NPs and AC towards the reduction of nitrophenols.

Keywords: Au nanoparticles; Activated coke; Catalytic reduction; Nitrophenols;

31 Azo dyes.

1. Introduction

Noble metal nanoparticles (MNPs) in catalytic applications have received significant interest because the nanoparticles possess unusual physiochemical properties with large number of exposed metal atoms, which greatly enhance the catalytic activity [1-5]. Gold nanoparticles (Au NPs) with features of high specific surface area, less prone to metal leaching and self-poisoning are one of the most inspiring developments in catalysis field [5-8]. Among all the Au NPs-catalyzed reaction, catalytic reduction of 4-nitrophenol (4-NP) to 4-aminophenol (4-AP) by $NaBH_4$ has been used widely as model reaction to test its catalytic activity, since 4-NP exhibits high toxicity and stability for a long time in water, causing harm to ecosystem [9-13]. And most importantly, the generated aminophenol is known to be an important intermediate chemical in many industries as well as easier to be mineralized and removed compared to the nitrophenols [14]. However, Au NPs suffer from serious stability problems such as aggregation in practice due to their high surface energy, eventually losing of their intrinsic activity [15-17]. In addition, considering facile catalyst recovery and recycling, immobilizing Au NPs on the surface of solid supports (e.g. silica, metal oxides and polymer) is regarded as an efficient approach for preventing aggregation of Au NPs and warranting high catalytic activity [18-21]. However, the stability of mentioned solid supports is compromised in some chemical environments of high or low pH solutions, resulting in the inability to achieve highly distributed Au NPs and dissolution of solid supports [22-24]. Thus, it is desirable to find a rational support with high stability to enhance

54 the catalytic activity and efficiency of Au NPs.

55 Activated coke (AC), as a kind of carbon-based material, exhibits excellent
56 properties with graphite-like layer crystallite and possesses appreciable
57 environmental and economic benefits owing to its better mechanical strength, easier
58 regeneration and lower cost compared with other carbon-based materials [25-27].
59 AC with mesopore and macropore structures can reduce the influence of internal
60 diffusion on the general rate of adsorption and catalytic process greatly [22, 28-30],
61 which is different from microporous activated carbon. In addition, with abundant
62 functional groups, AC could provide the active sites and is beneficial for MNPs
63 anchoring and dispersion [31, 32]. Moreover, AC possesses a graphite-like layer
64 crystallite structure and flourishing hole structure, leading to high adsorption ability
65 via π-π stacking interactions and thus facilitating the interface reaction with organic
66 compounds, which could enhance the catalytic efficiency [33-35]. Therefore, AC can
67 be considered as a promising, suitable and novel support, particularly, in catalytic
68 applications.

69 To date, AC has been used as a carrier for supporting CuO-CeO_2, MnO_x-CeO_2
70 mixed oxides for fuel gas desulfurization, denitrification and mercury removal [31,
71 36-38]. However, to the best of our knowledge, few papers thus far have reported on
72 the utilization of MNPs decorated on AC and on their application of catalytic activity
73 for organic transformation in wastewater treatment. In this regard, ideas of Au NPs
74 supported on AC for the application in catalytic reaction of organic compounds are
75 encouraged. The presence of abundant amount of oxygen-containing groups and

thiol group endows its hydrophilic character and provides sufficient reactive sites for Au NPs anchoring, which is beneficial for catalytic reaction [28, 39]. And, the good conductivity of AC can favor the electron transfer between Au NPs and AC [28]. It is well documented that electron transfer effect can conduce to negative shift in Fermi level of Au [16]. What's more, the utilization of AC as supports can expand its application in wastewater treatment in view of low cost of AC. On one hand, AC is able to prevent Au NPs from aggregation, warranting high catalytic activity. On the other hand, the synergistic effects between decorated Au NPs and AC were supposed to play the vital role in enhancing catalytic activity. Hence, using AC as a support for Au NPs anchoring seems to be a potential approach to fabricate a novel catalyst with enhanced catalytic activity for organic transformation in wastewater treatment.

Herein, taking full advantage of AC, we prepared Au/AC catalysts via a facile and one step method employed ascorbic acid as a mild reducing agent. The Au/AC catalysts were characterized by XRD, TEM, FTIR and XPS. The catalytic performance of Au/AC was investigated in the reduction of 4-NP in the presence of $NaBH_4$, with the rate constant evaluated in accordance with pseudo-first-order kinetic reaction under different Au loading amounts, catalyst dosage and $NaBH_4$ concentration. Besides, Au/AC was tested for the reduction of other nitrophenols such as 2-nitrophenol (2-NP), 2, 4-dinitrophenol (2, 4-DNP) and reductive degradation of azo dyes, including congo red (CR), methly orange (MO) and erichrome black T (EBT). The reusability of catalysts was tested up to six cycle run in the catalytic reduction of 4-NP. In addition, the feasible mechanism was discussed

for the catalytic reduction of nitrophenols.

2. Experimental

2.1 Materials

Virgin activated coke (AC) used in the experiment is commercial cokes from Clear Science Technology Co., Ltd. (Shanghai, China). AC was washed with ultrapure water for several times and dried 12 h at 60°C in an vacuum oven before grated with ball mill and sieved to 200 mesh size for further use. Hydrogen tetrachloroaurate hydrate ($HAuCl_4 \cdot 4H_2O$), sodium borohydride ($NaBH_4$), ascorbic acid (AA), 2-nitrophenol (2-NP), 4-nitrophenol (4-NP), 2,4-dinitrophenol (2,4-DNP), Methyl orange (MO) were purchased from Sinopharm Chemistry Reagent Co., Ltd. (Beijing, China). Congo red (CR) was purchased from Yuanhang chemical plant (Shanghai, China). Erichrome black T (EBT) was obtained from Shanpu Chemistry Reagent Co., Ltd. (Shanghai, China). All chemicals were of analytic reagent grade and used without further purification.

2.2 Preparation of Au/AC

Au/AC catalysts with different Au loading amount (1, 2, 3 mL of 1 wt% $HAuCl_4 \cdot 4H_2O$) were synthesized by a facile one-step method and labeled as Au/AC-x (x=1, 2, 3), respectively. For the typical synthesis of Au/AC-1, 0.4 g of AC was added to 200 mL of ultrapure water under ultrasonicating for 0.5 h to obtain AC suspension. Then, 1 mL of $HAuCl_4 \cdot 4H_2O$ (24.28 mM) was added with stirring for 0.5 h. After that, 10 mL of ascorbic acid (0.1 M) was injected drop by drop into the above solution under stirring. Further, the reaction mixture was allowed for stirring

for 24 h under ambient environment. The resulting black products were collected by filtration and washed with ultrapure water for several times, and then dried overnight at 35°C in vacuum oven for further use. Similar synthetic procedure was applied for preparation of Au/AC-2 and Au/AC-3 catalysts with different Au loading amount.

2.3 Catalytic reduction of nitrophenols and azo dyes

The catalytic activity of as-prepared catalyst Au/AC for nitrophenols reduction in the presence of excess sodium borohydride was studied by UV-Vis spectrophotometer in a 3 mL quartz cuvette. In a typical procedure, 30 mL of 4-NP aqueous solution (0.2 mM) was taken in a cuvette followed by adding 15 mL of freshly-prepared $NaBH_4$ solution (0.1 M). Then, 9 mg of catalyst was added into the cuvette. 3 mL aliquots were collected followed by the solid-liquid separation, then the absorbance of samples was immediately monitored at different time intervals using a UV-Vis spectrophotometer in a scanning range of 200 - 800 nm. In addition, the catalytic reduction of 2-NP and 2, 4-DNP were carried out following the same procedure. The similar procedure was applied for examining the performance on catalytic degradation of azo dyes (CR, MO and EBT). All the experiments were carried out under ambient experiment. The reusability of catalyst was examined via Au/AC separated by centrifugation after completely catalytic reduction of 4-NP in the first run.

2.4 Characterizations

UV-Vis spectrophotometer was recorded from 200 to 800 nm on a UV-2700 spectrophotometer (SHIMADZU (JAPAN) Co., Ltd.). The X-Ray diffraction (XRD)

patterns were collected using a XRD-6100 powder diffractometer (SHIMADZU (JAPAN) Co., Ltd.). Transmission electron microscopy (TEM) and high-resolution TEM (HRTEM) were carried out using a transmission electron microscope Tecnai G2 F20 (FEI USA), attached with selected area electron diffraction (SAED) to observe the morphology and composition of the samples. Scanning transmission electron microscope with high-angle annular dark-field detector (HAADF-STEM) was used to record the elemental mappings. Fourier transform infrared spectroscopy (FT-IR) studies were conducted using FTIR-8400 S IRprestige-21 (SHIMADZU (JAPAN) Co., Ltd.), recorded from 4000 - 400 cm^{-1-} at a resolution of 2 cm^{-1}. The X-ray photoelectron spectroscopy (XPS) measurements were performed on K-Alpha 1063 spectrometer (Thermo Fisher Scientific, UK). The Au loading amount was determined by inductively coupled plasma atomic emission spectrometry (ICP-OES, Perkin-Elmer Optima 5300DV, USA).

3. Results and discussion

3.1 Characterization of Au/AC catalyst

The XRD measurements were conducted to identify the phase purity and crystallite structure of virgin AC and as-prepared catalysts. As shown in Fig. 1, the characteristic diffraction peaks of AC appeared at 2θ = 26.66°, indicating AC possesses a graphite-like layer crystallite structure with hexagonal lattice [30]. The peak intensity at 26.66° decreased with increase of AC loading amount. The increase of Au loading amount may occupy more grain boundaries and affected the interplanar spacing of AC [31, 40], thus leading to a decrease of crystalline quality

of AC. The above results could also be inferred that the interaction may exist between Au and AC, as demonstrated as follows in TEM, FTIR and XPS. What's more, the peak at nearly 29.4° corresponding to AC was also detected over virgin AC. Interestingly, compared with the virgin AC, the peak at 29.4° disappeared in XRD pattern of AC that reacted with AA only. This indicates the synthesis process has an influence on the crystallinity of activated coke. As reported by Costanzo et al., the oxidation or reduction of ascorbic acid would affect the hydrogen bonding of hydrogen and oxygen atom [41, 42], thus resulting in a decrease of crystalline quality of AC. Besides, the minor peaks at 20.8°, 38.9° and 50.83° were ascribed to the presence of trace quantity of silica, aluminum and calcium as shown in Fig. S1B, which was corresponding with previous report that these elements were inert for the catalytic reaction [43]. In each pattern of catalyst with different Au loading amount, the crystallite structure of Au NPs was confirmed by the presence of diffraction peaks at 38.18°, 44.38°, 64.52°, and 77.54°, corresponding to the diffraction of the (111), (200), (220) and (311) lattice plane for Au(0) crystals, respectively (JCPDS NO. 04-0784). The XRD patterns of catalysts matched the face-centered-cubic (fcc) nature of Au NPs [16]. With the increment of Au loading amounts, the intensity of scattering peaks heightened, which could be attributed to the growth and formation of larger Au NPs as the Au loading amounts increasing [16].

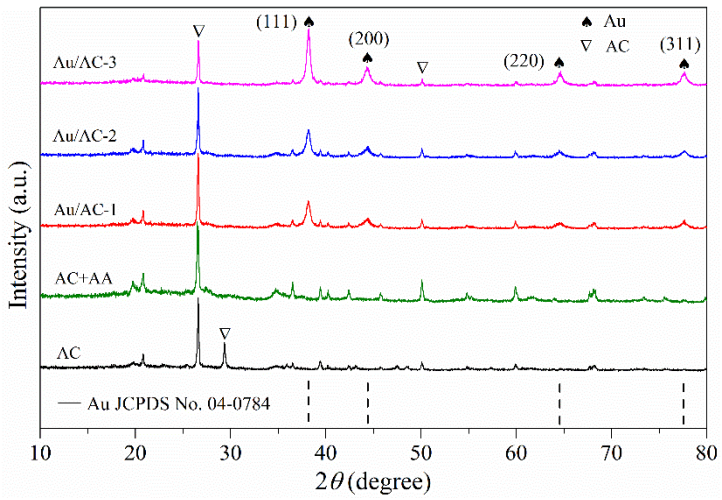

Fig. 1. X-ray diffraction patterns of virgin AC and Au/AC catalysts with different Au content.

In order to study the morphology and microstructure of the virgin AC and obtained Au/AC, TEM measurements were performed (Fig. 2). By the morphology image of virgin AC as indicated in Fig. 2A, it is clear that virgin AC contains some wrinkles composed by some thin layers with relatively smooth and planar surfaces. As revealed from Fig. 2B, the Au NPs were dispersed uniformly on the stacking AC layers. From Fig. 2C and 2D, it could be observed that Au NPs with a size smaller than 5 nm existed in AC with interplanar spacing of 0.235 nm corresponding to the (111) crystal planes. This was because the pore structure of AC restricted the growing of Au NPs adsorbed into the AC. As shown in Fig. 2E, HRTEM image reveals distinct lattice fringes with an interplanar spacing measured to be 0.235 nm and 0.205 nm, corresponding to the (111) and (200) crystal planes of fcc Au, respectively. Moreover, the SAED pattern was inserted in Fig. 2E, displaying the characteristic rings for the (111), (200), (220) and (311) planes of fcc Au. Both results confirm the polycrystalline structure of Au NPs supported on AC and are in

good accordance with the XRD results. Besides, the SEM images of Au/AC-3 in Fig. S2A further displayed that there were Au NPs dispersed on the surface of AC. Base on the Fig. 2C, Fig. 2D, Fig. S2B and Fig. S2C, the particle size of Au NPs supported on AC was counted for at least 200 nanoparticles, which would make the size distributions more representative and accurate. Fig. 2F shows the presence of dispersed Au NPs with a diameter of 14.9 ± 10.8 nm. In addition, to further confirm the elemental distribution and chemical composition of Au/AC-3, HAADF-STEM image and EDS spectrum were carried out (Fig. S1). The HAADF-STEM image shows a clear luminance of Au NPs, revealing homogenous distribution of Au NPs on AC. The presence of Au element confirmed the synthesis of Au NPs. These TEM images further indicate the successful preparation of Au NPs supported on AC as well, and illustrate Au NPs dispersed well on AC surface.

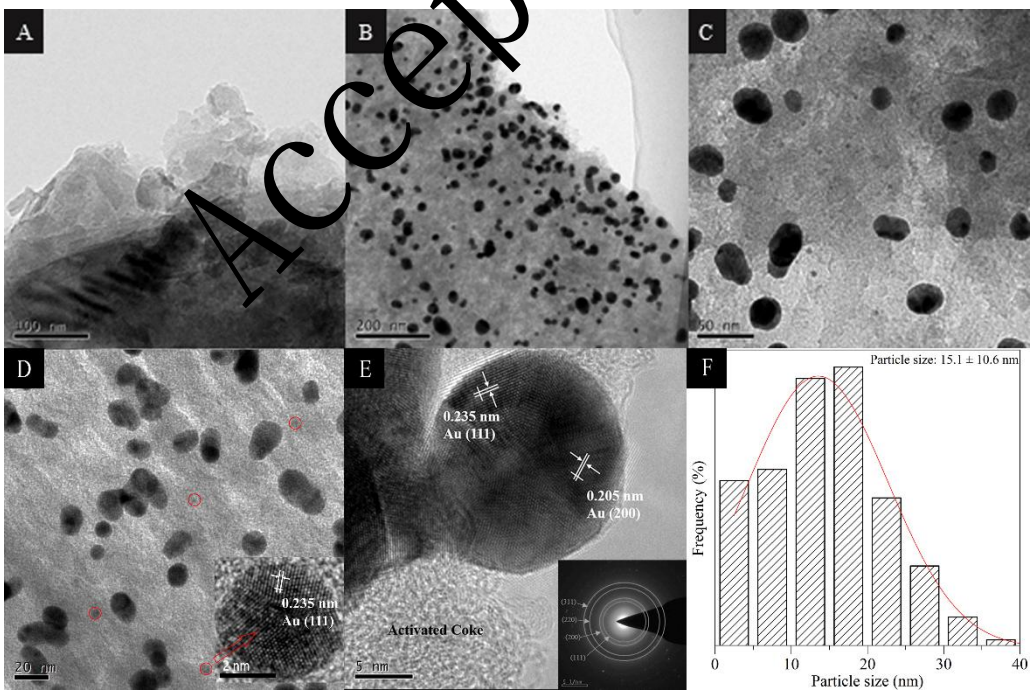

Fig. 2. TEM images of virgin AC (A) and the Au/AC-3 catalyst (B, C and D) (the inset is HRTEM image of the tiny NPs); HRTEM image (E) of Au/AC-3 catalyst (the

inset is SAED pattern); Size distribution of Au NPs (F).

FTIR measurements were performed to further obtain valid information of functional group about virgin AC and Au/AC-3 catalyst. In the region of 3600-3200 cm^{-1}, the most pronounced broad and intense band around 3421 cm^{-1} was due to the overlapping of –OH as exhibited in the FTIR spectrum of activated carbon or a displaced amino group [38, 44]. And the band located at 2362 cm^{-1} was assigned to the vibration of C=O [45]. The peaks at 1635 and 1445 cm^{-1} corresponded to the skeletal vibrations stretching of aromatic C=C [19]. The peak at 1037 cm^{-1} represented a stretching vibration of C-O or primary alcohols[46]. In addition, the peaks at 670-872 cm^{-1} represented out of plane bending vibrations of the C-H bonds [38]. It can be seen from the FTIR spectrum of Au/AC-3 that after the deposition with Au NPs on AC, some adsorption peaks drifted, appeared and disappeared. The attenuated peaks at 3421 and 1445 cm^{-1} indicated that the amount of O-H bonds decreased after active sites of AC were occupied by Au NPs. In addition, the shift of the band at 2626, 2362 and 1635 cm^{-1} may be accounted for the interaction of Au NPs with hydroxyl groups of AC [47]. The gradual variation in this band region of 900-700 cm^{-1} was owing to Au-O bonds stretching vibration. These variation and vibration indicated the reduction of oxygen-containing groups [48]. However, on account of the weak dipoles exhibited by S-H groups, the thiol group in FTIR is invisible under current conditions [49]. Fig. 3 indicates that the surface functional groups in AC contain oxygen-containing functional groups such as hydroxyl and carboxyl, possessing hydrophilic property in solvents which may favor catalytic

reaction [39, 50].

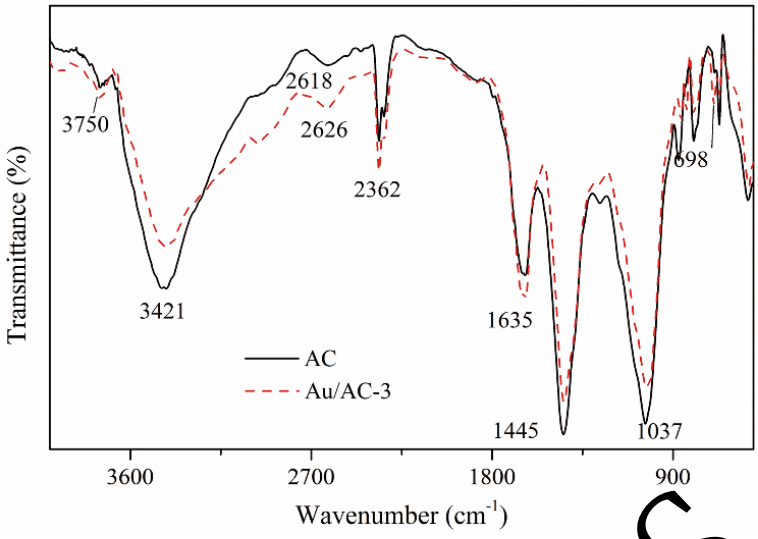

Fig. 3. FTIR spectra of AC and Au/AC-3 catalyst.

The XPS was employed to further analyze the composition and surface-functional groups of prepared catalysts. As shown in Fig. 4A, the binding energies (BE) of about 530, 284 and 163 eV indexed to O 1s, C 1s and S 2p, respectively. As shown in Fig. 4B, in the high-resolution XPS spectrum of Au 4f region, the peaks of Au $4f_{7/2}$ an Au $4f_{5/2}$ peaks were observed at 84.2 and 87.9 eV respectively, with a gap of 3.7 eV between two peaks [51]. It should be noted that the typical characteristic peaks of Au(III) were absent in the spectrum, illustrating the almost completed reduction of the small amount of Au(III) to Au(0) in the reaction system [51]. The O 1s spectra of Au/AC-3 and AC are shown in Fig. 4C. The photoelectron line of about 531.8 and 532.9 eV were attributed to oxygen in carboxylate/carbonyl (O-C=O/C=O) and in the epoxy/hydroxyl (C-OH) of the AC [52, 53]. It has been found that the shifting BE of O 1s ascribed to O-C=O/C=O and C-OH were occupied by Au NPs, revealing the oxygenated functional group like hydroxyl were reduced during the preparation of catalysts, and Au NPs occupied the sites of these functional groups

[54]. The claim was further verified by the C 1s spectra of Au/AC-3 and AC in Fig. 4D. The C 1s spectra could be deconvoluted into five components corresponding to sp^2 carbon (284.6 eV), -CONH (285.1 eV), C-O-C (286.6 eV), C=O (287.7 eV) and O-C=O (288.8 eV) [28, 46, 54, 55]. They were attributed to the presence of carboxylate, carbonyl and hydroxyl functional groups of AC. Obviously, after AC loaded with Au NPs, the peak intensity of oxygenated functional groups (C-C, C=O) decreased (Table S1), which was assigned to the formation of Au NPs on these functional groups [48]. The peak of C-O-C showed a slight shift compared with the virgin AC, owing to the galvanic displacement reaction between catechol groups and Au NPs [56]. Thus, the XPS measurements validate the presence of sulfur-containing and oxygen-containing groups in AC surface.

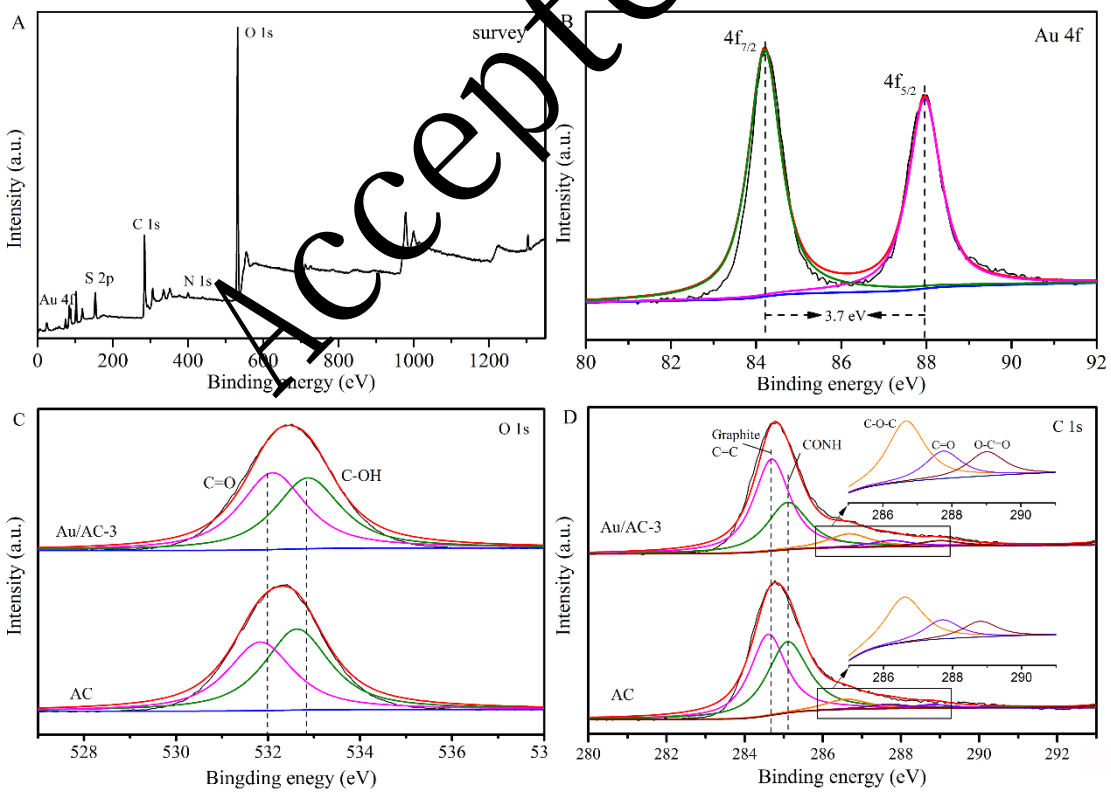

Fig. 4. XPS survey spectra (A) of Au/AC-3 catalyst; High-resolution XPS spectra of Au 4f (B), O1s (C) and C 1s (D) of Au/AC-3 and AC.

3.2 Catalytic reduction studies of nitrophenols

Before checking out the catalytic nature of synthesized catalysts Au/AC, it has to check whether self-hydrolysis of $NaBH_4$ reduces the 4-NP and the support material AC catalyzes the reduction of 4-NP. For these reason, two control experiments were performed in which the reductions of 4-NP were investigated in the presence of $NaBH_4$ and AC+$NaBH_4$. After the additional of $NaBH_4$ in the 4-NP, the color of the mixture aqueous turned to bright yellow rapidly, indicating the 4-NP was converted into nitrophenolate anion ($C_6H_4NO_3^-$). As shown in Fig. S3, the initial maximum absorbance at 400 nm indexed to the 4-NP in the natural and alkaline conditions. The maximum absorbance peak of the mixture solution centered at 400 nm over reaction time within 20 min in the absence of catalyst wherein excess $NaBH_4$ was used exclusively, indicating the reduction does not occur by the self-hydrolysis of $NaBH_4$ [57]. This can be ascribed to that there is a kinetic negative barrier and mutual repulsion between BH_4^- and 4-NP [58]. On the other hand, the absorbance peak at 400 nm also decreased slightly within 20 minutes but no peak appeared at 298 nm in the control experiment in the presence of virgin AC + $NaBH_4$, indicating the catalytic reaction did not proceed at all and AC has adsorption ability towards 4-NP. Nevertheless, it should be point out the adsorption efficiency is modest. Thus, the adsorption effects of AC towards nitrophenols can be ignored.

In order to study the catalytic performance of synthesized catalyst, catalytic reduction of 4-nitreophenol in the presence of excess sodium borohydride was carried out. The convincing evidence for reduction of 4-NP came from

time-dependent UV-Vis absorption spectra. Fig. 5A provides time-dependent UV-Vis absorption spectra of 4-NP catalyzed by 9 mg of Au/AC-3. The absorbance peak at 400 nm quickly decreased and disappeared within 20 s. Simultaneously, a new peak appeared at 298 nm, accompanied with an increase intensity of the peak over reaction time, which was assigned to the formation of 4-aminophenol. In order to confirm the product, the determination of 4-AP was recorded with UV-Vis absorbance spectra (Fig. 5B). Moreover, the isosbestic points at 313 nm also provided evidence to the catalytic reduction of 4-NP yields 4-AP without any byproduct [59]. As the initial concentration of $NaBH_4$ (0.1 M) was excess with respect to the concentration of 4-NP (0.2 mM), the reduction can be treated as pseudo-first-kinetic. The reduction rate of 4-nitrophenol was calculated using the following equation:

$$-\ln(C_t/C_0) = -\ln(A_t/A_0) = k_{app}$$

wherein C_t is 4-NP concentration at reaction time *t*, and C_0 is the initial concentration of 4-NP, and the rate constant k_{app} is the first order constant, determined by a liner plot of $\ln(C_t/C_0)$ versus reaction time. Liner relationships between $\ln(C_t/C_0)$ and reaction time t was shown in Fig. 5A, and the rate constant k_{app} was calculated as 0.1916 s^{-1} for the reaction. As presented in Table 1, it is obvious that the catalytic performance of Au/AC-3 was comparable or even superior when compared with other Au-based catalysts supported by other materials. It is well documented that the high catalytic activity of Au NPs is owing to their highly dispersed and nanosized properties, which is corresponding to the above characterization of Au/AC. In the

cases of other loading amounts of the Au catalysts, the catalytic reduction of 4-NP was performed under similar conditions. The catalytic reduction of 4-NP completed within 50 s, 30 s and 20 s, respectively. For apparent comparison of rate constant k_{app} of different Au loading amounts catalysts, the C/C_0 and ln (C/C_0) versus reaction time were plotted in Fig. 6A and 6B. The rate constant k_{app} was 0.0737, 0.1347, and 0.1916 s^{-1}, respectively. As expected, the rate constant k_{app} was proportional to the concentration of the $HAuCl_4$ solutions, indicating that the catalytic efficiency increased with the increased loading amounts of Au NPs on AC. It is obviously shown in Fig. S4 that with the lower Au loading amounts, the sparse distribution of Au NPs resulted in the low catalytic activity. In Au/AC-3 catalyst, Au NPs were well dispersed on AC, with the better surface morphology, which relates to the higher catalytic activity. This result is in well consistent with previous studies, demonstrating that the catalytic activity is proportional to the quantity of nanoparticles [60]. Furthermore, the Au content determined by ICP-OES was about 1.37 wt%, 2.45 wt% and 3.49 wt%, corresponding to Au/AC-1, Au/AC-2 and Au/AC-3, respectively. According to the previous research, the turn-over frequency (TOF: moles of 4-NP reduced by per gram of Au NPs per second) has been calculated to estimate the catalytic efficiency of catalysts in our research [61, 62]. TOF was calculated to be 0.287, 0.268 and 0.282 $mol \cdot g^{-1} \cdot s^{-1}$, for the case of Au/AC-1, Au/AC-2 and Au/AC-3, respectively. It is higher than those of Au NPs catalysts recently reported. Thus we have a workable and efficient Au/AC catalyst with relatively high TOF, which is important to the value of a catalyst in industrial

334 applications.

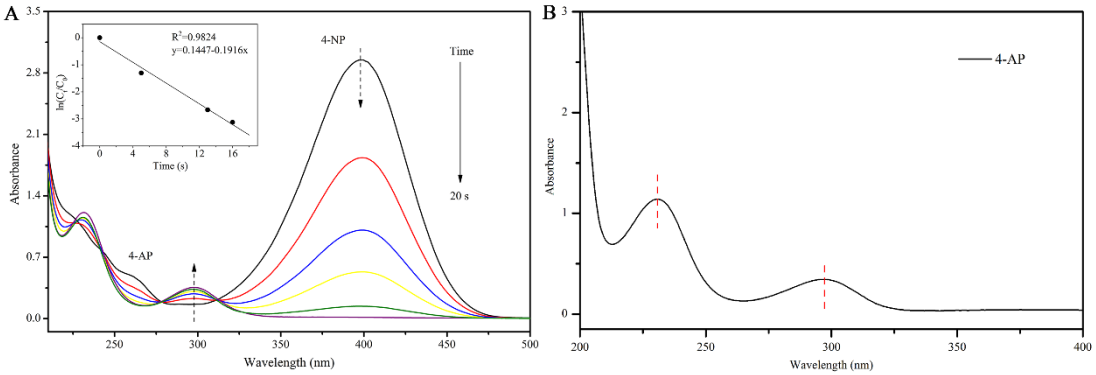

335

336 **Fig. 5.** Time-dependent UV-Vis absorption spectra of the reduction of 4-NP

337 catalyzed by Au/AC-3 (A) and plot of ln(C/C$_0$) versus the reaction time (B).

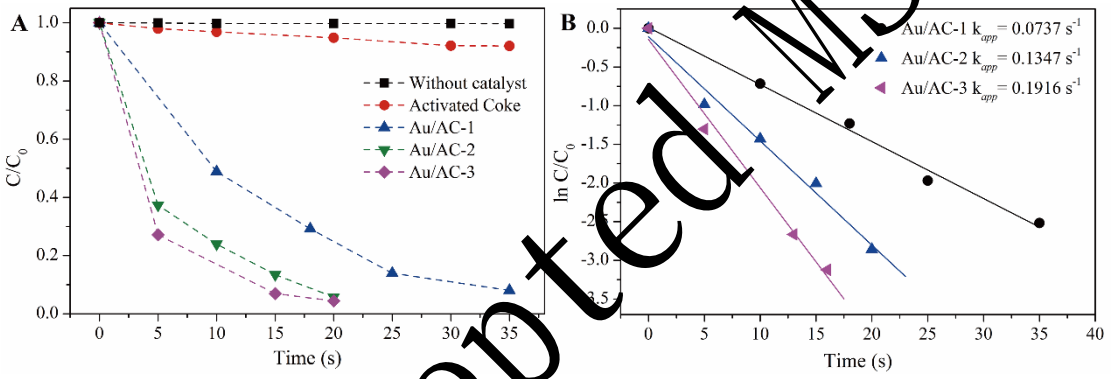

338

339 **Fig. 6.** C$_t$/C$_0$ (A) and ln(C$_t$/C$_0$) (B) versus the reaction time for the reduction of 4-NP

340 catalyzed by different Au loading amounts catalysts, respectively.

341 **Table 1** Compaision of the catalytic performances of Au/AC with the reported

342 AuNPs catalysts supported on orther materials for the reduction of 4-NP.

Catalysts	Supported materials	Catalyst dosage (mg)	Time (s)	k_{app} (10^{-3} s^{-1})	k_{nor} (s^{-1} g^{-1})	Ref
Au/AC[a]	Activated coke	9	20	191.6	21.3	This work
Au_3-Cu_1/rGO[b]	Graphene Oxide	0.1	30	96	960	[63]
Ag-Au-rGO[b]	Reduced grapheme oxide	0.1	360	3.47	34.7	[6]

Au/GO[c]	Graphene Oxide	-	45	107.97	-	[64]
GO-Fe_3O_4[d]-Au NPs	Graphene Oxide	0.02	100	0.322	16.1	[19]
Au@CMK-3-O[e]	Mesoporous carbon	75	300	7.75	0.103	[65]
Au/g-C_3N_4[f]	g-C_3N_4	1	600	5.936	5.936	[16]
CNFs[g]@Au core–shell network	Carbon nanofibers	0.1	300	5.42	54.2	[66]
Au@PZS@CNTs[h]	Carbon nanotubes	0.3	960	1.78	5.93	[67]
AuNPs/Chitosan	Chitosan	50	67	0.561	0.011	[61]
Au/MgO[i]	magnesium oxide	15	150	7.6	0.507	[68]

[a] AC, activated carbon. [b] rGO, reduced graphene oxide. [c] GO, graphene oxide. [d] GO-Fe_3O_4, graphene oxide–Fe_3O_4 nanocomposite. [e] CMK-3-O, oxidized mesoporous carbon. [f] g-C_3N_4, Graphitic carbon nitride. [g] CNFs, carbon nanofibers. [h] PZS@CNTs, polyphosphazene functionalized carbon nanotubes. [i] MgO, magnesium oxide. k_{nor}, the rate constant normalized with the catalyst dosage (k_{app}/the mass of catalyst, s^{-1} g^{-1})

According to the Sabatier principle, the interaction between substrate and catalyst should be optimum with regard to the higher catalytic activity [69]. Thus, the effect of the catalyst dosage on the reduction of 4-NP was also investigated under identical conditions. It can be seen from Fig. 7A, the rate constant k_{app} increased intensively with the catalyst dosage increasing until the catalyst dosage was 9 mg. This can be ascribed to the more availability site of active catalytic surfaces with the increase in catalyst dosage [70]. However, the rate constant k_{app} increased slowly as the catalyst dosage increased from 9 to 12 mg. When the dosage was over 9 mg and reached 12 mg, the increasing amount of rate constant k_{app} was very small, from 0.1916 to

358 0.2210 s^{-1}. This could be ascribed to that the reactants were saturated that even more
359 availability sites of active catalytic surfaces could not further enhance the reaction
360 rate at the same initial concentration of 4-NP [71]. For the balance of the highest rate
361 and minimum catalyst dosage in the concept of economic friendly, the catalyst
362 dosage of 9 mg was used with the current experimental conditions. Moreover, the
363 study of the optimization of the $NaBH_4$ concentration was also investigated. With the
364 initial $NaBH_4$ concentration increasing, the concentration of nitrophenolate anion
365 increased (Fig. S5). Similarly, the catalytic efficiency of Au/AC catalysts tends to
366 increase upon addition of more $NaBH_4$. Fig. 7B shows that the rate constant k_{app}
367 increased intensively by increasing the $NaBH_4$ concentration, and increased slowly
368 after the $NaBH_4$ concentration of 0.10 M. Therefore, the optimum $NaBH_4$
369 concentration was 0.10 M for the catalytic reduction in the study.

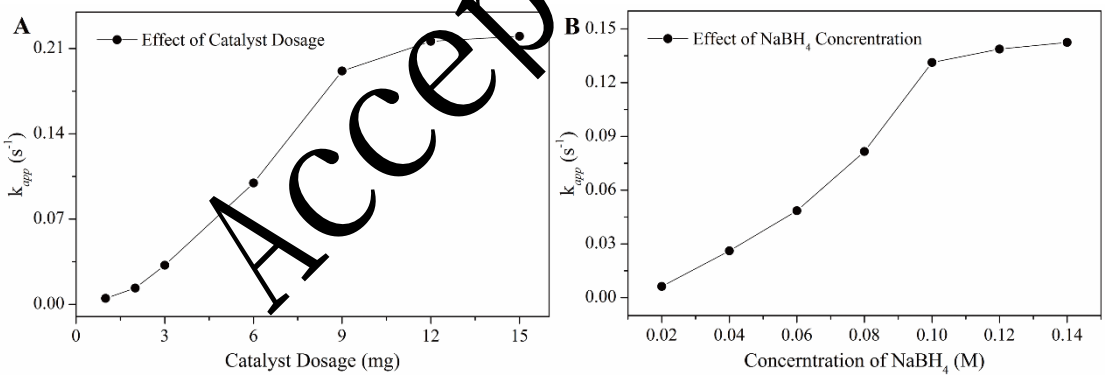

370

371 **Fig. 7.** The effect of catalyst dosage (A) and $NaBH_4$ concentration (B) on the
372 catalytic reduction of 4-NP catalyzed by Au/AC-3.

373 Furthermore, the catalytic reduction of other nitrophenols (2-NP and 2, 4-DNP)
374 was investigated to confirm the catalytic activity. The time-dependent UV-Vis
375 absorption spectra of 2-NP and 2, 4-DNP is presented in Fig. 8A and 8B. In natural
376 and alkaline conditions, the distinct bands of 2-NP and 2, 4-DNP were 415 and 359

377 nm, respectively [72]. Then, the intensity of their absorbance peak gradually
378 decreased within 40 s and 50 s, accompanied with decolorization upon the additional
379 of Au/AC-3 catalysts. As shown in Fig. 8C, we found that Au/AC-3 exhibited high
380 catalytic activity with excellent yields towards other nitrophenols regardless of the
381 position of the substituents. When the reduction of 4-NP, 2-NP and 2, 4-DNP was
382 catalyzed by Au/AC-3, the rate constant k_{app} was 0.1916, 0.1399 and 0.1229 s^{-1},
383 respectively. It can be conclude that the catalytic activity of reduction of 4-NP
384 showed a better activity than that of 2-NP and 2,4-DNP, which may related to the
385 substituent positions [73]. Nonetheless, the Au/AC catalyst exhibits magnificent
386 catalytic activity towards various nitrophenols.

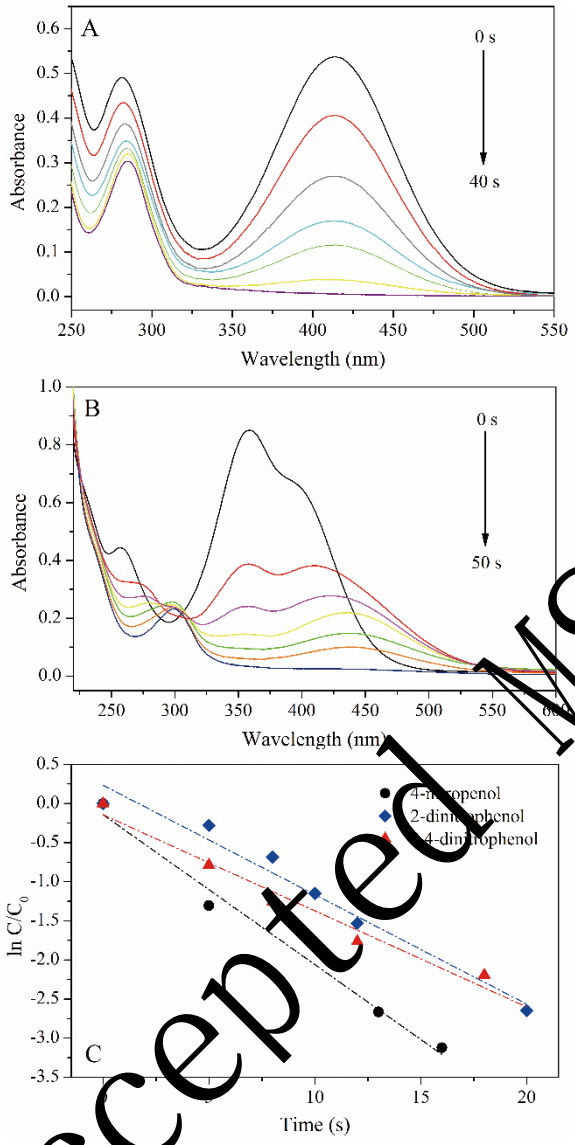

Fig. 8. Time-dependent UV-Vis absorption spectra of the reduction of 2-NP (A) and 2, 4-DNP (B) and $\ln(C_t/C_0)$ versus the reaction time (C) for the reduction of 4-NP, 2-NP and 2,4-DNP catalyzed by Au/AC-3, respectively.

The reusability of the catalyst was also investigated with the reduction of 4-NP. After completely catalytic reduction of 4-NP in the first run, the Au/AC could be easily separated by centrifugation from reaction solution, and then washed three times and dried for the further use in next cycle of the reduction of 4-NP. As shown in Fig. 9, the conversion of 4-NP to 4-AP was 84% in 20 s after six cycles. Thus, the

Au/AC still exhibited good catalytic activity after six cycles without significant loss of active sites, owing to the supporting effect of AC. It should be noted that although novel catalyst with superior catalytic performance has been developed, the method for addressing the problem of weight loss after each cycles and higher catalytic activity should be focused on further study. Hence, more experiments will be carried out to address above issues in our further research.

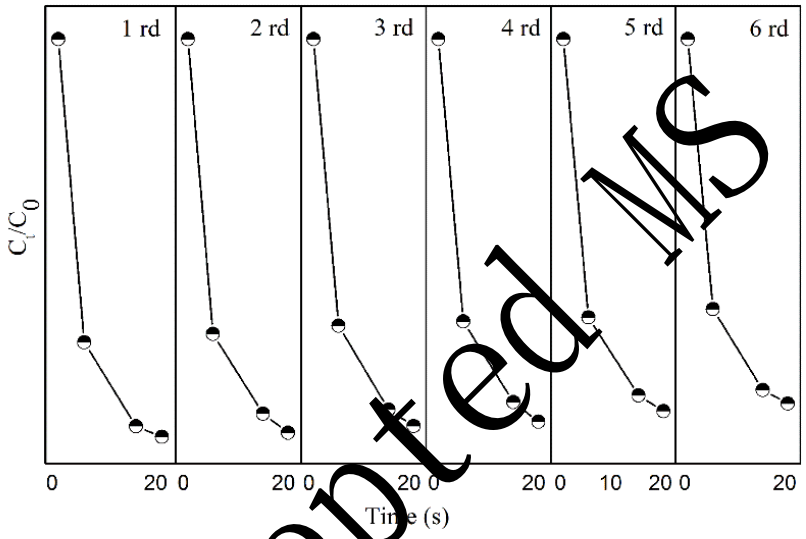

Fig. 9. Six cycling reduction curves of 4-NP catalyzed by Au/AC-3 in the presence of $NaBH_4$.

3.3 Feasible mechanism for reduction of nitrophenols

It has been widely accepted that the catalytic reduction of nitrophenols in the presence of $NaBH_4$ obeys the classical Langmuir-Hinshelwood model on account of the surface catalysis of catalytic reduction reactions [74]. Based on the experimental data, a feasible mechanism for the reduction of nitrophenols catalyzed by Au/AC was proposed in Scheme 1: (i) BH_4^- is adsorbed on to the catalytic surface, then generating BO_2- by the self-hydrolysis of $NaBH_4$. Meanwhile, BH_4^- reacts with Au NPs, transferring active hydrogen species to form the active surface-hydrogen Au-H

[69, 75]. (ii) From Fig. 5, it can be speculated that there is an induce time for 4-NP adsorption, which is in good agreement with the results that the concentration of 4-NP decreased at the initial but the concentration of 4-AP was no significant increase. Thus, 4-NP would adhere reversibly to the surface of Au/AC owing to the adsorption of AC [75]. Simultaneously, the active surface-hydrogen transfers to the nitro groups $–NO_2$, attacking $–NO_2$ to reduce to form corresponding amino groups with the electron transferring from BH_4^- to $–NO_2$ [19]. It has been reported that the catalytic reduction is owing to electron transfer between the $NaBH_4$ and the $–NO_2$ when there is direct contact between the Au NPs and $–NO_2$ [19, 76]. (iii) The generated aminophenol compounds were desorbed from the surface of Au/AC.

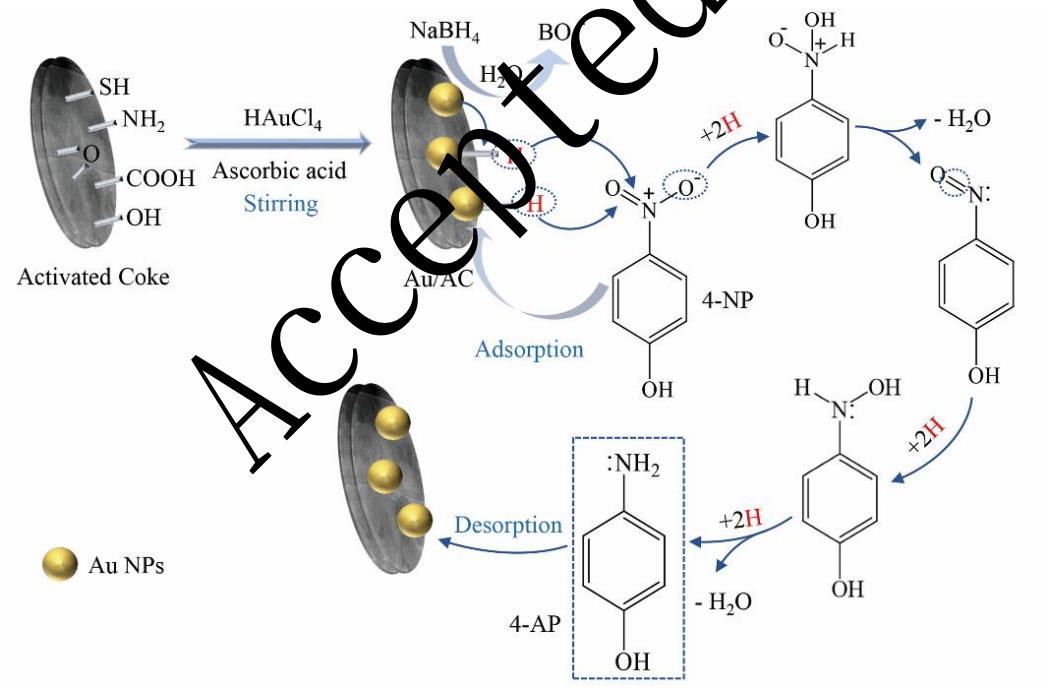

Scheme 1. Possible mechanism of catalyst preparation and catalytic reduction of 4-NP.

In summary, it can be concluded that Au/AC exhibits high catalytic activity towards the reduction of nitrophenols, which can be postulated that such high

catalytic activity of Au/AC is ascribed to these factors: (1) It has been well documented that Au NPs can be easily bonded to the sulfur atom on the surface of AC [49], guaranteeing the relative tightly combination of Au NPs and AC. Besides, with electron-rich feature of other abundant oxygen-containing groups, the AC as support is in favor to anchor and disperse Au NPs firmly through complexing or electrostatic interaction, which is vital in using metal nanoparticles catalyst in organic transformation [28, 46, 64]. (2) AC can promote the adsorption of reactants, which provides a higher concentration of nitrophenols near to Au NPs on AC. This could provide more opportunity for nitrophenols molecules to expose onto active sites of the catalysts and thus accelerate the reaction kinetics [28, 64]. (3) AC possesses a graphite-like layer crystallite structure, which is beneficial for the adsorption of 4-NP via π-π stacking interactions. This can shorten the distance between 4-NP and Au NPs supported on AC. Besides, the electrical conductivity of AC is in favor of the electron transfer during reaction. (4) Previous research has shown that the high catalytic activity also can be attributed to the use of a weakly binding agent ascorbic acid in the synthesis and the large defect to volume ratio of the Au NPs [77, 78]. Furthermore, the nanosized Au NPs with a higher redox potential value, are beneficial for accelerating the electron transfer in the catalytic system and consequently lower the kinetic negative barrier for the reduction [61]. It is concluded that the well-dispersed and nanosized Au NPs, the synergistic effects of the good adsorption capacity and electrical conductivity of AC as well as large defect to volume ratio may be responsible for the high catalytic performance of the Au/AC

450 catalysts.

451 **3.4 Degradation of azo dyes**

452 Azo dyes, as a kind of toxic and hard-biodegraded industrial pollutant containing
453 one or more azo bonds (–N=N–), are hazardous to environment at low concentrations
454 and carcinogenic to human [79, 80]. Thus, we extended the Au/AC catalysts to
455 catalytic degradation of azo dyes to further investigate the catalytic performance of
456 Au/AC. In this study, three kinds of azo dyes including CR, EBT and MO have been
457 chosen as substrates. All the catalytic conditions of these azo dyes were same to that
458 of 4-NP and the convincing evidence for degradation of azo dyes came from
459 time-dependent UV-Vis absorption spectra.

460 As shown in Fig. S6, the initial maximum absorbance of CR, EBT and MO was at
461 495, 526 and 465 nm [81]. After the as-prepared Au/AC-3 was tried on CR, EBT and
462 MO adsorption, the characteristic peaks in the corresponding UV-Vis spectra of CR,
463 EBT and MO decreased within initial 15 min (Fig. S6A, Fig. S6C and Fig. S6E).
464 With continuously stirring for another 15 min, these solutions achieved the
465 adsorption equilibrium, with the adsorption efficiency of 30%, 35% and 12% for CR,
466 EBT and MO, respectively. Especially, the adsorption efficiency of MO by Au/AC-3
467 was 32% at first 15 min and then decreased to 12% until equilibrium was achieved.
468 Besides, the BET surface area (S_{BET}), pore volume, and average pore size of
469 Au/AC-3 were determined to be 21.383 $m^2 g^{-1}$, 0.0938 $cm^3 g^{-1}$ and 17.55 nm (Table
470 S2). It validates that Au/AC-3 possesses low adsorption ability [82].

471 Then, the reductant $NaBH_4$ was added to the above solution for triggering the

catalytic degradation. As we can see from Fig. S6B, the characteristic peaks at 344 and 495 nm ascribed to the CR decreased rapidly over reaction time. However, a new peak at 250 nm occurred with the decolorization of solutions within several seconds (Fig. S7). After reaction, there was almost no absorbance at 344 and 495 nm, and the absorbance at 250 nm was maximized, confirming that the removal of CR and the formation of intermediates were caused by catalytic degradation [83]. Similarly, the characteristic peaks of EBT and MO disappeared accompanied with the decolorization within several seconds after adding the Au/AC-3 catalysts (Fig. S7), while the new peaks at 240 and 258 nm were emerged corresponding to the produced intermediates of EBT and MO (Fig. S6D and Fig. S6E) [84, 85].

To sum up, the characteristic peaks of azo dyes decreased and the color of these solutions was decolorization during the reaction. Besides, new peaks were formed in the UV- range, suggesting azo dyes was indeed degraded, instead of just being absorbed by Au/AC-3 and the –N=N– bonds of azo dyes was broken down by Au/AC-3 [84]. The emerging absorption at about 250 nm appeared simultaneously with –N=N– cleavage, indicating that there were newly produced colorless compounds [71]. These peaks were originated from the absorption from aromatic intermediates, which may ascribed to the two sides of the cleavage azo bond or their derivatives, corresponding to the results in previous reports [83, 84]. Thus, the most of azo dyes were removed by the catalytic degradation by Au/AC-3. As is well-known, adsorption process can play a critical role on the removal of pollutants, including catalysis [19]. Compared with other study of catalytic degradation of azo

494 dyes, the reductive degradation efficiency of Au/AC catalyst is obviously superior to
495 that of other catalysts (Table S3). These results confirm the high reductive
496 degradation activity towards various azo dyes of our catalyst. However, as shown in
497 Fig. S8 the catalytic efficiency was different for the three azo dyes with the rate
498 constant k_{app} followed the order by MO (0.1863 s^{-1}) > EBT (0.1197 s^{-1}) > CR
499 (0.0692 s^{-1}), attributed to the molecular formula and size, as well as the electrical
500 feature of dyes [86]. The structural formulas of these dyes are given in Fig. S7, it can
501 be concluded that with the fewer azo bonds and simpler molecular, the azo dyes
502 could be degraded more easily. The structural formula of MO and EBT possesses
503 single azo bonds, while CR contains a couple of azo bonds, causing that MO was
504 reductive degraded more easily within 30 s. A speculated reason is that the less steric
505 hindrance of dyes with the simpler molecular structural and easier electrostatic
506 attraction between catalyst and dyes can promote these dyes to expose on the
507 catalytic active sites, thus accelerating the catalytic degradation [86].

508 **4. Conclusions**

509 In this study, a facile one-step method was developed to prepare a novel Au/AC
510 catalyst. Au NPs with a diameter of 16 ± 6 nm were supported on the surface of AC.
511 The Au/AC catalyst exhibited excellent catalytic performance for the reduction of
512 4-NP with the rate constant k_{app} of 0.1916 s^{-1}. The catalyst also manifested
513 remarkable catalytic activity for the reduction of other nitrophenols and degradation
514 of azo dyes. It was found that the catalytic performance was comparable or even
515 superior to that of some other Au-based catalyst. This could be attributed to the

abundant oxygen-containing functional groups and thiol groups on the surface of AC, promoting the Au NPs firmly anchored and dispersed on AC. The AC in this study is an excellent supporting material and beneficial for the catalytic reaction. In addition, the synergistic effect of nanosized Au NPs, the good adsorption capacity of AC and large defect to volume ratio could enhance the catalytic activity. The catalyst exhibited good stability and the catalytic performance remained 84% over six recycles. Considering the low cost of AC, facile preparation method and excellent catalytic performance, Au/AC catalysts seem to have potential to serve as an efficient catalyst for the reduction of nitrophenols and azo dyes as a pretreatment for wastewater treatment in diversified applications.

Conflicts of interest

There are no conflicts to declare.

Acknowledgements

This study was financially supported by the Program for the National Natural Science Foundation of China (51579098, 51879101, 51779090, 51709101, 51278176, 51408206, 51521006, 51809090, 51378190), Science and Technology Plan Project of Hunan Province (2018SK20410, 2017SK2243, 2016RS3026), the National Program for Support of Top-Notch Young Professionals of China (2014), the Program for New Century Excellent Talents in University (NCET-13-0186), the Program for Changjiang Scholars and Innovative Research Team in University (IRT-13R17), and the Fundamental Research Funds for the Central Universities (531109200027, 531107050978, 531107051080). Hunan Provincial Innovation

538 Foundation for Postgraduate.

References

[1] R. Ciriminna, E. Falletta, C. Della Pina, J.H. Teles, M. Pagliaro, Industrial Applications of Gold Catalysis, Angewandte Chemie International Edition, 55 (2016) 14210-14217.

[2] H. Mou, C. Song, Y. Zhou, B. Zhang, D. Wang, Design and synthesis of porous Ag/ZnO nanosheets assemblies as super photocatalysts for enhanced visible-light degradation of 4-nitrophenol and hydrogen evolution, Applied Catalysis B: Environmental, 221 (2018) 565-573.

[3] C. Lai, X. Liu, L. Qin, C. Zhang, G. Zeng, D. Huang, M. Cheng, P. Xu, H. Yi, D. Huang, Chitosan-wrapped gold nanoparticles for hydrogen-bonding recognition and colorimetric determination of the antibiotic kanamycin, Microchimica Acta, 184 (2017) 2097-2105.

[4] P. Xu, G.M. Zeng, D.L. Huang, C.L. Feng, S. Hu, M.H. Zhao, C. Lai, Z. Wei, C. Huang, G.X. Xie, Z.F. Liu, Use of iron oxide nanomaterials in wastewater treatment: A review, Science of The Total Environment, 424 (2012) 1-10.

[5] O. Ramirez, S. Bonardd, C. Saldias, D. Radic, A. Leiva, Biobased Chitosan Nanocomposite Films Containing Gold Nanoparticles: Obtainment, Characterization, and Catalytic Activity Assessment, ACS applied materials & interfaces, 9 (2017) 16561-16570.

[6] H. K, R.P. Joshi, S. D.V, V.N. Bhoraskar, S.D. Dhole, Anchoring of Ag-Au alloy nanoparticles on reduced graphene oxide sheets for the reduction of 4-nitrophenol, Applied Surface Science, 389 (2016) 1050-1055.

[7] A. Balanta, C. Godard, C. Claver, Pd nanoparticles for C–C coupling reactions, Chemical Society Reviews, 40 (2011) 4973-4985.

[8] L. Qin, G. Zeng, C. Lai, D. Huang, P. Xu, C. Zhang, M. Cheng, X. Liu, S. Liu, B. Li, H. Yi, "Gold rush" in modern science: Fabrication strategies and typical advanced applications of gold nanoparticles in sensing, Coordination Chemistry Reviews, 359 (2018) 1-31.

[9] X. Ren, G. Zeng, L. Tang, J. Wang, J. Wan, Y. Liu, J. Yu, H. Yi, S. Ye, R. Deng, Sorption, transport and biodegradation – An insight into bioavailability of persistent organic pollutants in soil, Science of The Total Environment, 610-611 (2018) 1154-1163.

[10] C. Zhang, C. Lai, G. Zeng, D. Huang, C. Yang, Y. Wang, Y. Zhou, M. Cheng, Efficacy of carbonaceous nanocomposites for sorbing ionizable antibiotic sulfamethazine from aqueous solution, Water Research, 95 (2016) 103-112.

[11] F. Long, J.-L. Gong, G.-M. Zeng, L. Chen, X.-Y. Wang, J.-H. Deng, Q.-Y. Niu, H.-Y. Zhang, X.-R. Zhang, Removal of phosphate from aqueous solution by magnetic Fe–Zr binary oxide, Chemical Engineering Journal, 171 (2011) 448-455.

[12] W.W. Tang, G.M. Zeng, J.L. Gong, J. Liang, P. Xu, C. Zhang, B.B. Huang, Impact of humic/fulvic acid on the removal of heavy metals from aqueous solutions using nanomaterials: a review, The Science of the total environment, 468-469 (2014) 1014-1027.

[13] X. Tan, Y. Liu, G. Zeng, X. Wang, X. Hu, Y. Gu, Z. Yang, Application of biochar for the removal of pollutants from aqueous solutions, Chemosphere, 125 (2015) 70-85.

[14] R. Rajesh, E. Sujanthi, S. Senthil Kumar, R. Venkatesan, Designing versatile heterogeneous catalysts based on Ag and Au nanoparticles decorated on chitosan functionalized graphene oxide, Physical chemistry chemical physics : PCCP, 17 (2015) 11329-11340.

[15] P. Zhao, X. Feng, D. Huang, G. Yang, D. Astruc, Basic concepts and recent advances in nitrophenol reduction by gold- and other transition metal nanoparticles, Coordination Chemistry Reviews, 287 (2015) 114-136.

[16] Y. Fu, T. Huang, B. Jia, J. Zhu, X. Wang, Reduction of nitrophenols to aminophenols under concerted catalysis by Au/g-C_3N_4 contact system, Applied Catalysis B: Environmental, 202 (2017) 430-437.
[17] L. Qin, G. Zeng, C. Lai, D. Huang, C. Zhang, P. Xu, T. Hu, X. Liu, M. Cheng, Y. Liu, A visual application of gold nanoparticles: simple, reliable and sensitive detection of kanamycin based on hydrogen-bonding recognition, Sensors and Actuators B: Chemical, 243 (2017) 946-954.
[18] Q. Ji, J.P. Hill, K. Ariga, Shell-adjustable hollow 'soft' silica spheres as a support for gold nanoparticles, Journal of Materials Chemistry A, 1 (2013) 3600.
[19] J. Hu, Y.-l. Dong, X.-j. Chen, H.-j. Zhang, J.-m. Zheng, Q. Wang, X.-g. Chen, A highly efficient catalyst: In situ growth of Au nanoparticles on graphene oxide–Fe_3O_4 nanocomposite support, Chemical Engineering Journal, 236 (2014) 1-8.
[20] J. Zheng, Y. Dong, W. Wang, Y. Ma, J. Hu, X. Chen, X. Chen, In situ loading of gold nanoparticles on Fe_3O_4@SiO_2 magnetic nanocomposites and their high catalytic activity, Nanoscale, 5 (2013) 4894-4901.
[21] B. Le Droumaguet, R. Poupart, D. Grande, "Clickable" thiol-functionalized nanoporous polymers: from their synthesis to further adsorption of gold nanoparticles and subsequent use as efficient catalytic supports, Polymer Chemistry, 6 (2015) 8105-8111.
[22] F. Cárdenas-Lizana, Z.M.D. Pedro, S. Gómez-Quero, L. Kiwi-Minsker, M.A. Keane, Carbon supported gold and silver: Application in the gas phase hydrogenation of m -dinitrobenzene, Journal of Molecular Catalysis A: Chemical, 408 (2015) 138-146.
[23] F. Ke, J. Zhu, L.-G. Qiu, X. Jiang, Controlled synthesis of novel Au@MIL-100(Fe) core-shell nanoparticles with enhanced catalytic performance, Chemical Communications, 49 (2013) 1267-1269.
[24] A.D. Quast, M. Bornstein, B.J. Greylandus, I. Zharov, J.S. Shumaker-Parry, Robust Polymer-Coated Diamond Supports for Noble Metal Nanoparticle Catalysts, ACS Catalysis, 6 (2016) 4729-4738.
[25] J.-H. Deng, X.-R. Zhang, G.-M. Zeng, J.-L. Gong, Q.-Y. Niu, J. Liang, Simultaneous removal of Cd(II) and ionic dyes from aqueous solution using magnetic graphene oxide nanocomposite as an adsorbent, Chemical Engineering Journal, 226 (2013) 189-200.
[26] J.-L. Gong, B. Wang, G.-M. Zeng, C.-P. Yang, C.-G. Niu, Q.-Y. Niu, W.-J. Zhou, Y. Liang, Removal of cationic dyes from aqueous solution using magnetic multi-wall carbon nanotube nanocomposite as adsorbent, Journal of Hazardous Materials, 164 (2009) 1517-1522.
[27] H. Yi, D. Huang, G. Zeng, C. Lai, L. Qin, M. Cheng, S. Ye, B. Song, X. Ren, X. Guo, Selective prepared carbon nanomaterials for advanced photocatalytic application in environmental pollutant treatment and hydrogen production, Applied Catalysis B: Environmental, (2018).
[28] X. Du, C. Li, L. Zhao, J. Zhang, L. Gao, J. Sheng, Y. Yi, J. Chen, G. Zeng, Promotional removal of HCHO from simulated flue gas over Mn-Fe oxides modified activated coke, Applied Catalysis B: Environmental, 232 (2018) 37-48.
[29] S. Álvarez-Torrellas, M. Martin-Martinez, H.T. Gomes, G. Ovejero, J. García, Enhancement of p-nitrophenol adsorption capacity through N_2-thermal-based treatment of activated carbons, Applied Surface Science, 414 (2017) 424-434.
[30] H. Chen, D. He, Q. He, P. Jiang, G. Zhou, W. Fu, Selective hydrogenation of p-chloronitrobenzene over an Fe promoted Pt/AC catalyst, RSC Advances, 7 (2017) 29143-29148.
[31] Y. Xie, C. Li, L. Zhao, J. Zhang, G. Zeng, X. Zhang, W. Zhang, S. Tao, Experimental study on

626 Hg^0 removal from flue gas over columnar MnO_x-CeO_2/activated coke, Applied Surface Science, 333
627 (2015) 59-67.
628 [32] S. Tao, C. Li, X. Fan, G. Zeng, P. Lu, X. Zhang, Q. Wen, W. Zhao, D. Luo, C. Fan, Activated
629 coke impregnated with cerium chloride used for elemental mercury removal from simulated flue gas,
630 Chemical Engineering Journal, 210 (2012) 547-556.
631 [33] B.F. Machado, P. Serp, Graphene-based materials for catalysis, Catalysis Science & Technology,
632 2 (2012) 54-75.
633 [34] P. Zhang, C. Shao, Z. Zhang, M. Zhang, J. Mu, Z. Guo, Y. Liu, TiO_2@carbon core/shell
634 nanofibers: Controllable preparation and enhanced visible photocatalytic properties, Nanoscale, 3
635 (2011) 2943-2949.
636 [35] C. Lai, M.-M. Wang, G.-M. Zeng, Y.-G. Liu, D.-L. Huang, C. Zhang, R.-Z. Wang, P. Xu, M.
637 Cheng, C. Huang, H.-P. Wu, L. Qin, Synthesis of surface molecular imprinted TiO_2/graphene
638 photocatalyst and its highly efficient photocatalytic degradation of target pollutant under visible light
639 irradiation, Applied Surface Science, 390 (2016) 368-376.
640 [36] J. Sheng, C. Li, L. Zhao, X. Du, L. Gao, G. Zeng, Efficient removal of HCHO from simulated
641 coal combustion flue gas using CuO-CeO_2 supported on cylindrical activated coke, Fuel, 197 (2017)
642 397-406.
643 [37] K. Tong, Y. Zhang, D. Fu, X. Meng, Q. An, P.K. Chu, Removal of organic pollutants from super
644 heavy oil wastewater by lignite activated coke, Colloids and Surfaces A: Physicochemical and
645 Engineering Aspects, 447 (2014) 120-130.
646 [38] K. Tong, A. Lin, G. Ji, D. Wang, X. Wang, The effects of adsorbing organic pollutants from super
647 heavy oil wastewater by lignite activated coke, J Hazard Mater, 308 (2016) 113-119.
648 [39] H. Guo, Y. Ren, Q. Cheng, D. Wang, Y. Liu, Gold nanoparticles on cyanuric acid-based support:
649 A highly active catalyst for the reduction of 4-nitrophenol in water, Catalysis Communications, 102
650 (2017) 136-140.
651 [40] L. Ouarez, A. Chelouche, T. Touam, R. Mahiou, D. Djouadi, A. Potdevin, Au-doped ZnO sol-gel
652 thin films: An experimental investigation of physical and photoluminescence properties, Journal of
653 Luminescence, 203 (2018) 223-229.
654 [41] F. Costanzo, M. Sulpizi, J. Vandevondele, R.G.D. Valle, M. Sprik, Ab initiomolecular dynamics
655 study of ascorbic acid in aqueous solution, Molecular Physics, 105 (2007) 17-23.
656 [42] H. Li, Y. Liu, Y. Yang, D. Yang, J. Sun, Influences of hydrogen bonding dynamics on adsorption
657 of ethyl mercaptan onto functionalized activated carbons: A DFT/TDDFT study, Journal of
658 Photochemistry and Photobiology A: Chemistry, 291 (2014) 9-15.
659 [43] M. Nemanashi-Maumela, I. Nongwe, R.C. Motene, B.L. Davids, R. Meijboom, Au and Ag
660 nanoparticles encapsulated within silica nanospheres using dendrimers as dual templating agent and
661 their catalytic activity, Molecular Catalysis, 438 (2017) 184-196.
662 [44] H. Sharififard, F. Zokaee Ashtiani, M. Soleimani, Adsorption of palladium and platinum from
663 aqueous solutions by chitosan and activated carbon coated with chitosan, Asia-Pacific Journal of
664 Chemical Engineering, 8 (2013) 384-395.
665 [45] L. Qi, B. Cheng, J. Yu, W. Ho, High-surface area mesoporous Pt/TiO_2 hollow chains for efficient
666 formaldehyde decomposition at ambient temperature, Journal of Hazardous Materials, 301 (2016)
667 522-530.
668 [46] Z. Li, L. Wu, H. Liu, H. Lan, J. Qu, Improvement of aqueous mercury adsorption on activated
669 coke by thiol-functionalization, Chemical Engineering Journal, 228 (2013) 925-934.

[47] S. Nellaiappan, A.S. Kumar, S. Nisha, K. Chandrasekara Pillai, In-situ preparation of Au(111) oriented nanoparticles trapped carbon nanofiber-chitosan modified electrode for enhanced bifunctional electrocatalysis and sensing of formaldehyde and hydrogen peroxide in neutral pH solution, Electrochimica Acta, 249 (2017) 227-240.
[48] B. Adhikari, A. Biswas, A. Banerjee, Graphene oxide-based hydrogels to make metal nanoparticle-containing reduced graphene oxide-based functional hybrid hydrogels, ACS applied materials & interfaces, 4 (2012) 5472-5482.
[49] S. Wang, Q. Zhao, H. Wei, J.Q. Wang, M. Cho, H.S. Cho, O. Terasaki, Y. Wan, Aggregation-free gold nanoparticles in ordered mesoporous carbons: toward highly active and stable heterogeneous catalysts, Journal of the American Chemical Society, 135 (2013) 11849-11860.
[50] M.-B. Li, S.-K. Tian, Z. Wu, R. Jin, Cu2+ induced formation of $Au_{44}(SC_2H_4Ph)_{32}$ and its high catalytic activity for the reduction of 4-nitrophenol at low temperature, Chemical Communications, 51 (2015) 4433-4436.
[51] F. Zhang, X. Zhao, C. Feng, B. Li, T. Chen, W. Lu, X. Lei, S. Xu, Crystal-Face-Selective Supporting of Gold Nanoparticles on Layered Double Hydroxide as Efficient Catalyst for Epoxidation of Styrene, ACS Catalysis, 1 (2011) 232-237.
[52] X. Hu, B. Liu, Y. Deng, H. Chen, S. Luo, C. Sun, P. Yang, S. Yang, Adsorption and heterogeneous Fenton degradation of 17α-methyltestosterone on nano Fe_3O_4/MWCNTs in aqueous solution, Applied Catalysis B: Environmental, 107 (2011) 274-283.
[53] D. Huang, C. Hu, G. Zeng, M. Cheng, P. Xu, X. Gong, R. Wang, W. Xue, Combination of Fenton processes and biotreatment for wastewater treatment and soil remediation, Science of the Total Environment, 574 (2017) 1599-1610.
[54] L. Li, M. Chen, G. Huang, N. Yang, L. Zhang, H. Wang, Y. Liu, W. Wang, J. Gao, A green method to prepare Pd–Ag nanoparticles supported on reduced graphene oxide and their electrochemical catalysis of methanol and ethanol oxidation, Journal of Power Sources, 263 (2014) 13-21.
[55] F. Montagne, J. Polesel-Maris, R. Pugin, H. Heinzelmann, Poly(N-isopropylacrylamide) Thin Films Densely Grafted onto Gold Surface: Preparation, Characterization, and Dynamic AFM Study of Temperature-Induced Chain Conformational Changes, Langmuir, 25 (2009) 983-991.
[56] F. Wei, J. Liu, Y.-H. Zhu, X.-S. Wang, C.-Y. Cao, W.-G. Song, In situ facile loading of noble metal nanoparticles on polydopamine nanospheres via galvanic replacement reaction for multifunctional catalysis, Science China Chemistry, 60 (2017) 1236-1242.
[57] F. Ali, S.B. Khan, T. Kamal, Y. Anwar, K.A. Alamry, A.M. Asiri, Bactericidal and catalytic performance of green nanocomposite based-on chitosan/carbon black fiber supported monometallic and bimetallic nanoparticles, Chemosphere, 188 (2017) 588-598.
[58] S. Praharaj, S. Nath, S.K. Ghosh, S. Kundu, T. Pal, Immobilization and Recovery of Au Nanoparticles from Anion Exchange Resin: Resin-Bound Nanoparticle Matrix as a Catalyst for the Reduction of 4-Nitrophenol, Langmuir, 20 (2004) 9889-9892.
[59] Y. Deng, Y. Cai, Z. Sun, J. Liu, C. Liu, J. Wei, W. Li, C. Liu, Y. Wang, D. Zhao, Multifunctional Mesoporous Composite Microspheres with Well-Designed Nanostructure: A Highly Integrated Catalyst System, Journal of the American Chemical Society, 132 (2010) 8466-8473.
[60] Y. Liu, L. Xu, X. Liu, M. Cao, Hybrids of Gold Nanoparticles with Core-Shell Hyperbranched Polymers: Synthesis, Characterization, and Their High Catalytic Activity for Reduction of 4-Nitrophenol, Catalysts, 6 (2015) 3.

[61] Y. Qiu, Z. Ma, P. Hu, Environmentally benign magnetic chitosan/Fe_3O_4 composites as reductant and stabilizer for anchoring Au NPs and their catalytic reduction of 4-nitrophenol, Journal of Materials Chemistry A, 2 (2014) 13471-13478.
[62] W. Zhao, L. Xie, M. Zhang, Z. Ai, H. Xi, Y. Li, Q. Shi, J. Chen, Enhanced photocatalytic activity of all-solid-state g-C_3N_4/Au/P_{25} Z-scheme system for visible-light-driven H2 evolution, International Journal of Hydrogen Energy, 41 (2016) 6277-6287.
[63] L. Rout, A. Kumar, R.S. Dhaka, G.N. Reddy, S. Giri, P. Dash, Bimetallic Au-Cu alloy nanoparticles on reduced graphene oxide support: Synthesis, catalytic activity and investigation of synergistic effect by DFT analysis, Applied Catalysis A: General, 538 (2017) 107-122.
[64] Y. Choi, H.S. Bae, E. Seo, S. Jang, K.H. Park, B.-S. Kim, Hybrid gold nanoparticle-reduced graphene oxide nanosheets as active catalysts for highly efficient reduction of nitroarenes, Journal of Materials Chemistry, 21 (2011) 15431.
[65] P. Guo, L. Tang, J. Tang, G. Zeng, B. Huang, H. Dong, Y. Zhang, Y. Zhou, Y. Deng, L. Ma, S. Tan, Catalytic reduction-adsorption for removal of p-nitrophenol and its conversion p-aminophenol from water by gold nanoparticles supported on oxidized mesoporous carbon, Journal of colloid and interface science, 469 (2016) 78-85.
[66] P. Zhang, C. Shao, X. Li, M. Zhang, X. Zhang, C. Su, N. Lu, K. Wang, Y. Liu, An electron-rich free-standing carbon@Au core-shell nanofiber network as a highly active and recyclable catalyst for the reduction of 4-nitrophenol, Physical chemistry chemical physics : PCCP, 15 (2013) 10453-10458.
[67] X. Wang, J. Fu, M. Wang, Y. Wang, Z. Chen, J. Zhang, J. Chen, Q. Xu, Facile synthesis of Au nanoparticles supported on polyphosphazene functionalized carbon nanotubes for catalytic reduction of 4-nitrophenol, Journal of Materials Science, 49 (2014) 5056-5065.
[68] K. Layek, M.L. Kantam, M. Shirai, D. Nishio-Hamane, T. Sasaki, H. Maheswaran, Gold nanoparticles stabilized on nanocrystalline magnesium oxide as an active catalyst for reduction of nitroarenes in aqueous medium at room temperature, Green Chemistry, 14 (2012) 3164.
[69] X. Li, Y. Ma, Z. Yang, D. Huang, S. Xu, T. Wang, Y. Su, N. Hu, Y. Zhang, In situ preparation of magnetic Ni-Au/graphene nanocomposites with electron-enhanced catalytic performance, Journal of Alloys and Compounds, 706 (2017) 377-386.
[70] V.K. Gupta, N. Atar, M.L. Yola, Z. Ustundag, L. Uzun, A novel magnetic Fe@Au core-shell nanoparticles anchored graphene oxide recyclable nanocatalyst for the reduction of nitrophenol compounds, Water Res, 48 (2014) 210-217.
[71] L. Qin, D. Huang, P. Xu, G. Zeng, C. Lai, Y. Fu, H. Yi, B. Li, C. Zhang, M. Cheng, C. Zhou, X. Wen, In-situ deposition of gold nanoparticles onto polydopamine-decorated g-C_3N_4 for highly efficient reduction of nitroaromatics in environmental water purification, Journal of colloid and interface science, 534 (2018) 357-369.
[72] X. Zhou, C. Lai, D. Huang, G. Zeng, L. Chen, L. Qin, P. Xu, M. Cheng, C. Huang, C. Zhang, Preparation of water-compatible molecularly imprinted thiol-functionalized activated titanium dioxide: Selective adsorption and efficient photodegradation of 2, 4-dinitrophenol in aqueous solution, Journal of hazardous materials, 346 (2018) 113-123.
[73] J. Xia, G. He, L. Zhang, X. Sun, X. Wang, Hydrogenation of nitrophenols catalyzed by carbon black-supported nickel nanoparticles under mild conditions, Applied Catalysis B: Environmental, 180 (2016) 408-415.
[74] S. Wunder, F. Polzer, Y. Lu, Y. Mei, M. Ballauff, Kinetic Analysis of Catalytic Reduction of 4-Nitrophenol by Metallic Nanoparticles Immobilized in Spherical Polyelectrolyte Brushes, The

758 Journal of Physical Chemistry C, 114 (2010) 8814-8820.
759 [75] T. Aditya, A. Pal, T. Pal, Nitroarene reduction: a trusted model reaction to test nanoparticle
760 catalysts, Chem Commun (Camb), 51 (2015) 9410-9431.
761 [76] W. Xie, B. Walkenfort, S. Schlücker, Label-Free SERS Monitoring of Chemical Reactions
762 Catalyzed by Small Gold Nanoparticles Using 3D Plasmonic Superstructures, Journal of the
763 American Chemical Society, 135 (2013) 1657-1660.
764 [77] Q. Cui, B. Xia, S. Mitzscherling, A. Masic, L. Li, M. Bargheer, H. Möhwald, Preparation of gold
765 nanostars and their study in selective catalytic reactions, Colloids and Surfaces A: Physicochemical
766 and Engineering Aspects, 465 (2015) 20-25.
767 [78] S. Biella, L. Prati, M. Rossi, Selective Oxidation of D-Glucose on Gold Catalyst, Journal of
768 Catalysis, 206 (2002) 242-247.
769 [79] H. Zhang, D. Chen, X. Lv, Y. Wang, H. Chang, J. Li, Energy-Efficient Photodegradation of Azo
770 Dyes with TiO_2 Nanoparticles Based on Photoisomerization and Alternate UV−Visible Light,
771 Environmental Science & Technology, 44 (2010) 1107-1111.
772 [80] M. Chen, P. Xu, G. Zeng, C. Yang, D. Huang, J. Zhang, Bioremediation of soils contaminated
773 with polycyclic aromatic hydrocarbons, petroleum, pesticides, chlorophenols and heavy metals by
774 composting: Applications, microbes and future research needs, Biotechnology Advances, 33 (2015)
775 745-755.
776 [81] C. Umamaheswari, A. Lakshmanan, N.S. Nagarajan, Green synthesis, characterization and
777 catalytic degradation studies of gold nanoparticles against congo red and methyl orange, J Photochem
778 Photobiol B, 178 (2018) 33-39.
779 [82] U. Tyagi, N. Anand, D. Kumar, Synergistic effect of modified activated carbon and ionic liquid
780 in the conversion of microcrystalline cellulose to 5-Hydroxymethyl Furfural, Bioresour Technol, 267
781 (2018) 326-332.
782 [83] Y. Zhu, X. Cao, Y. Cheng, T. Zhu, Performances and structures of functional microbial
783 communities in the mono azo dye decolorization and mineralization stages, Chemosphere, 210 (2018)
784 1051-1060.
785 [84] W. Zhong, T. Jiang, Y. Long, . He, S.-Y. Chen, C.-H. Kuo, D. Kriz, Y. Meng, A.G.
786 Meguerdichian, S.L. Suib, Mechanism studies on methyl orange dye degradation by perovskite-type
787 $LaNiO_3$-δ under dark ambient conditions, Applied Catalysis A: General, 549 (2018) 302-309.
788 [85] N. Srivastava, M. Mukhopadhyay, Biosynthesis of SnO_2 Nanoparticles Using Bacterium Erwinia
789 herbicola and Their Photocatalytic Activity for Degradation of Dyes, Industrial & Engineering
790 Chemistry Research, 53 (2014) 13971-13979.
791 [86] J. Hu, Y.-l. Dong, Z.u. Rahman, Y.-h. Ma, C.-l. Ren, X.-g. Chen, In situ preparation of
792 core-satellites nanostructural magnetic-Au NPs composite for catalytic degradation of organic
793 contaminants, Chemical Engineering Journal, 254 (2014) 514-523.

794

Au nanoparticles decorated on activated coke via a facile preparation for efficient catalytic reduction of nitrophenols and azo dyes

Yukui Fu [a,b,1], Piao Xu [a,b,1], Danlian Huang [a,b,1], Guangming Zeng [a,b,*], Cui Lai [a,b,*], Lei Qin [a,b], Bisheng Li [a,b], Jiangfan He [a, b], Huan Yi [a,b], Min Cheng [a,b], Chen Zhang [a,b]

[a] *College of Environmental Science and Engineering, Hunan University, Changsha, 410082, PR China,*

[b] *Key Laboratory of Environmental Biology and Pollution Control, Hunan University, Ministry of Education*

* Corresponding author.

E-mail address: zgming@hnu.edu.cn (G.M. Zeng) and laicui@hnu.edu.cn (C.Lai).

1 These authors contributed equally to this article.

Abstract

Activated coke (AC) exhibits excellent properties with a graphite-like layer crystallite structure and possesses mesopore and macropore structures, which can reduce the influence of internal diffusion on the general rate of adsorption and catalytic process greatly. In this work, AC was served as a support for gold nanoparticles (Au NPs) anchoring to prepare Au /AC catalysts via a facile synthesis using ascorbic acid as a mild reducing agent. The morphology and structure of catalysts were characterized by XRD, TEM, FTIR, and XPS analysis. Our experiment results showed that the abundant functional groups on the surface of AC play a vital role in the immobilization of Au NPs. Au/AC was employed as a highly efficient catalyst with a rate constant of 0.1916 s^{-1} for the reduction of 4-nitrophenols by $NaBH_4$. Au/AC was also tested for the catalytic reduction of other nitrophenols (2-nitrophenol and 2, 4-dinitrophenol) and azo dyes (congo red, methyl orange and erichrome black T), demonstrating that Au/AC exhibited superior catalytic efficiency compared with other Au NPs catalysts. The catalysts showed good reusability, with conversion of 84% in the reduction of 4-NP in 20 s after six cycles. The Au/AC with high TOF has potential to be a workable and efficient catalyst in industrial applications. Present study not only provides a facile preparation route of catalysts using AC as a promising support, but also sheds light on the understanding of mechanism of the synergistic effect between Au NPs and AC towards the reduction of nitrophenols.

Keywords: Au nanoparticles; Activated coke; Catalytic reduction; Nitrophenols;

Azo dyes.

1. Introduction

Noble metal nanoparticles (MNPs) in catalytic applications have received significant interest because the nanoparticles possess unusual physiochemical properties with large number of exposed metal atoms, which greatly enhance the catalytic activity [1-5]. Gold nanoparticles (Au NPs) with features of high specific surface area, less prone to metal leaching and self-poisoning are one of the most inspiring developments in catalysis field [5-8]. Among all the Au NPs-catalyzed reaction, catalytic reduction of 4-nitrophenol (4-NP) to 4-aminophenol (4-AP) by $NaBH_4$ has been used widely as model reaction to test its catalytic activity, since 4-NP exhibits high toxicity and stability for a long time in water, causing harm to ecosystem [9-13]. And most importantly, the generated aminophenol is known to be an important intermediate chemical in many industries as well as easier to be mineralized and removed compared to the nitrophenols [14]. However, Au NPs suffer from serious stability problems such as aggregation in practice due to their high surface energy, eventually losing of their intrinsic activity [15-17]. In addition, considering facile catalyst recovery and recycling, immobilizing Au NPs on the surface of solid supports (e.g. silica, metal oxides and polymer) is regarded as an efficient approach for preventing aggregation of Au NPs and warranting high catalytic activity [18-21]. However, the stability of mentioned solid supports is compromised in some chemical environments of high or low pH solutions, resulting in the inability to achieve highly distributed Au NPs and dissolution of solid supports [22-24]. Thus, it is desirable to find a rational support with high stability to enhance

the catalytic activity and efficiency of Au NPs.

Activated coke (AC), as a kind of carbon-based material, exhibits excellent properties with graphite-like layer crystallite and possesses appreciable environmental and economic benefits owing to its better mechanical strength, easier regeneration and lower cost compared with other carbon-based materials [25-27]. AC with mesopore and macropore structures can reduce the influence of internal diffusion on the general rate of adsorption and catalytic process greatly [22, 28-30], which is different from microporous activated carbon. In addition, with abundant functional groups, AC could provide the active sites and is beneficial for MNPs anchoring and dispersion [31, 32]. Moreover, AC possesses a graphite-like layer crystallite structure and flourishing hole structure, leading to high adsorption ability via π-π stacking interactions and thus facilitating the interface reaction with organic compounds, which could enhance the catalytic efficiency [33-35]. Therefore, AC can be considered as a promising, suitable and novel support, particularly, in catalytic applications.

To date, AC has been used as a carrier for supporting CuO-CeO_2, MnO_x-CeO_2 mixed oxides for fuel gas desulfurization, denitrification and mercury removal [31, 36-38]. However, to the best of our knowledge, few papers thus far have reported on the utilization of MNPs decorated on AC and on their application of catalytic activity for organic transformation in wastewater treatment. In this regard, ideas of Au NPs supported on AC for the application in catalytic reaction of organic compounds are encouraged. The presence of abundant amount of oxygen-containing groups and

thiol group endows its hydrophilic character and provides sufficient reactive sites for Au NPs anchoring, which is beneficial for catalytic reaction [28, 39]. And, the good conductivity of AC can favor the electron transfer between Au NPs and AC [28]. It is well documented that electron transfer effect can conduce to negative shift in Fermi level of Au [16]. What's more, the utilization of AC as supports can expand its application in wastewater treatment in view of low cost of AC. On one hand, AC is able to prevent Au NPs from aggregation, warranting high catalytic activity. On the other hand, the synergistic effects between decorated Au NPs and AC were supposed to play the vital role in enhancing catalytic activity. Hence, using AC as a support for Au NPs anchoring seems to be a potential approach to fabricate a novel catalyst with enhanced catalytic activity for organic transformation in wastewater treatment.

Herein, taking full advantage of AC, we prepared Au/AC catalysts via a facile and one step method employed ascorbic acid as a mild reducing agent. The Au/AC catalysts were characterized by XRD, TEM, FTIR and XPS. The catalytic performance of Au/AC was investigated in the reduction of 4-NP in the presence of $NaBH_4$, with the rate constant evaluated in accordance with pseudo-first-order kinetic reaction under different Au loading amounts, catalyst dosage and $NaBH_4$ concentration. Besides, Au/AC was tested for the reduction of other nitrophenols such as 2-nitrophenol (2-NP), 2, 4-dinitrophenol (2, 4-DNP) and reductive degradation of azo dyes, including congo red (CR), methly orange (MO) and erichrome black T (EBT). The reusability of catalysts was tested up to six cycle run in the catalytic reduction of 4-NP. In addition, the feasible mechanism was discussed

for the catalytic reduction of nitrophenols.

2. Experimental

2.1 Materials

Virgin activated coke (AC) used in the experiment is commercial cokes from Clear Science Technology Co., Ltd. (Shanghai, China). AC was washed with ultrapure water for several times and dried 12 h at 60°C in an vacuum oven before grated with ball mill and sieved to 200 mesh size for further use. Hydrogen tetrachloroaurate hydrate ($HAuCl_4 \cdot 4H_2O$), sodium borohydride ($NaBH_4$), ascorbic acid (AA), 2-nitrophenol (2-NP), 4-nitrophenol (4-NP), 2,4-dinitrophenol (2,4-DNP), Methyl orange (MO) were purchased from Sinopharm Chemistry Reagent Co., Ltd. (Beijing, China). Congo red (CR) was purchased from Yuanhang chemical plant (Shanghai, China). Erichrome black T (EBT) was obtained from Shanpu Chemistry Reagent Co., Ltd. (Shanghai, China). All chemicals were of analytic reagent grade and used without further purification.

2.2 Preparation of Au/AC

Au/AC catalysts with different Au loading amount (1, 2, 3 mL of 1 wt% $HAuCl_4 \cdot 4H_2O$) were synthesized by a facile one-step method and labeled as Au/AC-x (x=1, 2, 3), respectively. For the typical synthesis of Au/AC-1, 0.4 g of AC was added to 200 mL of ultrapure water under ultrasonicating for 0.5 h to obtain AC suspension. Then, 1 mL of $HAuCl_4 \cdot 4H_2O$ (24.28 mM) was added with stirring for 0.5 h. After that, 10 mL of ascorbic acid (0.1 M) was injected drop by drop into the above solution under stirring. Further, the reaction mixture was allowed for stirring

for 24 h under ambient environment. The resulting black products were collected by filtration and washed with ultrapure water for several times, and then dried overnight at 35°C in vacuum oven for further use. Similar synthetic procedure was applied for preparation of Au/AC-2 and Au/AC-3 catalysts with different Au loading amount.

2.3 Catalytic reduction of nitrophenols and azo dyes

The catalytic activity of as-prepared catalyst Au/AC for nitrophenols reduction in the presence of excess sodium borohydride was studied by UV-Vis spectrophotometer in a 3 mL quartz cuvette. In a typical procedure, 30 mL of 4-NP aqueous solution (0.2 mM) was taken in a cuvette followed by adding 15 mL of freshly-prepared $NaBH_4$ solution (0.1 M). Then, 9 mg of catalyst was added into the cuvette. 3 mL aliquots were collected followed by the solid-liquid separation, then the absorbance of samples was immediately monitored at different time intervals using a UV-Vis spectrophotometer in a scanning range of 200 - 800 nm. In addition, the catalytic reduction of 2-NP and 2, 4-DNP were carried out following the same procedure. The similar procedure was applied for examining the performance on catalytic degradation of azo dyes (CR, MO and EBT). All the experiments were carried out under ambient experiment. The reusability of catalyst was examined via Au/AC separated by centrifugation after completely catalytic reduction of 4-NP in the first run.

2.4 Characterizations

UV-Vis spectrophotometer was recorded from 200 to 800 nm on a UV-2700 spectrophotometer (SHIMADZU (JAPAN) Co., Ltd.). The X-Ray diffraction (XRD)

patterns were collected using a XRD-6100 powder diffractometer (SHIMADZU (JAPAN) Co., Ltd.). Transmission electron microscopy (TEM) and high-resolution TEM (HRTEM) were carried out using a transmission electron microscope Tecnai G2 F20 (FEI USA), attached with selected area electron diffraction (SAED) to observe the morphology and composition of the samples. Scanning transmission electron microscope with high-angle annular dark-field detector (HAADF-STEM) was used to record the elemental mappings. Fourier transform infrared spectroscopy (FT-IR) studies were conducted using FTIR-8400 S IRprestige-21 (SHIMADZU (JAPAN) Co., Ltd.), recorded from 4000 - 400 cm^{-1-} at a resolution of 2 cm^{-1}. The X-ray photoelectron spectroscopy (XPS) measurements were performed on K-Alpha 1063 spectrometer (Thermo Fisher Scientific, UK). The Au loading amount was determined by inductively coupled plasma atomic emission spectrometry (ICP-OES, Perkin-Elmer Optima 5300DV, USA).

3. Results and discussion

3.1 Characterization of Au/AC catalyst

The XRD measurements were conducted to identify the phase purity and crystallite structure of virgin AC and as-prepared catalysts. As shown in Fig. 1, the characteristic diffraction peaks of AC appeared at 2θ = 26.66°, indicating AC possesses a graphite-like layer crystallite structure with hexagonal lattice [30]. The peak intensity at 26.66° decreased with increase of AC loading amount. The increase of Au loading amount may occupy more grain boundaries and affected the interplanar spacing of AC [31, 40], thus leading to a decrease of crystalline quality

of AC. The above results could also be inferred that the interaction may exist between Au and AC, as demonstrated as follows in TEM, FTIR and XPS. What's more, the peak at nearly 29.4° corresponding to AC was also detected over virgin AC. Interestingly, compared with the virgin AC, the peak at 29.4° disappeared in XRD pattern of AC that reacted with AA only. This indicates the synthesis process has an influence on the crystallinity of activated coke. As reported by Costanzo et al., the oxidation or reduction of ascorbic acid would affect the hydrogen bonding of hydrogen and oxygen atom [41, 42], thus resulting in a decrease of crystalline quality of AC. Besides, the minor peaks at 20.8°, 38.9° and 50.83° were ascribed to the presence of trace quantity of silica, aluminum and calcium as shown in Fig. S1B, which was corresponding with previous report that these elements were inert for the catalytic reaction [43]. In each pattern of catalyst with different Au loading amount, the crystallite structure of Au NPs was confirmed by the presence of diffraction peaks at 38.18°, 44.38°, 64.52°, and 77.54°, corresponding to the diffraction of the (111), (200), (220) and (311) lattice plane for Au(0) crystals, respectively (JCPDS NO. 04-0784). The XRD patterns of catalysts matched the face-centered-cubic (fcc) nature of Au NPs [16]. With the increment of Au loading amounts, the intensity of scattering peaks heightened, which could be attributed to the growth and formation of larger Au NPs as the Au loading amounts increasing [16].

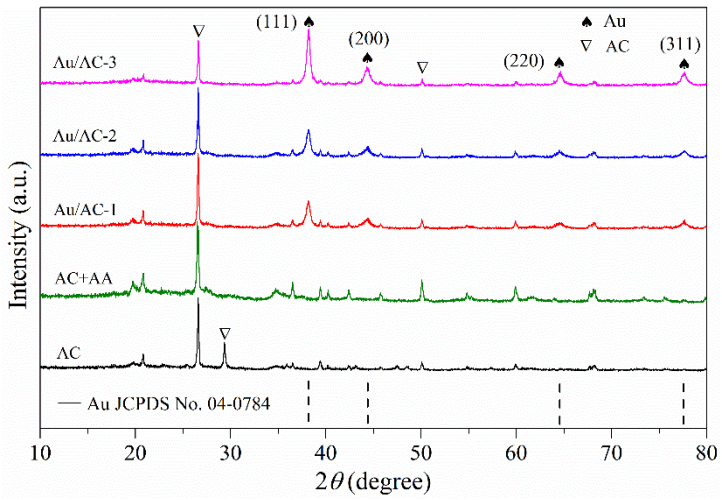

Fig. 1. X-ray diffraction patterns of virgin AC and Au/AC catalysts with different Au content.

In order to study the morphology and microstructure of the virgin AC and obtained Au/AC, TEM measurements were performed (Fig. 2). By the morphology image of virgin AC as indicated in Fig. 2A, it is clear that virgin AC contains some wrinkles composed by some thin layers with relatively smooth and planar surfaces. As revealed from Fig. 2B, the Au NPs were dispersed uniformly on the stacking AC layers. From Fig. 2C and 2D, it could be observed that Au NPs with a size smaller than 5 nm existed in AC with interplanar spacing of 0.235 nm corresponding to the (111) crystal planes. This was because the pore structure of AC restricted the growing of Au NPs adsorbed into the AC. As shown in Fig. 2E, HRTEM image reveals distinct lattice fringes with an interplanar spacing measured to be 0.235 nm and 0.205 nm, corresponding to the (111) and (200) crystal planes of fcc Au, respectively. Moreover, the SAED pattern was inserted in Fig. 2E, displaying the characteristic rings for the (111), (200), (220) and (311) planes of fcc Au. Both results confirm the polycrystalline structure of Au NPs supported on AC and are in

good accordance with the XRD results. Besides, the SEM images of Au/AC-3 in Fig. S2A further displayed that there were Au NPs dispersed on the surface of AC. Base on the Fig. 2C, Fig. 2D, Fig. S2B and Fig. S2C, the particle size of Au NPs supported on AC was counted for at least 200 nanoparticles, which would make the size distributions more representative and accurate. Fig. 2F shows the presence of dispersed Au NPs with a diameter of 14.9 ± 10.8 nm. In addition, to further confirm the elemental distribution and chemical composition of Au/AC-3, HAADF-STEM image and EDS spectrum were carried out (Fig. S1). The HAADF-STEM image shows a clear luminance of Au NPs, revealing homogenous distribution of Au NPs on AC. The presence of Au element confirmed the synthesis of Au NPs. These TEM images further indicate the successful preparation of Au NPs supported on AC as well, and illustrate Au NPs dispersed well on AC surface.

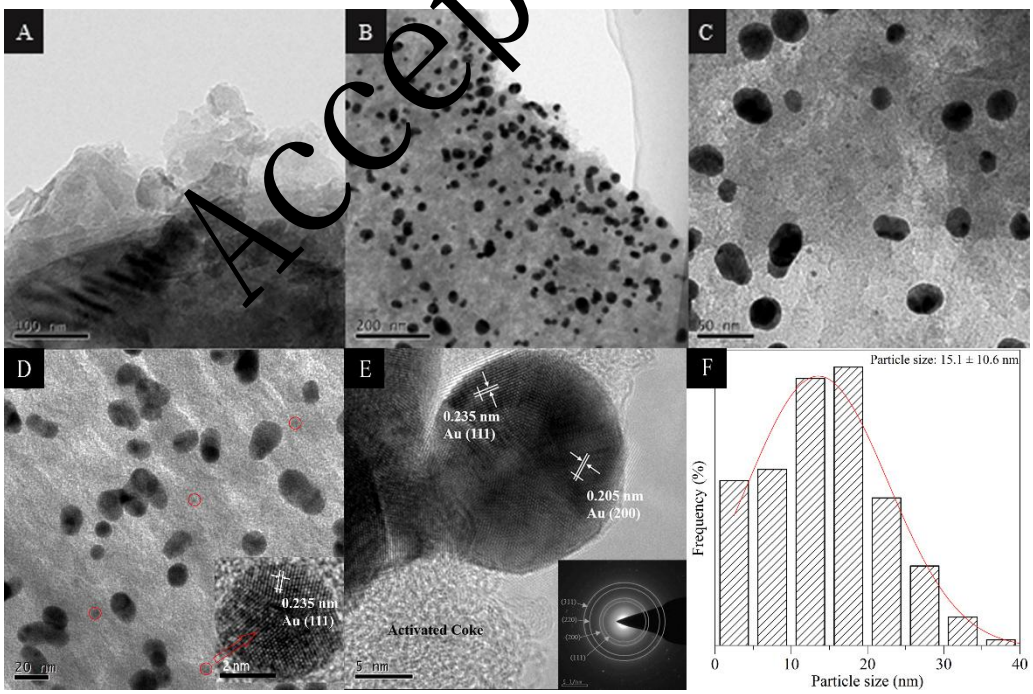

Fig. 2. TEM images of virgin AC (A) and the Au/AC-3 catalyst (B, C and D) (the inset is HRTEM image of the tiny NPs); HRTEM image (E) of Au/AC-3 catalyst (the

inset is SAED pattern); Size distribution of Au NPs (F).

FTIR measurements were performed to further obtain valid information of functional group about virgin AC and Au/AC-3 catalyst. In the region of 3600-3200 cm^{-1}, the most pronounced broad and intense band around 3421 cm^{-1} was due to the overlapping of –OH as exhibited in the FTIR spectrum of activated carbon or a displaced amino group [38, 44]. And the band located at 2362 cm^{-1} was assigned to the vibration of C=O [45]. The peaks at 1635 and 1445 cm^{-1} corresponded to the skeletal vibrations stretching of aromatic C=C [19]. The peak at 1037 cm^{-1} represented a stretching vibration of C-O or primary alcohols[46]. In addition, the peaks at 670-872 cm^{-1} represented out of plane bending vibrations of the C-H bonds [38]. It can be seen from the FTIR spectrum of Au/AC-3 that after the deposition with Au NPs on AC, some adsorption peaks drifted, appeared and disappeared. The attenuated peaks at 3421 and 1445 cm^{-1} indicated that the amount of O-H bonds decreased after active sites of AC were occupied by Au NPs. In addition, the shift of the band at 2626, 2362 and 1635 cm^{-1} may be accounted for the interaction of Au NPs with hydroxyl groups of AC [47]. The gradual variation in this band region of 900-700 cm^{-1} was owing to Au-O bonds stretching vibration. These variation and vibration indicated the reduction of oxygen-containing groups [48]. However, on account of the weak dipoles exhibited by S-H groups, the thiol group in FTIR is invisible under current conditions [49]. Fig. 3 indicates that the surface functional groups in AC contain oxygen-containing functional groups such as hydroxyl and carboxyl, possessing hydrophilic property in solvents which may favor catalytic

reaction [39, 50].

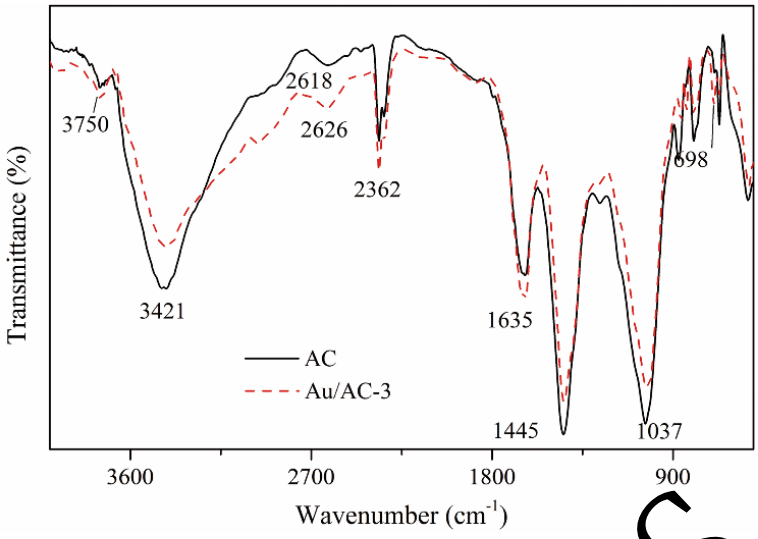

Fig. 3. FTIR spectra of AC and Au/AC-3 catalyst.

The XPS was employed to further analyze the composition and surface-functional groups of prepared catalysts. As shown in Fig. 4A, the binding energies (BE) of about 530, 284 and 163 eV indexed to O 1s, C 1s and S 2p, respectively. As shown in Fig. 4B, in the high-resolution XPS spectrum of Au 4f region, the peaks of Au $4f_{7/2}$ an Au $4f_{5/2}$ peaks were observed at 84.2 and 87.9 eV respectively, with a gap of 3.7 eV between two peaks [51]. It should be noted that the typical characteristic peaks of Au(III) were absent in the spectrum, illustrating the almost completed reduction of the small amount of Au(III) to Au(0) in the reaction system [51]. The O 1s spectra of Au/AC-3 and AC are shown in Fig. 4C. The photoelectron line of about 531.8 and 532.9 eV were attributed to oxygen in carboxylate/carbonyl (O-C=O/C=O) and in the epoxy/hydroxyl (C-OH) of the AC [52, 53]. It has been found that the shifting BE of O 1s ascribed to O-C=O/C=O and C-OH were occupied by Au NPs, revealing the oxygenated functional group like hydroxyl were reduced during the preparation of catalysts, and Au NPs occupied the sites of these functional groups

[54]. The claim was further verified by the C 1s spectra of Au/AC-3 and AC in Fig. 4D. The C 1s spectra could be deconvoluted into five components corresponding to sp^2 carbon (284.6 eV), -CONH (285.1 eV), C-O-C (286.6 eV), C=O (287.7 eV) and O-C=O (288.8 eV) [28, 46, 54, 55]. They were attributed to the presence of carboxylate, carbonyl and hydroxyl functional groups of AC. Obviously, after AC loaded with Au NPs, the peak intensity of oxygenated functional groups (C-C, C=O) decreased (Table S1), which was assigned to the formation of Au NPs on these functional groups [48]. The peak of C-O-C showed a slight shift compared with the virgin AC, owing to the galvanic displacement reaction between catechol groups and Au NPs [56]. Thus, the XPS measurements validate the presence of sulfur-containing and oxygen-containing groups in AC surface.

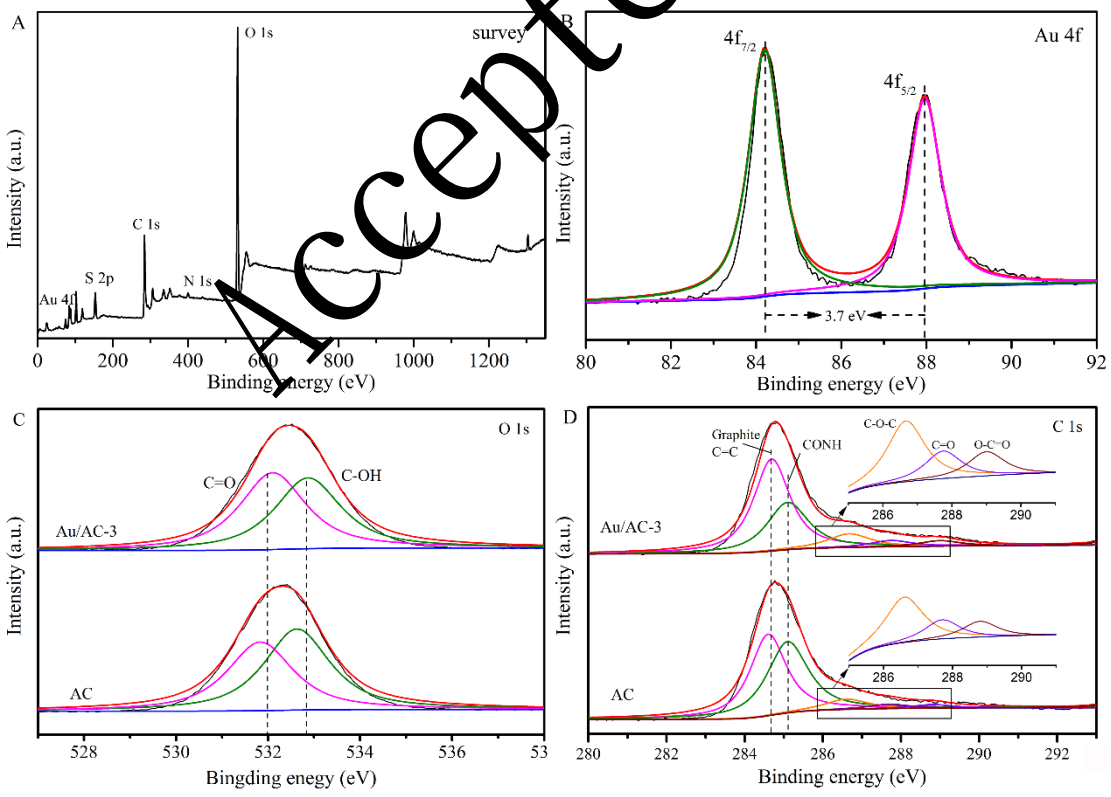

Fig. 4. XPS survey spectra (A) of Au/AC-3 catalyst; High-resolution XPS spectra of Au 4f (B), O1s (C) and C 1s (D) of Au/AC-3 and AC.

3.2 Catalytic reduction studies of nitrophenols

Before checking out the catalytic nature of synthesized catalysts Au/AC, it has to check whether self-hydrolysis of $NaBH_4$ reduces the 4-NP and the support material AC catalyzes the reduction of 4-NP. For these reason, two control experiments were performed in which the reductions of 4-NP were investigated in the presence of $NaBH_4$ and AC+$NaBH_4$. After the additional of $NaBH_4$ in the 4-NP, the color of the mixture aqueous turned to bright yellow rapidly, indicating the 4-NP was converted into nitrophenolate anion ($C_6H_4NO_3^-$). As shown in Fig. S3, the initial maximum absorbance at 400 nm indexed to the 4-NP in the natural and alkaline conditions. The maximum absorbance peak of the mixture solution centered at 400 nm over reaction time within 20 min in the absence of catalyst wherein excess $NaBH_4$ was used exclusively, indicating the reduction does not occur by the self-hydrolysis of $NaBH_4$ [57]. This can be ascribed to that there is a kinetic negative barrier and mutual repulsion between BH_4^- and 4-NP [58]. On the other hand, the absorbance peak at 400 nm also decreased slightly within 20 minutes but no peak appeared at 298 nm in the control experiment in the presence of virgin AC + $NaBH_4$, indicating the catalytic reaction did not proceed at all and AC has adsorption ability towards 4-NP. Nevertheless, it should be point out the adsorption efficiency is modest. Thus, the adsorption effects of AC towards nitrophenols can be ignored.

In order to study the catalytic performance of synthesized catalyst, catalytic reduction of 4-nitreophenol in the presence of excess sodium borohydride was carried out. The convincing evidence for reduction of 4-NP came from

time-dependent UV-Vis absorption spectra. Fig. 5A provides time-dependent UV-Vis absorption spectra of 4-NP catalyzed by 9 mg of Au/AC-3. The absorbance peak at 400 nm quickly decreased and disappeared within 20 s. Simultaneously, a new peak appeared at 298 nm, accompanied with an increase intensity of the peak over reaction time, which was assigned to the formation of 4-aminophenol. In order to confirm the product, the determination of 4-AP was recorded with UV-Vis absorbance spectra (Fig. 5B). Moreover, the isosbestic points at 313 nm also provided evidence to the catalytic reduction of 4-NP yields 4-AP without any byproduct [59]. As the initial concentration of $NaBH_4$ (0.1 M) was excess with respect to the concentration of 4-NP (0.2 mM), the reduction can be treated as pseudo-first-kinetic. The reduction rate of 4-nitrophenol was calculated using the following equation:

$$-\ln(C_t/C_0) = -\ln(A_t/A_0) = k_{app}$$

wherein C_t is 4-NP concentration at reaction time *t*, and C_0 is the initial concentration of 4-NP, and the rate constant k_{app} is the first order constant, determined by a liner plot of $\ln(C_t/C_0)$ versus reaction time. Liner relationships between $\ln(C_t/C_0)$ and reaction time t was shown in Fig. 5A, and the rate constant k_{app} was calculated as 0.1916 s^{-1} for the reaction. As presented in Table 1, it is obvious that the catalytic performance of Au/AC-3 was comparable or even superior when compared with other Au-based catalysts supported by other materials. It is well documented that the high catalytic activity of Au NPs is owing to their highly dispersed and nanosized properties, which is corresponding to the above characterization of Au/AC. In the

cases of other loading amounts of the Au catalysts, the catalytic reduction of 4-NP was performed under similar conditions. The catalytic reduction of 4-NP completed within 50 s, 30 s and 20 s, respectively. For apparent comparison of rate constant k_{app} of different Au loading amounts catalysts, the C/C_0 and ln (C/C_0) versus reaction time were plotted in Fig. 6A and 6B. The rate constant k_{app} was 0.0737, 0.1347, and 0.1916 s^{-1}, respectively. As expected, the rate constant k_{app} was proportional to the concentration of the $HAuCl_4$ solutions, indicating that the catalytic efficiency increased with the increased loading amounts of Au NPs on AC. It is obviously shown in Fig. S4 that with the lower Au loading amounts, the sparse distribution of Au NPs resulted in the low catalytic activity. In Au/AC-3 catalyst, Au NPs were well dispersed on AC, with the better surface morphology, which relates to the higher catalytic activity. This result is in well consistent with previous studies, demonstrating that the catalytic activity is proportional to the quantity of nanoparticles [60]. Furthermore, the Au content determined by ICP-OES was about 1.37 wt%, 2.45 wt% and 3.49 wt%, corresponding to Au/AC-1, Au/AC-2 and Au/AC-3, respectively. According to the previous research, the turn-over frequency (TOF: moles of 4-NP reduced by per gram of Au NPs per second) has been calculated to estimate the catalytic efficiency of catalysts in our research [61, 62]. TOF was calculated to be 0.287, 0.268 and 0.282 $mol \cdot g^{-1} \cdot s^{-1}$, for the case of Au/AC-1, Au/AC-2 and Au/AC-3, respectively. It is higher than those of Au NPs catalysts recently reported. Thus we have a workable and efficient Au/AC catalyst with relatively high TOF, which is important to the value of a catalyst in industrial

applications.

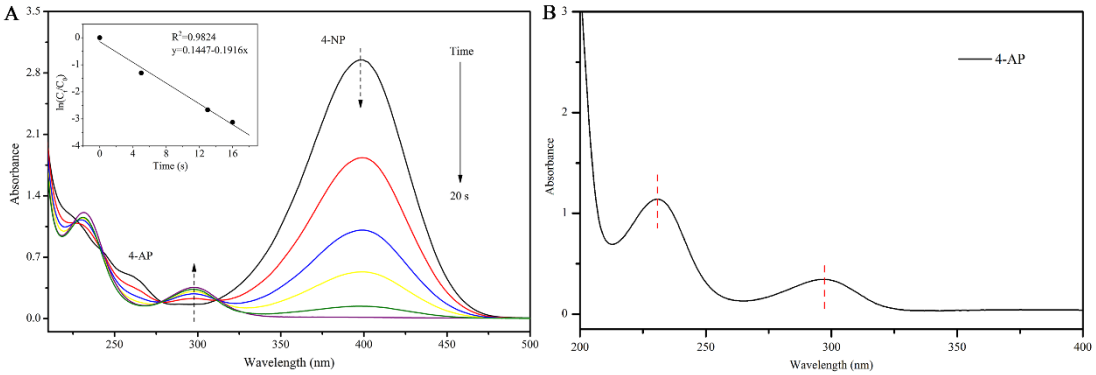

Fig. 5. Time-dependent UV-Vis absorption spectra of the reduction of 4-NP catalyzed by Au/AC-3 (A) and plot of $\ln(C/C_0)$ versus the reaction time (B).

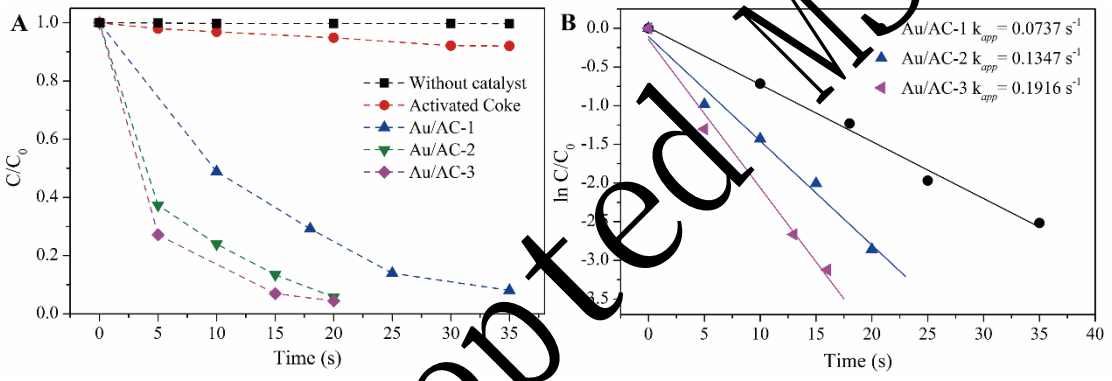

Fig. 6. C_t/C_0 (A) and $\ln(C_t/C_0)$ (B) versus the reaction time for the reduction of 4-NP catalyzed by different Au loading amounts catalysts, respectively.

Table 1 Compaision of the catalytic performances of Au/AC with the reported AuNPs catalysts supported on orther materials for the reduction of 4-NP.

Catalysts	Supported materials	Catalyst dosage (mg)	Time (s)	k_{app} (10^{-3} s^{-1})	k_{nor} (s^{-1} g^{-1})	Ref
Au/AC[a]	Activated coke	9	20	191.6	21.3	This work
Au_3-Cu_1/rGO[b]	Graphene Oxide	0.1	30	96	960	[63]
Ag-Au-rGO[b]	Reduced grapheme oxide	0.1	360	3.47	34.7	[6]

Au/GO[c]	Graphene Oxide	-	45	107.97	-	[64]
GO-Fe_3O_4[d]-Au NPs	Graphene Oxide	0.02	100	0.322	16.1	[19]
Au@CMK-3-O[e]	Mesoporous carbon	75	300	7.75	0.103	[65]
Au/g-C_3N_4[f]	g-C_3N_4	1	600	5.936	5.936	[16]
CNFs[g]@Au core–shell network	Carbon nanofibers	0.1	300	5.42	54.2	[66]
Au@PZS@CNTs[h]	Carbon nanotubes	0.3	960	1.78	5.93	[67]
AuNPs/Chitosan	Chitosan	50	67	0.561	0.011	[61]
Au/MgO[i]	magnesium oxide	15	150	7.6	0.507	[68]

[a] AC, activated carbon. [b] rGO, reduced graphene oxide. [c] GO, graphene oxide. [d] GO-Fe_3O_4, graphene oxide–Fe_3O_4 nanocomposite. [e] CMK-3-O, oxidized mesoporous carbon. [f] g-C_3N_4, Graphitic carbon nitride. [g] CNFs, carbon nanofibers. [h] PZS@CNTs, polyphosphazene functionalized carbon nanotubes. [i] MgO, magnesium oxide. k_{nor}, the rate constant normalized with the catalyst dosage (k_{app}/the mass of catalyst, s^{-1} g^{-1})

According to the Sabatier principle, the interaction between substrate and catalyst should be optimum with regard to the higher catalytic activity [69]. Thus, the effect of the catalyst dosage on the reduction of 4-NP was also investigated under identical conditions. It can be seen from Fig. 7A, the rate constant k_{app} increased intensively with the catalyst dosage increasing until the catalyst dosage was 9 mg. This can be ascribed to the more availability site of active catalytic surfaces with the increase in catalyst dosage [70]. However, the rate constant k_{app} increased slowly as the catalyst dosage increased from 9 to 12 mg. When the dosage was over 9 mg and reached 12 mg, the increasing amount of rate constant k_{app} was very small, from 0.1916 to

0.2210 s^{-1}. This could be ascribed to that the reactants were saturated that even more availability sites of active catalytic surfaces could not further enhance the reaction rate at the same initial concentration of 4-NP [71]. For the balance of the highest rate and minimum catalyst dosage in the concept of economic friendly, the catalyst dosage of 9 mg was used with the current experimental conditions. Moreover, the study of the optimization of the $NaBH_4$ concentration was also investigated. With the initial $NaBH_4$ concentration increasing, the concentration of nitrophenolate anion increased (Fig. S5). Similarly, the catalytic efficiency of Au/AC catalysts tends to increase upon addition of more $NaBH_4$. Fig. 7B shows that the rate constant k_{app} increased intensively by increasing the $NaBH_4$ concentration, and increased slowly after the $NaBH_4$ concentration of 0.10 M. Therefore, the optimum $NaBH_4$ concentration was 0.10 M for the catalytic reduction in the study.

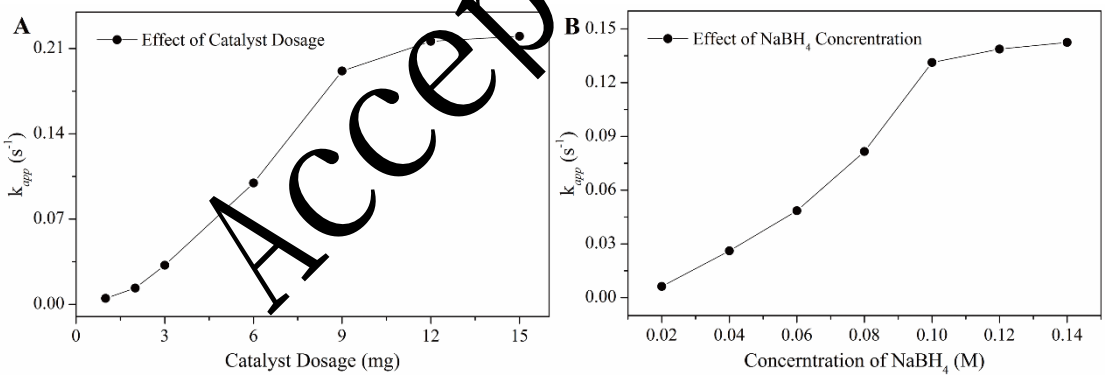

Fig. 7. The effect of catalyst dosage (A) and $NaBH_4$ concentration (B) on the catalytic reduction of 4-NP catalyzed by Au/AC-3.

Furthermore, the catalytic reduction of other nitrophenols (2-NP and 2, 4-DNP) was investigated to confirm the catalytic activity. The time-dependent UV-Vis absorption spectra of 2-NP and 2, 4-DNP is presented in Fig. 8A and 8B. In natural and alkaline conditions, the distinct bands of 2-NP and 2, 4-DNP were 415 and 359

nm, respectively [72]. Then, the intensity of their absorbance peak gradually decreased within 40 s and 50 s, accompanied with decolorization upon the additional of Au/AC-3 catalysts. As shown in Fig. 8C, we found that Au/AC-3 exhibited high catalytic activity with excellent yields towards other nitrophenols regardless of the position of the substituents. When the reduction of 4-NP, 2-NP and 2, 4-DNP was catalyzed by Au/AC-3, the rate constant k_{app} was 0.1916, 0.1399 and 0.1229 s^{-1}, respectively. It can be conclude that the catalytic activity of reduction of 4-NP showed a better activity than that of 2-NP and 2,4-DNP, which may related to the substituent positions [73]. Nonetheless, the Au/AC catalyst exhibits magnificent catalytic activity towards various nitrophenols.

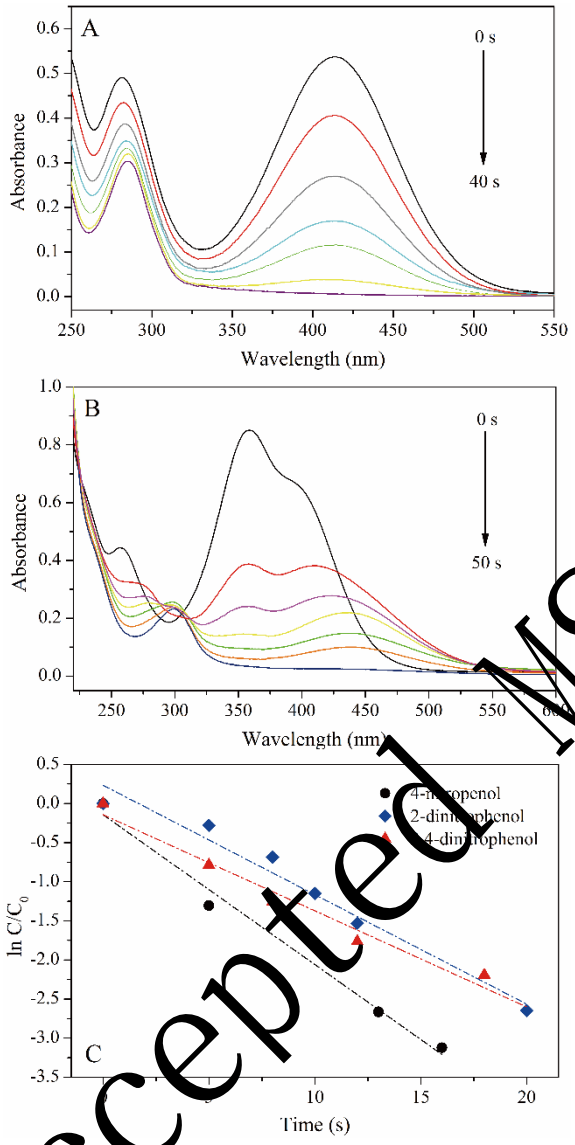

Fig. 8. Time-dependent UV-Vis absorption spectra of the reduction of 2-NP (A) and 2, 4-DNP (B) and $\ln(C_t/C_0)$ versus the reaction time (C) for the reduction of 4-NP, 2-NP and 2,4-DNP catalyzed by Au/AC-3, respectively.

The reusability of the catalyst was also investigated with the reduction of 4-NP. After completely catalytic reduction of 4-NP in the first run, the Au/AC could be easily separated by centrifugation from reaction solution, and then washed three times and dried for the further use in next cycle of the reduction of 4-NP. As shown in Fig. 9, the conversion of 4-NP to 4-AP was 84% in 20 s after six cycles. Thus, the

Au/AC still exhibited good catalytic activity after six cycles without significant loss of active sites, owing to the supporting effect of AC. It should be noted that although novel catalyst with superior catalytic performance has been developed, the method for addressing the problem of weight loss after each cycles and higher catalytic activity should be focused on further study. Hence, more experiments will be carried out to address above issues in our further research.

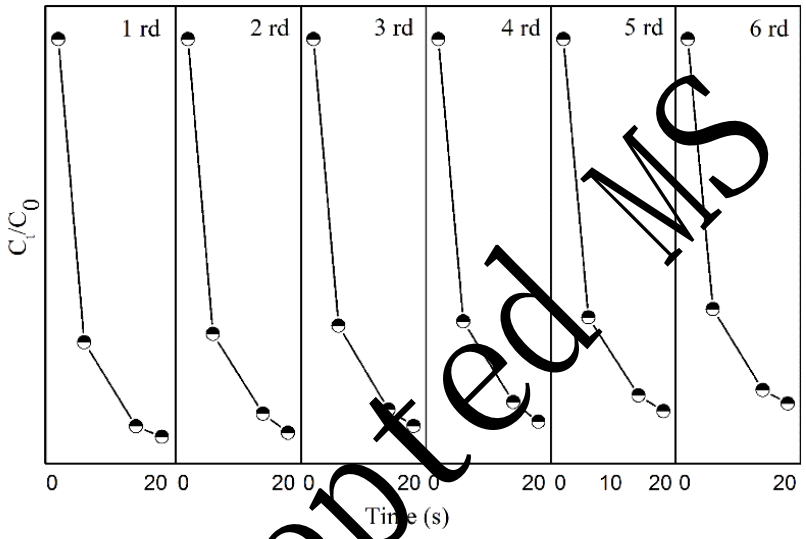

Fig. 9. Six cycling reduction curves of 4-NP catalyzed by Au/AC-3 in the presence of $NaBH_4$.

3.3 Feasible mechanism for reduction of nitrophenols

It has been widely accepted that the catalytic reduction of nitrophenols in the presence of $NaBH_4$ obeys the classical Langmuir-Hinshelwood model on account of the surface catalysis of catalytic reduction reactions [74]. Based on the experimental data, a feasible mechanism for the reduction of nitrophenols catalyzed by Au/AC was proposed in Scheme 1: (i) BH_4^- is adsorbed on to the catalytic surface, then generating BO_2- by the self-hydrolysis of $NaBH_4$. Meanwhile, BH_4^- reacts with Au NPs, transferring active hydrogen species to form the active surface-hydrogen Au-H

[69, 75]. (ii) From Fig. 5, it can be speculated that there is an induce time for 4-NP adsorption, which is in good agreement with the results that the concentration of 4-NP decreased at the initial but the concentration of 4-AP was no significant increase. Thus, 4-NP would adhere reversibly to the surface of Au/AC owing to the adsorption of AC [75]. Simultaneously, the active surface-hydrogen transfers to the nitro groups $–NO_2$, attacking $–NO_2$ to reduce to form corresponding amino groups with the electron transferring from BH_4^- to $–NO_2$ [19]. It has been reported that the catalytic reduction is owing to electron transfer between the $NaBH_4$ and the $–NO_2$ when there is direct contact between the Au NPs and $–NO_2$ [19, 76]. (iii) The generated aminophenol compounds were desorbed from the surface of Au/AC.

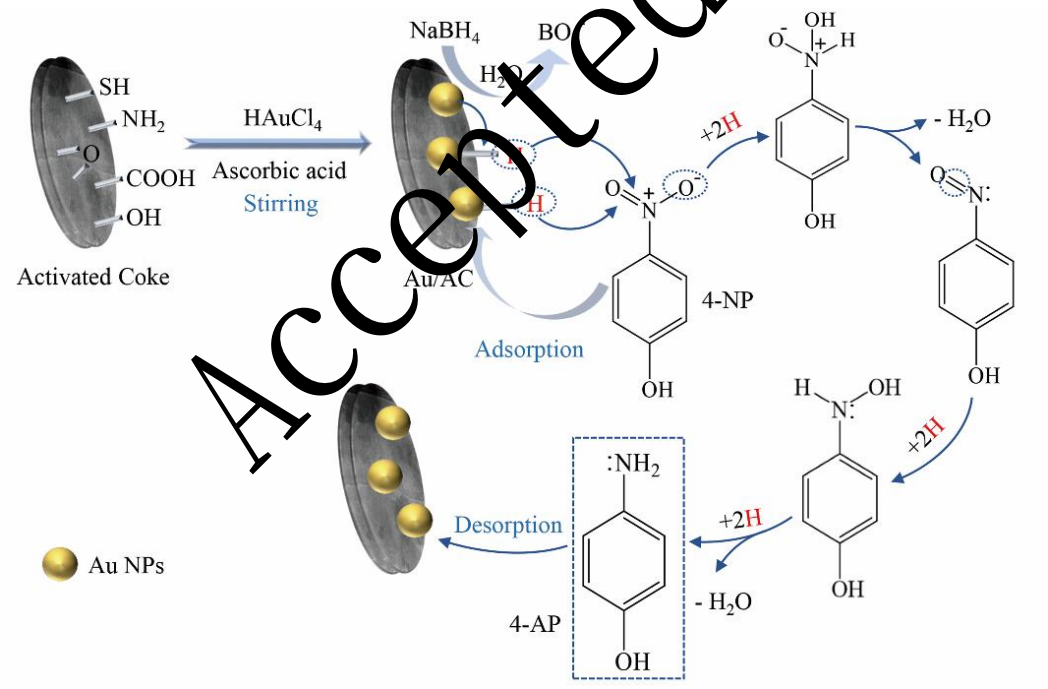

Scheme 1. Possible mechanism of catalyst preparation and catalytic reduction of 4-NP.

In summary, it can be concluded that Au/AC exhibits high catalytic activity towards the reduction of nitrophenols, which can be postulated that such high

catalytic activity of Au/AC is ascribed to these factors: (1) It has been well documented that Au NPs can be easily bonded to the sulfur atom on the surface of AC [49], guaranteeing the relative tightly combination of Au NPs and AC. Besides, with electron-rich feature of other abundant oxygen-containing groups, the AC as support is in favor to anchor and disperse Au NPs firmly through complexing or electrostatic interaction, which is vital in using metal nanoparticles catalyst in organic transformation [28, 46, 64]. (2) AC can promote the adsorption of reactants, which provides a higher concentration of nitrophenols near to Au NPs on AC. This could provide more opportunity for nitrophenols molecules to expose onto active sites of the catalysts and thus accelerate the reaction kinetics [28, 64]. (3) AC possesses a graphite-like layer crystallite structure, which is beneficial for the adsorption of 4-NP via π-π stacking interactions. This can shorten the distance between 4-NP and Au NPs supported on AC. Besides, the electrical conductivity of AC is in favor of the electron transfer during reaction. (4) Previous research has shown that the high catalytic activity also can be attributed to the use of a weakly binding agent ascorbic acid in the synthesis and the large defect to volume ratio of the Au NPs [77, 78]. Furthermore, the nanosized Au NPs with a higher redox potential value, are beneficial for accelerating the electron transfer in the catalytic system and consequently lower the kinetic negative barrier for the reduction [61]. It is concluded that the well-dispersed and nanosized Au NPs, the synergistic effects of the good adsorption capacity and electrical conductivity of AC as well as large defect to volume ratio may be responsible for the high catalytic performance of the Au/AC

catalysts.

3.4 Degradation of azo dyes

Azo dyes, as a kind of toxic and hard-biodegraded industrial pollutant containing one or more azo bonds (–N=N–), are hazardous to environment at low concentrations and carcinogenic to human [79, 80]. Thus, we extended the Au/AC catalysts to catalytic degradation of azo dyes to further investigate the catalytic performance of Au/AC. In this study, three kinds of azo dyes including CR, EBT and MO have been chosen as substrates. All the catalytic conditions of these azo dyes were same to that of 4-NP and the convincing evidence for degradation of azo dyes came from time-dependent UV-Vis absorption spectra.

As shown in Fig. S6, the initial maximum absorbance of CR, EBT and MO was at 495, 526 and 465 nm [81]. After the as-prepared Au/AC-3 was tried on CR, EBT and MO adsorption, the characteristic peaks in the corresponding UV-Vis spectra of CR, EBT and MO decreased within initial 15 min (Fig. S6A, Fig. S6C and Fig. S6E). With continuously stirring for another 15 min, these solutions achieved the adsorption equilibrium, with the adsorption efficiency of 30%, 35% and 12% for CR, EBT and MO, respectively. Especially, the adsorption efficiency of MO by Au/AC-3 was 32% at first 15 min and then decreased to 12% until equilibrium was achieved. Besides, the BET surface area (S_{BET}), pore volume, and average pore size of Au/AC-3 were determined to be 21.383 $m^2 g^{-1}$, 0.0938 $cm^3 g^{-1}$ and 17.55 nm (Table S2). It validates that Au/AC-3 possesses low adsorption ability [82].

Then, the reductant $NaBH_4$ was added to the above solution for triggering the

catalytic degradation. As we can see from Fig. S6B, the characteristic peaks at 344 and 495 nm ascribed to the CR decreased rapidly over reaction time. However, a new peak at 250 nm occurred with the decolorization of solutions within several seconds (Fig. S7). After reaction, there was almost no absorbance at 344 and 495 nm, and the absorbance at 250 nm was maximized, confirming that the removal of CR and the formation of intermediates were caused by catalytic degradation [83]. Similarly, the characteristic peaks of EBT and MO disappeared accompanied with the decolorization within several seconds after adding the Au/AC-3 catalysts (Fig. S7), while the new peaks at 240 and 258 nm were emerged corresponding to the produced intermediates of EBT and MO (Fig. S6D and Fig. S6E) [84, 85].

To sum up, the characteristic peaks of azo dyes decreased and the color of these solutions was decolorization during the reaction. Besides, new peaks were formed in the UV- range, suggesting azo dyes was indeed degraded, instead of just being absorbed by Au/AC-3 and the –N=N– bonds of azo dyes was broken down by Au/AC-3 [84]. The emerging absorption at about 250 nm appeared simultaneously with –N=N– cleavage, indicating that there were newly produced colorless compounds [71]. These peaks were originated from the absorption from aromatic intermediates, which may ascribed to the two sides of the cleavage azo bond or their derivatives, corresponding to the results in previous reports [83, 84]. Thus, the most of azo dyes were removed by the catalytic degradation by Au/AC-3. As is well-known, adsorption process can play a critical role on the removal of pollutants, including catalysis [19]. Compared with other study of catalytic degradation of azo

dyes, the reductive degradation efficiency of Au/AC catalyst is obviously superior to that of other catalysts (Table S3). These results confirm the high reductive degradation activity towards various azo dyes of our catalyst. However, as shown in Fig. S8 the catalytic efficiency was different for the three azo dyes with the rate constant k_{app} followed the order by MO (0.1863 s^{-1}) > EBT (0.1197 s^{-1}) > CR (0.0692 s^{-1}), attributed to the molecular formula and size, as well as the electrical feature of dyes [86]. The structural formulas of these dyes are given in Fig. S7, it can be concluded that with the fewer azo bonds and simpler molecular, the azo dyes could be degraded more easily. The structural formula of MO and EBT possesses single azo bonds, while CR contains a couple of azo bonds, causing that MO was reductive degraded more easily within 30 s. A speculated reason is that the less steric hindrance of dyes with the simpler molecular structural and easier electrostatic attraction between catalyst and dyes can promote these dyes to expose on the catalytic active sites, thus accelerating the catalytic degradation [86].

4. Conclusions

In this study, a facile one-step method was developed to prepare a novel Au/AC catalyst. Au NPs with a diameter of 16 ± 6 nm were supported on the surface of AC. The Au/AC catalyst exhibited excellent catalytic performance for the reduction of 4-NP with the rate constant k_{app} of 0.1916 s^{-1}. The catalyst also manifested remarkable catalytic activity for the reduction of other nitrophenols and degradation of azo dyes. It was found that the catalytic performance was comparable or even superior to that of some other Au-based catalyst. This could be attributed to the

abundant oxygen-containing functional groups and thiol groups on the surface of AC, promoting the Au NPs firmly anchored and dispersed on AC. The AC in this study is an excellent supporting material and beneficial for the catalytic reaction. In addition, the synergistic effect of nanosized Au NPs, the good adsorption capacity of AC and large defect to volume ratio could enhance the catalytic activity. The catalyst exhibited good stability and the catalytic performance remained 84% over six recycles. Considering the low cost of AC, facile preparation method and excellent catalytic performance, Au/AC catalysts seem to have potential to serve as an efficient catalyst for the reduction of nitrophenols and azo dyes as a pretreatment for wastewater treatment in diversified applications.

Conflicts of interest

There are no conflicts to declare.

Acknowledgements

This study was financially supported by the Program for the National Natural Science Foundation of China (51579098, 51879101, 51779090, 51709101, 51278176, 51408206, 51521006, 51809090, 51378190), Science and Technology Plan Project of Hunan Province (2018SK20410, 2017SK2243, 2016RS3026), the National Program for Support of Top-Notch Young Professionals of China (2014), the Program for New Century Excellent Talents in University (NCET-13-0186), the Program for Changjiang Scholars and Innovative Research Team in University (IRT-13R17), and the Fundamental Research Funds for the Central Universities (531109200027, 531107050978, 531107051080). Hunan Provincial Innovation

538 Foundation for Postgraduate.

References

[1] R. Ciriminna, E. Falletta, C. Della Pina, J.H. Teles, M. Pagliaro, Industrial Applications of Gold Catalysis, Angewandte Chemie International Edition, 55 (2016) 14210-14217.

[2] H. Mou, C. Song, Y. Zhou, B. Zhang, D. Wang, Design and synthesis of porous Ag/ZnO nanosheets assemblies as super photocatalysts for enhanced visible-light degradation of 4-nitrophenol and hydrogen evolution, Applied Catalysis B: Environmental, 221 (2018) 565-573.

[3] C. Lai, X. Liu, L. Qin, C. Zhang, G. Zeng, D. Huang, M. Cheng, P. Xu, H. Yi, D. Huang, Chitosan-wrapped gold nanoparticles for hydrogen-bonding recognition and colorimetric determination of the antibiotic kanamycin, Microchimica Acta, 184 (2017) 2097-2105.

[4] P. Xu, G.M. Zeng, D.L. Huang, C.L. Feng, S. Hu, M.H. Zhao, C. Lai, Z. Wei, C. Huang, G.X. Xie, Z.F. Liu, Use of iron oxide nanomaterials in wastewater treatment: A review, Science of The Total Environment, 424 (2012) 1-10.

[5] O. Ramirez, S. Bonardd, C. Saldias, D. Radic, A. Leiva, Biobased Chitosan Nanocomposite Films Containing Gold Nanoparticles: Obtainment, Characterization, and Catalytic Activity Assessment, ACS applied materials & interfaces, 9 (2017) 16561-16570.

[6] H. K, R.P. Joshi, S. D.V, V.N. Bhoraskar, S.D. Dhole, Anchoring of Ag-Au alloy nanoparticles on reduced graphene oxide sheets for the reduction of 4-nitrophenol, Applied Surface Science, 389 (2016) 1050-1055.

[7] A. Balanta, C. Godard, C. Claver, Pd nanoparticles for C–C coupling reactions, Chemical Society Reviews, 40 (2011) 4973-4985.

[8] L. Qin, G. Zeng, C. Lai, D. Huang, P. Xu, C. Zhang, M. Cheng, X. Liu, S. Liu, B. Li, H. Yi, "Gold rush" in modern science: Fabrication strategies and typical advanced applications of gold nanoparticles in sensing, Coordination Chemistry Reviews, 359 (2018) 1-31.

[9] X. Ren, G. Zeng, L. Tang, J. Wang, J. Wan, Y. Liu, J. Yu, H. Yi, S. Ye, R. Deng, Sorption, transport and biodegradation – An insight into bioavailability of persistent organic pollutants in soil, Science of The Total Environment, 610-611 (2018) 1154-1163.

[10] C. Zhang, C. Lai, G. Zeng, D. Huang, C. Yang, Y. Wang, Y. Zhou, M. Cheng, Efficacy of carbonaceous nanocomposites for sorbing ionizable antibiotic sulfamethazine from aqueous solution, Water Research, 95 (2016) 103-112.

[11] F. Long, J.-L. Gong, G.-M. Zeng, L. Chen, X.-Y. Wang, J.-H. Deng, Q.-Y. Niu, H.-Y. Zhang, X.-R. Zhang, Removal of phosphate from aqueous solution by magnetic Fe–Zr binary oxide, Chemical Engineering Journal, 171 (2011) 448-455.

[12] W.W. Tang, G.M. Zeng, J.L. Gong, J. Liang, P. Xu, C. Zhang, B.B. Huang, Impact of humic/fulvic acid on the removal of heavy metals from aqueous solutions using nanomaterials: a review, The Science of the total environment, 468-469 (2014) 1014-1027.

[13] X. Tan, Y. Liu, G. Zeng, X. Wang, X. Hu, Y. Gu, Z. Yang, Application of biochar for the removal of pollutants from aqueous solutions, Chemosphere, 125 (2015) 70-85.

[14] R. Rajesh, E. Sujanthi, S. Senthil Kumar, R. Venkatesan, Designing versatile heterogeneous catalysts based on Ag and Au nanoparticles decorated on chitosan functionalized graphene oxide, Physical chemistry chemical physics : PCCP, 17 (2015) 11329-11340.

[15] P. Zhao, X. Feng, D. Huang, G. Yang, D. Astruc, Basic concepts and recent advances in nitrophenol reduction by gold- and other transition metal nanoparticles, Coordination Chemistry Reviews, 287 (2015) 114-136.

[16] Y. Fu, T. Huang, B. Jia, J. Zhu, X. Wang, Reduction of nitrophenols to aminophenols under concerted catalysis by Au/g-C_3N_4 contact system, Applied Catalysis B: Environmental, 202 (2017) 430-437.
[17] L. Qin, G. Zeng, C. Lai, D. Huang, C. Zhang, P. Xu, T. Hu, X. Liu, M. Cheng, Y. Liu, A visual application of gold nanoparticles: simple, reliable and sensitive detection of kanamycin based on hydrogen-bonding recognition, Sensors and Actuators B: Chemical, 243 (2017) 946-954.
[18] Q. Ji, J.P. Hill, K. Ariga, Shell-adjustable hollow 'soft' silica spheres as a support for gold nanoparticles, Journal of Materials Chemistry A, 1 (2013) 3600.
[19] J. Hu, Y.-l. Dong, X.-j. Chen, H.-j. Zhang, J.-m. Zheng, Q. Wang, X.-g. Chen, A highly efficient catalyst: In situ growth of Au nanoparticles on graphene oxide–Fe_3O_4 nanocomposite support, Chemical Engineering Journal, 236 (2014) 1-8.
[20] J. Zheng, Y. Dong, W. Wang, Y. Ma, J. Hu, X. Chen, X. Chen, In situ loading of gold nanoparticles on Fe_3O_4@SiO_2 magnetic nanocomposites and their high catalytic activity, Nanoscale, 5 (2013) 4894-4901.
[21] B. Le Droumaguet, R. Poupart, D. Grande, "Clickable" thiol-functionalized nanoporous polymers: from their synthesis to further adsorption of gold nanoparticles and subsequent use as efficient catalytic supports, Polymer Chemistry, 6 (2015) 8105-8111.
[22] F. Cárdenas-Lizana, Z.M.D. Pedro, S. Gómez-Quero, L. Kiwi-Minsker, M.A. Keane, Carbon supported gold and silver: Application in the gas phase hydrogenation of m -dinitrobenzene, Journal of Molecular Catalysis A: Chemical, 408 (2015) 138-146.
[23] F. Ke, J. Zhu, L.-G. Qiu, X. Jiang, Controlled synthesis of novel Au@MIL-100(Fe) core-shell nanoparticles with enhanced catalytic performance, Chemical Communications, 49 (2013) 1267-1269.
[24] A.D. Quast, M. Bornstein, B.J. Greylandus, I. Zharov, J.S. Shumaker-Parry, Robust Polymer-Coated Diamond Supports for Noble Metal Nanoparticle Catalysts, ACS Catalysis, 6 (2016) 4729-4738.
[25] J.-H. Deng, X.-R. Zhang, G.-M. Zeng, J.-L. Gong, Q.-Y. Niu, J. Liang, Simultaneous removal of Cd(II) and ionic dyes from aqueous solution using magnetic graphene oxide nanocomposite as an adsorbent, Chemical Engineering Journal, 226 (2013) 189-200.
[26] J.-L. Gong, B. Wang, G.-M. Zeng, C.-P. Yang, C.-G. Niu, Q.-Y. Niu, W.-J. Zhou, Y. Liang, Removal of cationic dyes from aqueous solution using magnetic multi-wall carbon nanotube nanocomposite as adsorbent, Journal of Hazardous Materials, 164 (2009) 1517-1522.
[27] H. Yi, D. Huang, G. Zeng, C. Lai, L. Qin, M. Cheng, S. Ye, B. Song, X. Ren, X. Guo, Selective prepared carbon nanomaterials for advanced photocatalytic application in environmental pollutant treatment and hydrogen production, Applied Catalysis B: Environmental, (2018).
[28] X. Du, C. Li, L. Zhao, J. Zhang, L. Gao, J. Sheng, Y. Yi, J. Chen, G. Zeng, Promotional removal of HCHO from simulated flue gas over Mn-Fe oxides modified activated coke, Applied Catalysis B: Environmental, 232 (2018) 37-48.
[29] S. Álvarez-Torrellas, M. Martin-Martinez, H.T. Gomes, G. Ovejero, J. García, Enhancement of p-nitrophenol adsorption capacity through N_2-thermal-based treatment of activated carbons, Applied Surface Science, 414 (2017) 424-434.
[30] H. Chen, D. He, Q. He, P. Jiang, G. Zhou, W. Fu, Selective hydrogenation of p-chloronitrobenzene over an Fe promoted Pt/AC catalyst, RSC Advances, 7 (2017) 29143-29148.
[31] Y. Xie, C. Li, L. Zhao, J. Zhang, G. Zeng, X. Zhang, W. Zhang, S. Tao, Experimental study on

626 Hg^0 removal from flue gas over columnar MnO_x-CeO_2/activated coke, Applied Surface Science, 333
627 (2015) 59-67.
628 [32] S. Tao, C. Li, X. Fan, G. Zeng, P. Lu, X. Zhang, Q. Wen, W. Zhao, D. Luo, C. Fan, Activated
629 coke impregnated with cerium chloride used for elemental mercury removal from simulated flue gas,
630 Chemical Engineering Journal, 210 (2012) 547-556.
631 [33] B.F. Machado, P. Serp, Graphene-based materials for catalysis, Catalysis Science & Technology,
632 2 (2012) 54-75.
633 [34] P. Zhang, C. Shao, Z. Zhang, M. Zhang, J. Mu, Z. Guo, Y. Liu, TiO_2@carbon core/shell
634 nanofibers: Controllable preparation and enhanced visible photocatalytic properties, Nanoscale, 3
635 (2011) 2943-2949.
636 [35] C. Lai, M.-M. Wang, G.-M. Zeng, Y.-G. Liu, D.-L. Huang, C. Zhang, R.-Z. Wang, P. Xu, M.
637 Cheng, C. Huang, H.-P. Wu, L. Qin, Synthesis of surface molecular imprinted TiO_2/graphene
638 photocatalyst and its highly efficient photocatalytic degradation of target pollutant under visible light
639 irradiation, Applied Surface Science, 390 (2016) 368-376.
640 [36] J. Sheng, C. Li, L. Zhao, X. Du, L. Gao, G. Zeng, Efficient removal of HCHO from simulated
641 coal combustion flue gas using CuO-CeO_2 supported on cylindrical activated coke, Fuel, 197 (2017)
642 397-406.
643 [37] K. Tong, Y. Zhang, D. Fu, X. Meng, Q. An, P.K. Chu, Removal of organic pollutants from super
644 heavy oil wastewater by lignite activated coke, Colloids and Surfaces A: Physicochemical and
645 Engineering Aspects, 447 (2014) 120-130.
646 [38] K. Tong, A. Lin, G. Ji, D. Wang, X. Wang, The effects of adsorbing organic pollutants from super
647 heavy oil wastewater by lignite activated coke, J Hazard Mater, 308 (2016) 113-119.
648 [39] H. Guo, Y. Ren, Q. Cheng, D. Wang, Y. Liu, Gold nanoparticles on cyanuric acid-based support:
649 A highly active catalyst for the reduction of 4-nitrophenol in water, Catalysis Communications, 102
650 (2017) 136-140.
651 [40] L. Ouarez, A. Chelouche, T. Touam, R. Mahiou, D. Djouadi, A. Potdevin, Au-doped ZnO sol-gel
652 thin films: An experimental investigation of physical and photoluminescence properties, Journal of
653 Luminescence, 203 (2018) 223-229.
654 [41] F. Costanzo, M. Sulpizi, J. Vandevondele, R.G.D. Valle, M. Sprik, Ab initiomolecular dynamics
655 study of ascorbic acid in aqueous solution, Molecular Physics, 105 (2007) 17-23.
656 [42] H. Li, Y. Liu, Y. Yang, D. Yang, J. Sun, Influences of hydrogen bonding dynamics on adsorption
657 of ethyl mercaptan onto functionalized activated carbons: A DFT/TDDFT study, Journal of
658 Photochemistry and Photobiology A: Chemistry, 291 (2014) 9-15.
659 [43] M. Nemanashi-Maumela, I. Nongwe, R.C. Motene, B.L. Davids, R. Meijboom, Au and Ag
660 nanoparticles encapsulated within silica nanospheres using dendrimers as dual templating agent and
661 their catalytic activity, Molecular Catalysis, 438 (2017) 184-196.
662 [44] H. Sharififard, F. Zokaee Ashtiani, M. Soleimani, Adsorption of palladium and platinum from
663 aqueous solutions by chitosan and activated carbon coated with chitosan, Asia-Pacific Journal of
664 Chemical Engineering, 8 (2013) 384-395.
665 [45] L. Qi, B. Cheng, J. Yu, W. Ho, High-surface area mesoporous Pt/TiO_2 hollow chains for efficient
666 formaldehyde decomposition at ambient temperature, Journal of Hazardous Materials, 301 (2016)
667 522-530.
668 [46] Z. Li, L. Wu, H. Liu, H. Lan, J. Qu, Improvement of aqueous mercury adsorption on activated
669 coke by thiol-functionalization, Chemical Engineering Journal, 228 (2013) 925-934.

63
64
65

[47] S. Nellaiappan, A.S. Kumar, S. Nisha, K. Chandrasekara Pillai, In-situ preparation of Au(111) oriented nanoparticles trapped carbon nanofiber-chitosan modified electrode for enhanced bifunctional electrocatalysis and sensing of formaldehyde and hydrogen peroxide in neutral pH solution, Electrochimica Acta, 249 (2017) 227-240.
[48] B. Adhikari, A. Biswas, A. Banerjee, Graphene oxide-based hydrogels to make metal nanoparticle-containing reduced graphene oxide-based functional hybrid hydrogels, ACS applied materials & interfaces, 4 (2012) 5472-5482.
[49] S. Wang, Q. Zhao, H. Wei, J.Q. Wang, M. Cho, H.S. Cho, O. Terasaki, Y. Wan, Aggregation-free gold nanoparticles in ordered mesoporous carbons: toward highly active and stable heterogeneous catalysts, Journal of the American Chemical Society, 135 (2013) 11849-11860.
[50] M.-B. Li, S.-K. Tian, Z. Wu, R. Jin, Cu2+ induced formation of $Au_{44}(SC_2H_4Ph)_{32}$ and its high catalytic activity for the reduction of 4-nitrophenol at low temperature, Chemical Communications, 51 (2015) 4433-4436.
[51] F. Zhang, X. Zhao, C. Feng, B. Li, T. Chen, W. Lu, X. Lei, S. Xu, Crystal-Face-Selective Supporting of Gold Nanoparticles on Layered Double Hydroxide as Efficient Catalyst for Epoxidation of Styrene, ACS Catalysis, 1 (2011) 232-237.
[52] X. Hu, B. Liu, Y. Deng, H. Chen, S. Luo, C. Sun, P. Yang, S. Yang, Adsorption and heterogeneous Fenton degradation of 17α-methyltestosterone on nano Fe_3O_4/MWCNTs in aqueous solution, Applied Catalysis B: Environmental, 107 (2011) 274-283.
[53] D. Huang, C. Hu, G. Zeng, M. Cheng, P. Xu, X. Gong, R. Wang, W. Xue, Combination of Fenton processes and biotreatment for wastewater treatment and soil remediation, Science of the Total Environment, 574 (2017) 1599-1610.
[54] L. Li, M. Chen, G. Huang, N. Yang, L. Zhang, H. Wang, Y. Liu, W. Wang, J. Gao, A green method to prepare Pd–Ag nanoparticles supported on reduced graphene oxide and their electrochemical catalysis of methanol and ethanol oxidation, Journal of Power Sources, 263 (2014) 13-21.
[55] F. Montagne, J. Polesel-Maris, R. Pugin, H. Heinzelmann, Poly(N-isopropylacrylamide) Thin Films Densely Grafted onto Gold Surface: Preparation, Characterization, and Dynamic AFM Study of Temperature-Induced Chain Conformational Changes, Langmuir, 25 (2009) 983-991.
[56] F. Wei, J. Liu, Y.-H. Zhu, X.-S. Wang, C.-Y. Cao, W.-G. Song, In situ facile loading of noble metal nanoparticles on polydopamine nanospheres via galvanic replacement reaction for multifunctional catalysis, Science China Chemistry, 60 (2017) 1236-1242.
[57] F. Ali, S.B. Khan, T. Kamal, Y. Anwar, K.A. Alamry, A.M. Asiri, Bactericidal and catalytic performance of green nanocomposite based-on chitosan/carbon black fiber supported monometallic and bimetallic nanoparticles, Chemosphere, 188 (2017) 588-598.
[58] S. Praharaj, S. Nath, S.K. Ghosh, S. Kundu, T. Pal, Immobilization and Recovery of Au Nanoparticles from Anion Exchange Resin: Resin-Bound Nanoparticle Matrix as a Catalyst for the Reduction of 4-Nitrophenol, Langmuir, 20 (2004) 9889-9892.
[59] Y. Deng, Y. Cai, Z. Sun, J. Liu, C. Liu, J. Wei, W. Li, C. Liu, Y. Wang, D. Zhao, Multifunctional Mesoporous Composite Microspheres with Well-Designed Nanostructure: A Highly Integrated Catalyst System, Journal of the American Chemical Society, 132 (2010) 8466-8473.
[60] Y. Liu, L. Xu, X. Liu, M. Cao, Hybrids of Gold Nanoparticles with Core-Shell Hyperbranched Polymers: Synthesis, Characterization, and Their High Catalytic Activity for Reduction of 4-Nitrophenol, Catalysts, 6 (2015) 3.

[61] Y. Qiu, Z. Ma, P. Hu, Environmentally benign magnetic chitosan/Fe_3O_4 composites as reductant and stabilizer for anchoring Au NPs and their catalytic reduction of 4-nitrophenol, Journal of Materials Chemistry A, 2 (2014) 13471-13478.
[62] W. Zhao, L. Xie, M. Zhang, Z. Ai, H. Xi, Y. Li, Q. Shi, J. Chen, Enhanced photocatalytic activity of all-solid-state g-C_3N_4/Au/P_{25} Z-scheme system for visible-light-driven H2 evolution, International Journal of Hydrogen Energy, 41 (2016) 6277-6287.
[63] L. Rout, A. Kumar, R.S. Dhaka, G.N. Reddy, S. Giri, P. Dash, Bimetallic Au-Cu alloy nanoparticles on reduced graphene oxide support: Synthesis, catalytic activity and investigation of synergistic effect by DFT analysis, Applied Catalysis A: General, 538 (2017) 107-122.
[64] Y. Choi, H.S. Bae, E. Seo, S. Jang, K.H. Park, B.-S. Kim, Hybrid gold nanoparticle-reduced graphene oxide nanosheets as active catalysts for highly efficient reduction of nitroarenes, Journal of Materials Chemistry, 21 (2011) 15431.
[65] P. Guo, L. Tang, J. Tang, G. Zeng, B. Huang, H. Dong, Y. Zhang, Y. Zhou, Y. Deng, L. Ma, S. Tan, Catalytic reduction-adsorption for removal of p-nitrophenol and its conversion p-aminophenol from water by gold nanoparticles supported on oxidized mesoporous carbon, Journal of colloid and interface science, 469 (2016) 78-85.
[66] P. Zhang, C. Shao, X. Li, M. Zhang, X. Zhang, C. Su, N. Lu, K. Wang, Y. Liu, An electron-rich free-standing carbon@Au core-shell nanofiber network as a highly active and recyclable catalyst for the reduction of 4-nitrophenol, Physical chemistry chemical physics : PCCP, 15 (2013) 10453-10458.
[67] X. Wang, J. Fu, M. Wang, Y. Wang, Z. Chen, J. Zhang, J. Chen, Q. Xu, Facile synthesis of Au nanoparticles supported on polyphosphazene functionalized carbon nanotubes for catalytic reduction of 4-nitrophenol, Journal of Materials Science, 49 (2014) 5056-5065.
[68] K. Layek, M.L. Kantam, M. Shirai, D. Nishio-Hamane, T. Sasaki, H. Maheswaran, Gold nanoparticles stabilized on nanocrystalline magnesium oxide as an active catalyst for reduction of nitroarenes in aqueous medium at room temperature, Green Chemistry, 14 (2012) 3164.
[69] X. Li, Y. Ma, Z. Yang, D. Huang, S. Xu, T. Wang, Y. Su, N. Hu, Y. Zhang, In situ preparation of magnetic Ni-Au/graphene nanocomposites with electron-enhanced catalytic performance, Journal of Alloys and Compounds, 706 (2017) 377-386.
[70] V.K. Gupta, N. Atar, M.L. Yola, Z. Ustundag, L. Uzun, A novel magnetic Fe@Au core-shell nanoparticles anchored graphene oxide recyclable nanocatalyst for the reduction of nitrophenol compounds, Water Res, 48 (2014) 210-217.
[71] L. Qin, D. Huang, P. Xu, G. Zeng, C. Lai, Y. Fu, H. Yi, B. Li, C. Zhang, M. Cheng, C. Zhou, X. Wen, In-situ deposition of gold nanoparticles onto polydopamine-decorated g-C_3N_4 for highly efficient reduction of nitroaromatics in environmental water purification, Journal of colloid and interface science, 534 (2018) 357-369.
[72] X. Zhou, C. Lai, D. Huang, G. Zeng, L. Chen, L. Qin, P. Xu, M. Cheng, C. Huang, C. Zhang, Preparation of water-compatible molecularly imprinted thiol-functionalized activated titanium dioxide: Selective adsorption and efficient photodegradation of 2, 4-dinitrophenol in aqueous solution, Journal of hazardous materials, 346 (2018) 113-123.
[73] J. Xia, G. He, L. Zhang, X. Sun, X. Wang, Hydrogenation of nitrophenols catalyzed by carbon black-supported nickel nanoparticles under mild conditions, Applied Catalysis B: Environmental, 180 (2016) 408-415.
[74] S. Wunder, F. Polzer, Y. Lu, Y. Mei, M. Ballauff, Kinetic Analysis of Catalytic Reduction of 4-Nitrophenol by Metallic Nanoparticles Immobilized in Spherical Polyelectrolyte Brushes, The

Journal of Physical Chemistry C, 114 (2010) 8814-8820.
[75] T. Aditya, A. Pal, T. Pal, Nitroarene reduction: a trusted model reaction to test nanoparticle catalysts, Chem Commun (Camb), 51 (2015) 9410-9431.
[76] W. Xie, B. Walkenfort, S. Schlücker, Label-Free SERS Monitoring of Chemical Reactions Catalyzed by Small Gold Nanoparticles Using 3D Plasmonic Superstructures, Journal of the American Chemical Society, 135 (2013) 1657-1660.
[77] Q. Cui, B. Xia, S. Mitzscherling, A. Masic, L. Li, M. Bargheer, H. Möhwald, Preparation of gold nanostars and their study in selective catalytic reactions, Colloids and Surfaces A: Physicochemical and Engineering Aspects, 465 (2015) 20-25.
[78] S. Biella, L. Prati, M. Rossi, Selective Oxidation of D-Glucose on Gold Catalyst, Journal of Catalysis, 206 (2002) 242-247.
[79] H. Zhang, D. Chen, X. Lv, Y. Wang, H. Chang, J. Li, Energy-Efficient Photodegradation of Azo Dyes with TiO_2 Nanoparticles Based on Photoisomerization and Alternate UV−Visible Light, Environmental Science & Technology, 44 (2010) 1107-1111.
[80] M. Chen, P. Xu, G. Zeng, C. Yang, D. Huang, J. Zhang, Bioremediation of soils contaminated with polycyclic aromatic hydrocarbons, petroleum, pesticides, chlorophenols and heavy metals by composting: Applications, microbes and future research needs, Biotechnology Advances, 33 (2015) 745-755.
[81] C. Umamaheswari, A. Lakshmanan, N.S. Nagarajan, Green synthesis, characterization and catalytic degradation studies of gold nanoparticles against congo red and methyl orange, J Photochem Photobiol B, 178 (2018) 33-39.
[82] U. Tyagi, N. Anand, D. Kumar, Synergistic effect of modified activated carbon and ionic liquid in the conversion of microcrystalline cellulose to 5-Hydroxymethyl Furfural, Bioresour Technol, 267 (2018) 326-332.
[83] Y. Zhu, X. Cao, Y. Cheng, T. Zhu, Performances and structures of functional microbial communities in the mono azo dye decolorization and mineralization stages, Chemosphere, 210 (2018) 1051-1060.
[84] W. Zhong, T. Jiang, Y. Long, . He, S.-Y. Chen, C.-H. Kuo, D. Kriz, Y. Meng, A.G. Meguerdichian, S.L. Suib, Mechanism studies on methyl orange dye degradation by perovskite-type $LaNiO_3$-δ under dark ambient conditions, Applied Catalysis A: General, 549 (2018) 302-309.
[85] N. Srivastava, M. Mukhopadhyay, Biosynthesis of SnO_2 Nanoparticles Using Bacterium Erwinia herbicola and Their Photocatalytic Activity for Degradation of Dyes, Industrial & Engineering Chemistry Research, 53 (2014) 13971-13979.
[86] J. Hu, Y.-l. Dong, Z.u. Rahman, Y.-h. Ma, C.-l. Ren, X.-g. Chen, In situ preparation of core-satellites nanostructural magnetic-Au NPs composite for catalytic degradation of organic contaminants, Chemical Engineering Journal, 254 (2014) 514-523.